Ancient TL

www.ancienttl.org · ISSN: 2693-0935

Issue 35(2) - December 2017
https://doi.org/10.26034/la.atl.v35.i2

ISSN 0735-1348

Ancient TL

A periodical devoted to Luminescence and ESR dating

Department of Physics, East Carolina University, 1000 East 5th Street, Greenville, NC 27858, USA
http://www.ecu.edu/cs-cas/physics/ancient-timeline/

December 2017, Volume 35 No.2
40th Anniversary Edition

Software in the context of luminescence dating: status, concepts and suggestions exemplified by the R package *Luminescence* 1
Sebastian Kreutzer, Christoph Burow, Michael Dietze, Margret C. Fuchs, Manfred Fischer and Christoph Schmidt

Bleaching of quartz OSL signals under natural and laboratory light conditions 12
Alma Lindvall, Rebecka Stjern and Helena Alexanderson

Les sables de Fontainebleau: A Natural Quartz Reference Sample and its Characterisation 21
Sebastian Kreutzer, Johannes Friedrich, David Sanderson, Grzegorz Adamiec, Alicja Chruścińska, Mauro Fasoli, Marco Martini, George S. Polymeris, Christopher I. Burbidge and Christoph Schmidt

Single-aliquot Regenerative-Dose (SAR) and Standardised Growth Curve (SGC) Equivalent Dose Determination in a Batch Model Using the R Package '*numOSL*' 32
Jun Peng and Bo Li

40 Years of Ancient TL 54
Steve Sutton, Ian Bailiff, Didier Miallier, Geoff Duller and Regina DeWitt

Thesis abstracts 61

Bibliography 65

Announcements 78

Obituaries 83

Ancient TL

Started by the late David Zimmerman in 1977

Ancient TL

Software in the context of luminescence dating: status, concepts and suggestions exemplified by the R package 'Luminescence'

Sebastian Kreutzer,[1*] Christoph Burow,[2] Michael Dietze,[3]
Margret C. Fuchs,[4] Manfred Fischer,[5] & Christoph Schmidt[5]

[1] IRAMAT-CRP2A, Université Bordeaux Montaigne, Pessac, France
[2] Institute of Geography, University of Cologne, Cologne, Germany
[3] Section 5.1: Geomorphology, Helmholtz Centre Potsdam, GFZ German Research Centre for Geosciences, Potsdam, Germany
[4] Helmholtz-Zentrum Dresden-Rossendorf, Helmholtz-Institut Freiberg for Resource Technology, Freiberg, Germany
[5] Chair of Geomorphology, University of Bayreuth, Bayreuth, Germany

*Corresponding Author: sebastian.kreutzer@u-bordeaux-montaigne.fr

Received: Nov 11, 2016; in final form: July 4, 2017

Abstract

The relevance of luminescence dating is reflected by the steadily growing quantity of published data. At the same time, the amount of data available for analysis has increased due to technological and methodological advances. Routinely, luminescence data are analysed using a mixture of commercially available software, self-written tools and specific solutions. Based on a luminescence dating literature screening we show how rarely articles report on the software used for the data analysis and we discuss potential problems arising from this. We explore the growing importance of the statistical programming language R in general and especially its reflection in recent software developments in the context of luminescence dating. Specifically, for the R package `'Luminescence'` we show how the transparency, flexibility and reliability of tools used for the data analysis have been improved. We finally advocate for more transparency if unvalidated software solutions are used and we emphasise that more attention should be paid to the tools used for analysing the data.

Keywords: R, Software, Luminescence dating, Data analysis

1. Introduction

Luminescence dating studies require comprehensive data analyses. Moreover, technological advances and methodological developments during the last decades have increased the amount of data available. However, how much emphasis is, or rather should be, put on the software used to analyse the data? Should we care about software development in general? For most of the researchers in the luminescence dating community, software is merely a tool to analyse data and conduct research. Moreover, not every update of such tools is worth publishing nor does every minor (or even major) change in, e.g., the *Analyst* (Duller, 2015) or the **R** package `'Luminescence'` (Kreutzer et al., 2012) always appeal to the vast majority of the luminescence dating community. Nevertheless, researchers may encounter problems, where no alternative software solution is readily available. Researchers are not usually skilled in programming or trained in managing software development projects, even though particular research questions sometimes demand such solutions. However, the design and the usage of self-written, specialised tools raises further challenges, such as verification and validation, bug tracking and even licensing questions. At the same time, scientific standards (e.g., documentation, transparency, reproducibility) need to be ensured.

In this study, we aim at shedding light on the role of software in the context of luminescence dating. Therefore we have conducted a literature screening and have compiled a list of software tools developed over the last years. We highlight the growing importance of the statistical programming language **R**. **R** and the package `'Luminescence'` are used to

exemplify standard software engineering practices and software test tools applied for developing research software. Finally, we discuss the advantages and challenges arising from the development of highly specialised software tools and we make suggestions for further developments. Our contribution consists of two parts: (I) a general presentation and discussion of the status quo of software tools used by the luminescence dating community and (II) a description of technical concepts embedded within the **R** package `'Luminescence'`.

Henceforth, we report names of software in *italic* letters and the names of **R** packages in single quotes and monospace letters (e.g., `'Luminescence'`). For program code we use `monospace` letters. Hyperlinks to internet resources, beyond the references, are provided as footnotes at their appropriate positions.

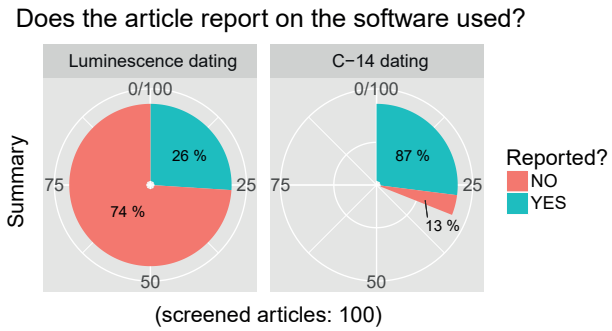

Figure 1. Results of the conducted literature study. 26 out of 100 screened articles report on the software tool used for analysing the luminescence data (left chart). By contrast, 31 out of these 100 articles additionally reported on ^{14}C dating results and from these 31 studies 27 (87 %) reported on the applied software to obtain the ^{14}C results. For details see main text. The graphic was produced using `'ggplot2'` (Wickham, 2009).

2. Software and its role in luminescence data analysis

2.1. Observations from the literature

To examine the role of software in the context of luminescence dating we conducted a literature study. The ten last published articles, presenting new luminescence dating results, of 10 international peer-reviewed journals (cf. Table S1, 100 items in total, closed volumes only, years 2016 to 2014, screening period: 2016-10-03 to 2016-10-08), were systematically screened for information given on the software used for the luminescence data analysis. Our chosen definition of data analysis includes equivalent dose modelling, age calculation and dosimetric calculations. Supplementary data provided with the screened articles were taken into account, but not referred articles. Exceptions were made for articles where substantial information on data and procedures were spread over more than one manuscript.

A table listing all screened articles is provided as supplement (Table S1). Screened journals were: *Boreas* (*BOR*), *CATENA* (*CAT*), *Earth and Planetary Science Letters* (*EPSL*), *Geomorphology* (*GM*), *Journal of Quaternary Science* (*JQS*), *Quaternary Geochronology* (*QG*), *Quaternary International* (*QI*), *Quaternary Research* (*QR*), *Quaternary Science Reviews* (*QSR*) and *The Holocene* (*HOL*). Note that this selection may be biased by preferring journals with an easy online accessibility; no further randomisation took place. Due to the applied selection articles published during the last two years were favoured. Hence, the overall explanatory power of the screening is limited.

In *CAT* and *JQS*, 5 out of 10 articles reported on the software used in the context of luminescence dating, in *EPSL*, *GM* and *QSR*, 3 out of 10 articles, in *QG*, *QR* and *HOL* it were 2 out of 10 articles each. In *BOR*, 1 out of 10 studies provided information, and none of the ten screened articles in *QI* reported on the software used. Thus, 26 out of 100 recently published articles reported on the software used for analysing the luminescence data (cf. Fig. 1). In 9 out of the 26 articles further details (e.g., software version number) were given and in only two of the articles, the references fully covered the data analysis carried out. Note: Software used for data visualisation only was not considered.

Software tools mentioned in these articles were (in alphabetical order):

- *ADELE* (Kulig, 2005, and one time *ADELE2015*, unpublished),
- *AGE* (Grün, 2009),
- *Analyst* (Duller, 2015),
- the **R** package `'Luminescence'`(Kreutzer et al., 2012, 2017),
- *DRAC* (Durcan et al., 2015),
- *DRc* (Tsakalos et al., 2015),
- *RadialPlotter* (Vermeesch, 2009),
- *PAST* (Hammer et al., 2001) (here for luminescence data regression analysis)
- and one self-written *Excel*® sheet.

Except for the programme *ADELE* (both versions) and the self-written *Excel*® sheet all cited tools were freely accessible at the time this article was written; links are given in the reference list.

Our observation differs for those articles that also include ^{14}C analysis. There, 87 % report on the software used to calculate the ^{14}C ages. In the ^{14}C community, specialised software such as *OxCal* (Ramsey, 1995) or *CALIB* (Stuiver et al., 2016) may have set a quasi-standard and their usage and citation may therefore be considered as indispensable for publishing an article. However, in other research communities (e.g., biology), Howison & Bullard (2015) encountered the similar problematic practise of missing citations and information on the software used.

2.2. Software in the wild

The previously mentioned observations from the literature are contrasted by the remarkable number of specialised software packages formally or informally released in the broader context of luminescence dating and related data analysis (in alphabetic order): *ADELE* (Kulig, 2005), *AGE* (Grün, 2009), *AgesGalore*[1] (Greilich et al., 2006), *AgesGalore2* (Greilich et al., 2015), *Analyst* (Duller, 2007, 2015), *DOSE* (Brumby, 1992), *DosiVox* (Martin et al., 2015), *DRc* (Tsakalos et al., 2015), *DRAC* (Durcan et al., 2015), *FitBin9* (Bailey, 2008), *FITT* (Grün & Macdonald, 1989), *Hybfit* (principle described in Bluszcz & Adamiec, 2006), *PTanalyse* (Lapp et al., 2009), *RadialPlotter* (Vermeesch, 2009), *RLanalyse* (Lapp et al., 2012). This list must be considered as non-exhaustive, which indicates a general demand for specialised solutions to deal with luminescence data. However, software may have not been taken into account or may have been overlooked. This includes various self-written *Excel*®, *MATLAB*®, *S* scripts and **R** scripts and individual software solutions that were never formally published, but circulate in the wild.

2.3. The R factor

Additionally, we observed a rising trend of published software based on the statistical programming language and environment **R** since 2012. Currently available **R** software (henceforth packages) dedicated to luminescence data analysis in a broader sense are listed in Table 1. All of them were first published during the last five years. The table lists the name of the package, the package maintainer as well as the latest available version and provides a short description. The columns 'Access via' (subcolumns CRAN and GitHub) and 'Licence' inform accessibility and on the selected legal statement. A licence sets the needed legal framework the software can be used in, modified and further propagated. Every software reported in Table 1 was published under GNU general public licence (GPL)[2] conditions.

3. The software dilemma

Considering the amount of software developed in the luminescence dating community over the time, it is remarkable how few articles (cf. Sec. 2.1) report on details of the software tools used for their data analysis. We consider this practice as problematic for several reasons:

1. The unanswered question "Which tool was used to analyse the data?" may lead to "How much trust can be put in presented data if important details on the data analysis remain undocumented?". Thus, reporting on the tools is indispensable to ensure transparency and reproducibility of published results.

2. Software is never free of bugs, might be inappropriately used and 'degrades' through time. Software that is no longer developed and not regularly maintained to function properly may suffer from increasingly frequent disabilities (e.g., unsupported new file structures, methods, operating systems) and eventually stop working at all. Changes are not always visible to the user and running software may undergo modifications causing changes for the data output. A proper reporting links the results to a particular tool and its version. It cannot prevent mistakes, but it helps to track them down.

3. Free and open-source software usually comes without any warranty. Hence, the user should not blindly trust every change undertaken and every new version released. Here, software quality assurance (e.g., testing, cross validation) is a responsibility that cannot be taken by the developers of analysis tools alone or should not be fully committed to them. If nothing is reported and software errors are discovered later, they are not linked to the article and can hardly be recognised.

The last point deserves further attention. Although the software tools reported in Sec. 2.2 were made freely available by the authors, the source code is not accessible to the public. By contrast, the source code of all the **R** software listed in Sec. 2.3 is available via public repositories. A non-accessible closed source tool is not by default inherently better or worse than a freely available open-source tool. However, if disagreements in the results from different software tools are encountered the ability to track down errors, such as deviations in calculations, are reduced. Open-source software balances the roles between developers and users, but only if recognised as an opportunity. At present, however, common reporting practice indicates that computational work and its developments are not yet part of the daily scientific routine in the luminescence dating community.

Beyond transparency, open-source software and in particular software published under GPL-3 (cf. Sec. 2.3) encourages code recycling, and tailored solutions can be built on existing code. The statistical programming language **R** provides a very robust and popular environment (Tippmann, 2014). The reuse and extension of code are capable of changing the way research is carried out. However, it comes at the cost of caretaking for reproducibility and reliability, and time must be invested to build up skills in programming.

In the second part of our paper, we explore some lesser known features of the programming language **R**. We further present and discuss concepts and development processing tools implemented in the **R** package `'Luminescence'`.

4. The popularity of the R environment

Since our first article on the **R** package `'Luminescence'` (Kreutzer et al., 2012), the popularity of **R** has risen remarkably. This development can be seen by the Comprehensive **R** Archive Network (CRAN)[3] statistics. The first **R** package on

[1] This software should not be confused with the **R** package `'AgesGalore'` (Greilich, 2013)

[2] https://www.gnu.org/licenses/gpl-3.0.en.html

[3] https://cran.r-project.org

Table 1. To date available **R** packages in alphabetic order dealing with luminescence and ESR data in a broader sense. URLs are given in the reference list.

Name	Maintainer	Version	Description	Licence	Access via CRAN	Access via GitHub[1]	Reference[2]
'AgesGalore'	Steffen Greilich	0.0.3 [2013-12-16]	Collection of routines complementing *AgesGalore 2*	GPL-3	-	-	unpublished, Greilich (2013)
'ArchaeoPhases'	Anne Philippe	1.2 [2017-06-13]	Post-Processing of the Markov Chain Simulated by *ChronoModel*, *Oxcal* or *BCal*	GPL-3	X	-	Philippe & Vibet (2017a)
'ESR'	Christoph Burow	0.1.0.9031 [2017-07-03]	Analysing and plotting Electron Resonance Spin (ESR) data	GPL-3	-	X	unpublished, Burow (2015)
'KMS'[2]	Jun Peng	no number [2015-11-04]	Collection of kinetic models for simulating quartz luminescence	custom & GPL-3	-	X	Peng & Pagonis (2016)
'Luminescence'	Sebastian Kreutzer	0.7.5 [2017-06-26]	Comprehensive luminescence dating data analysis	GPL-3	X	X	Kreutzer et al. (2012, 2017)
'LumReader'	David Strebler	0.1.0 [2017-01-27]	Package to simulate and visualise technical aspects of a luminesce reader	GPL-3	X	X	Strebler (2017)
'numOSL'	Jun Peng	2.3 [2017-05-18]	Numerical routines dealing for OSL dating, e.g., D_e calculation, dose response curve fitting	GPL-3	X	-	Peng et al. (2013); Peng & Li (2017)
'RChronoModel'	Anne Philippe	0.4 [2017-01-12]	Collection of functions for post-processing data returned by the software *ChronoModel* (Lanos et al., 2015), this includes chronological frameworks based on luminescence dating data	GPL-3	X	-	Philippe & Vibet (2017b)
'RLumModel'	Johannes Friedrich	0.2.1 [2017-04-13]	Simulate luminescence signals based on published models, e.g., Bailey (2001)	GPL-3	X	X	Friedrich et al. (2016, 2017)
'RLumShiny'	Christoph Burow	0.2.0 [2017-06-26]	Graphical interface for the **R** package 'Luminescence'	GPL-3	X	X	Burow et al. (2017, 2016a)
'rxylib'	Sebastian Kreutzer	0.1.1 [2017-07-07]	Functions to import xy-data into **R** (e.g., from γ-ray spectrometer)	GPL-3	X	X	Kreutzer (2017)
'TLdating'	David Strebler	0.1.3 [2016-08-31]	Functions dealing with TL data using the MAAD and SAR protocol	GPL-3	X	X	Strebler et al. (2016); Strebler (2016)
'tgcd'	Jun Peng	2.0 [2016-09-06]	Functions for TL curve deconvolution	GPL-3	X	-	Peng et al. (2016); Peng (2016)

[1] The source code of every **R** package on CRAN is additionally available on GitHub, but here only listed if the source code is actively managed by the package author(s) on GitHub

[2] A software is considered as published if it is (a) released via CRAN and/or (b) presented in a peer-reviewed journal

[3] Not available as a distinct **R** package, but as a collection of **R** functions

CRAN: comprehensive **R** Archive Network. https://cran.r-project.org

GitHub: online platform for the open-source version control system *Git*. https://github.com

CRAN was released in 1997. In 2012, the year the **R** package 'Luminescence' was introduced, the CRAN counted almost 4,000 packages and the package 'Luminescence' became number 3,918[4]. When this article was written there were 10,255 active **R** packages (07/2017: 11,018), 1,322 packages of which have been added from January to August 2016 alone (Hornik & Zeilis, 2016) and CRAN counted 6 to 7 million downloaded individual packages every week[5].

[4] https://gist.github.com/daroczig/3cf06d6db4be2bbe3368, accessed: 2016-10-06

[5] http://www.r-pkg.org; accessed: 2017-03-12 & 2017-07-10

Every package published on CRAN is well integrated in the **R** environment (convenient download and installation) and available for all three major platforms (*Windows*®, *macOS*® and *Linux*®) along with the source code and a reference manual. GitHub[6] is a commercial repository to maintain, develop and host the source code of software written in all kinds of programming languages. GitHub uses the version control system *Git* (e.g., Chacon & Straub, 2014) and can be used free of charge as long as the source code is made public and open-source. The popularity of GitHub amongst the **R** community may result from its good integration provided by the **R** community itself, e.g., packages under development can be directly downloaded and installed out of the **R** environment.

In Table 1 the columns CRAN and GitHub (Table 1) inform on how the package itself and the program code are made available to the public. As mentioned before, the term CRAN refers to the location a package can be submitted to after it has successfully passed some technical tests (cf. Sec. 5.4) and as long as it does not violate the repository rules[7]. At present, the source code of all **R** packages on CRAN is additionally mirrored on GitHub even if the package is not developed on GitHub itself. By contrast, Table 1 only lists packages available via GitHub if they are actively developed and maintained via GitHub.

General advantages of using **R** for luminescence data analyses have been outlined already elsewhere (Kreutzer et al., 2012; Dietze et al., 2013; Fuchs et al., 2015; Dietze et al., 2016). A lesser known fact is that CRAN automatically archives all packages ever published on the network. Thus even after a package was updated or removed, the older versions are still available. Additionally, automatic checks are run by the CRAN before every package submission and regularly after the package was released on CRAN. These tests provide a certain degree of technical compatibility and stability. They ensure, amongst other things, that the package can be installed without error (e.g., all dependencies are available) and it provides tests for all package examples. Packages failing the automatic tests are usually removed from CRAN and become archived until the developers have addressed the raised issues.

5. Transparency, flexibility and reliability

The development of software for scientific research demands extra care regarding transparency, flexibility and reliability. During the last five years of developing the **R** package `'Luminescence'`, we have adapted concepts established in computational science of which the most important aspects are presented below.

[6] https://github.com

[7] https://cran.r-project.org/submit.html, accessed: 2016-10-03

5.1. Transparent development process

All packages on CRAN are, including the source code, freely accessible. The development process itself is not always visible to the user. This can lead to situations where the developer might already be aware of a critical bug leading to a wrong calculation and eventually fixes that bug, but if the bug fix is not announced when the new version is released, the user might not even become aware of a faulty version that previously produced erroneous results. To improve the transparency of the development process, for the package `'Luminescence'` it was decided to move the entire development process, including the bug tracking, to an open repository, namely: GitHub.

In agreement with the GPL-3 licence conditions, the package still comes without any warranty, but now offers maximum transparency and an open handling of bugs. All modifications made to the software are recorded as so-called commits, usually enhanced by comments. Each of these commits keeps track of all individual changes, which enables a side-by-side comparison of a newer and older version of a piece of code or file. As shown in Table 1 this step is not limited to the `'Luminescence'` package and it is also not a new software development concept, but it is an important step which allow a proper peer-reviewing process of tools used for the data analysis.

5.2. Object standardisation

Working with **R** can sometimes become a rather disjointed experience, especially if different packages are involved (Boettiger, 2015). Many packages are tailored to deal with rather specific problems or to solve only one particular task. Some packages comprise only a few functions and even these few functions within one package may work with a different logic.

For example, the first version of the package `'Luminescence'` was just a collection of functions that could be used independently for one or the other purpose, e.g., analysing linearly modulated optically stimulated luminescence (LM-OSL) signals or plotting equivalent dose (D_e) distributions. Both are still possible, but due to the standardisation of function argument names and a changed package structure, more comprehensive data analyses are now possible.

Figure 2 shows the general package structure for the last version of the `'Luminescence'` package. The development of this structure was guided by the idea that the luminescence data need to be first imported independently of the initial data format and is then transformed into a coherent internal structure.

Therefore, an interface was integrated that converts all kinds of luminescence input data (e.g., a BIN- or XSYG-file) into a new unified data structure consisting of so-called `RLum-objects`. The details of this structure are beyond the scope of this contribution and may change in the future. Once the data are available as `RLum-objects`, they can be passed from one function to another. Thus, as long as the

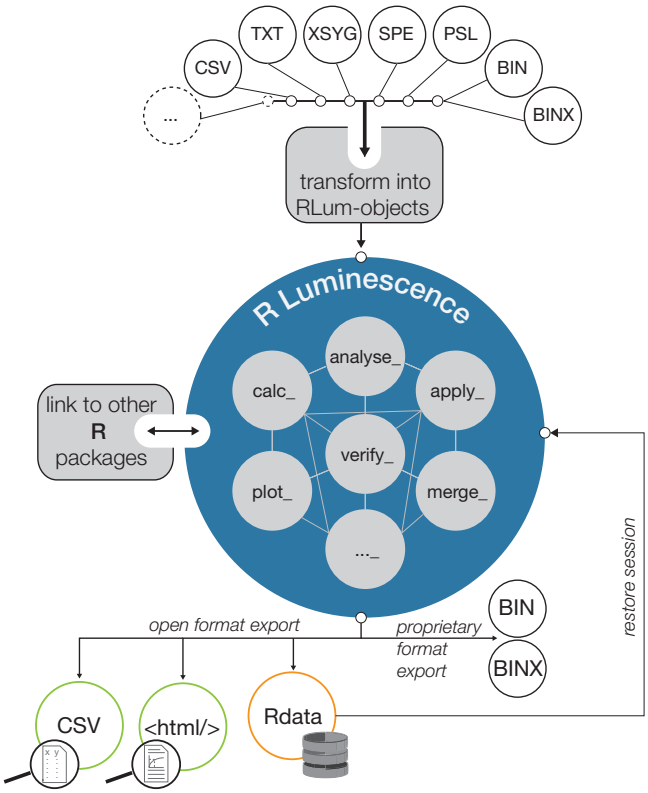

Figure 2. **R** ‘Luminescence’ package structure with indicated input/output interfaces. Once the raw measurement data have been transformed into an RLum-object, data can be passed without further transformation from one function to another within the package environment.

data are processed within the package environment (blue circle in Fig. 2), they can be analysed and combined in manifold ways, paving the way for new types of data analysis, e.g., data mining and big data analysis. For example, Burow et al. (2016b) reported the photo-ionisation cross section obtained from CW-OSL fitting of 5,488 CW-OSL curves extracted from 58 BIN-files (348 aliquots, 17 fine grain quartz loess samples from Europe). Their preliminary work showed the potential of data analyses carried out on a large scale, determining realistic distributions of expected natural variations.

The analytical output can be a graphic, a printed text in the **R** terminal, a new **R** object, an individual object created by the package ‘Luminescence’ (RLum-object) itself, or a combination of these possibilities. Numerical output can be exported to various formats natively supported by **R** (e.g., a CSV-file) or even proprietary formats (e.g., a BIN/BINX-file using the ‘Luminescence’ package). **R** allows for the export or archiving of an entire session (Rdata-file), which can be used to continue the data analysis with all previously created objects at any other time or to load the data and objects into a new session.

Another way to share analytical output with persons not familiar with **R** is the implemented possibility to export a function output to an HTML-file by creating a report using the function report_RLum(). Detailed examples are given in the package manual itself; an exemplary output is shown in Fig. 3.

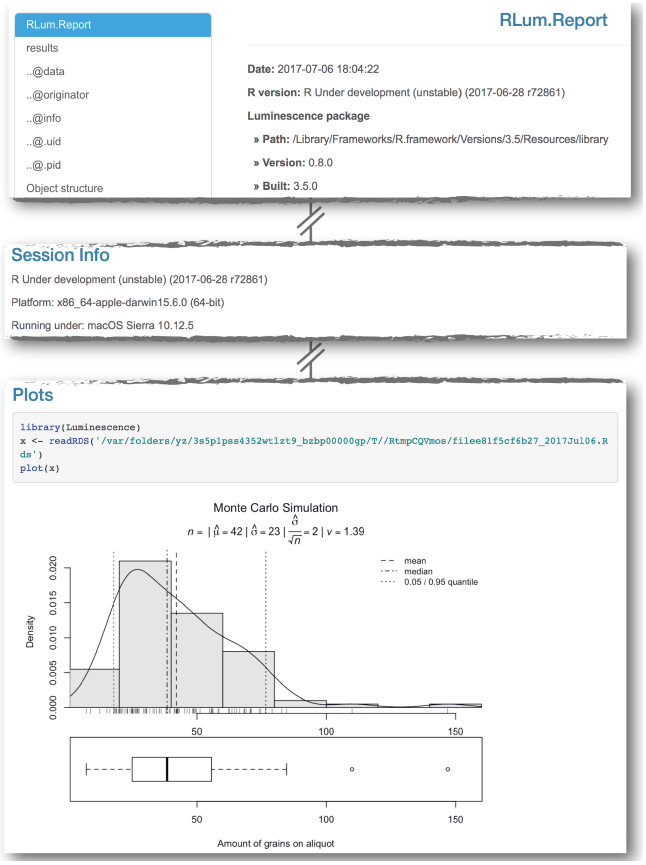

Figure 3. Screenshot of an HTML report produced using the function report_RLum() from the **R** package ‘Luminescence’. The output object used for the example was produced by the function calc_AliquotSize(). The output has been manually reduced for this figure.

The HTML-file can be opened with any modern web browser. It reports analytical output and parameters used for data analysis when producing the object, e.g., the **R** version, the package version, the operating system etc. Standard plot outputs are partly included. In this way, the provided information on a performed data analysis is optimised regarding a maximum transparency. Since HTML-files are human readable (non-binary) and can be opened by a web browser or by any text editor, the included information are available to every reviewer and reader.

5.3. Task modularisation

A programmer’s mantra is: do not repeat yourself. In other words, existing code designed for a particular task should be reused instead of implementing new code. With package modularisation, the **R** environment is well suited to reuse solutions developed by others. The ‘Luminescence’ package takes direct and indirect advantage of $>$ 50 other **R** packages. The packages are imported during installation or later (upon request) and are connected to the

'Luminescence' package based on the ability to link packages in the **R** environment and import functionalities from one package into another. Figure 4 illustrates how the package 'Luminescence' can be (and is) connected to other **R** packages.

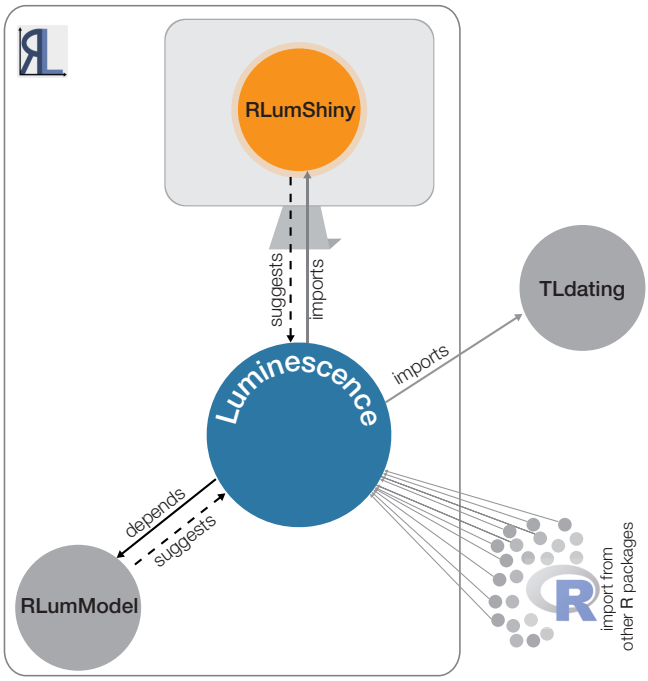

Figure 4. **R** package 'Luminescence' dependency sketch. For example: The package 'RLumShiny' is suggested by the package 'Luminescence' and therefore imported. Thus, the package 'Luminescence' can run without the package 'RLumShiny', but not the other way around.

To date, three packages import the 'Luminescence' package and using its core functionalities (e.g., data import, `RLum-object` structure). The package 'RLumShiny' (Burow et al., 2017) enhances the 'Luminescence' package by providing a graphical user interface for selected functions. 'RLumShiny' is not required to analyse data and is not installed by default while installing the 'Luminescence' package, but once installed it can improve the usability of supported functions tremendously (e.g., `plot_AbanicoPlot()`). The package 'RLumModel' (Friedrich et al., 2016, 2017) is a package to simulate quartz luminescence signals and it can be called out of the 'Luminescence' package using a so-called wrapper function (`model_LuminescenceSignals()`). To take advantage of its full functionality and for more complex use cases, the package functions should be called directly. The link established between both packages allows a very quick and focussed development of the 'RLumModel' package. It uses the entire object structure of the 'Luminescence' package, i.e., simulation outputs can be transferred to the analysis and plot functions of the 'Luminescence' package and can be treated as measurement output, i.e., as if it were produced by a luminescence reader. This connection makes writing custom plot and analysis functions for the 'RLumModel' package unnecessary and still allows a very efficient and independent development of the 'RLumModel' package, while keeping the model functions out of the 'Luminescence' package, where they are not needed for routine data analyses. The package 'TLdating' (Strebler, 2016; Strebler et al., 2016) took a different path. It imports functions (e.g., for plotting) from the 'Luminescence' package, but was further modified based on the underlying code structure of the 'Luminescence' package.

In all cases, the idea is similar concerning a preferred flexibility and task orientation of the packages, but avoiding a doubling of code wherever possible to reduce coding errors and to improve the overall reliability. The various possibilities to link **R** packages combined with the universally applicable object structure gives other package authors an independent platform for their projects without the need of taking care of the constraints provided by the 'Luminescence' package. For example, due to the complexity of 'Luminescence' not every function can be modified substantially without breaking other code and introducing errors.

5.4. Improving the code quality

Every new 'Luminescence' package release has passed internal tests performed by the programmers or by users working with the developer version from GitHub. But even after all of those tests, chance remains that bugs persist or that new bugs are introduced, which may lead to unexpected substantial errors or behaviours, i.e., the calculation output changes and remains undetected. And not every unexpected behaviour is a real bug, i.e. a coding mistake. For the package 'Luminescence', unexpected behaviour occurred with the change from package version 0.3.4 to 0.4.0. With the new version, the function `calc_FiniteMixture()` produced a different output; not because the function itself was changed, but the likelihood optimisation routine was taken from another package. The old and the new version gave different results. The results returned by the old version were not wrong, but the new results are considered to be more precise. Still, this behaviour remained unnoticed at first. Unexpected program behaviour and software errors can hardly be avoided, but can be reduced by adequate testing. Unfortunately, software testing is a tedious and time-consuming business that requires skilled users developing test scenarios. It is not the easily recognisable error in the graphical output that is most concerning, but the hard-to-track-down errors in basic calculations. Thus, errors may lead to a chain of misinterpretations and wrong scientific conclusions. Given that code errors will always exist, the aim is to recognise and reduce them. Figure 5 illustrates the development and testing process as implemented for the 'Luminescence' package (version $\geqslant 0.7.0$).

First, the implementation of a new feature (e.g., new function) starts with a feature request (induced internally or externally). After that, the developer drafts the first version and runs tests until the feature appears sufficiently implemented. Before making the new function part of the pack-

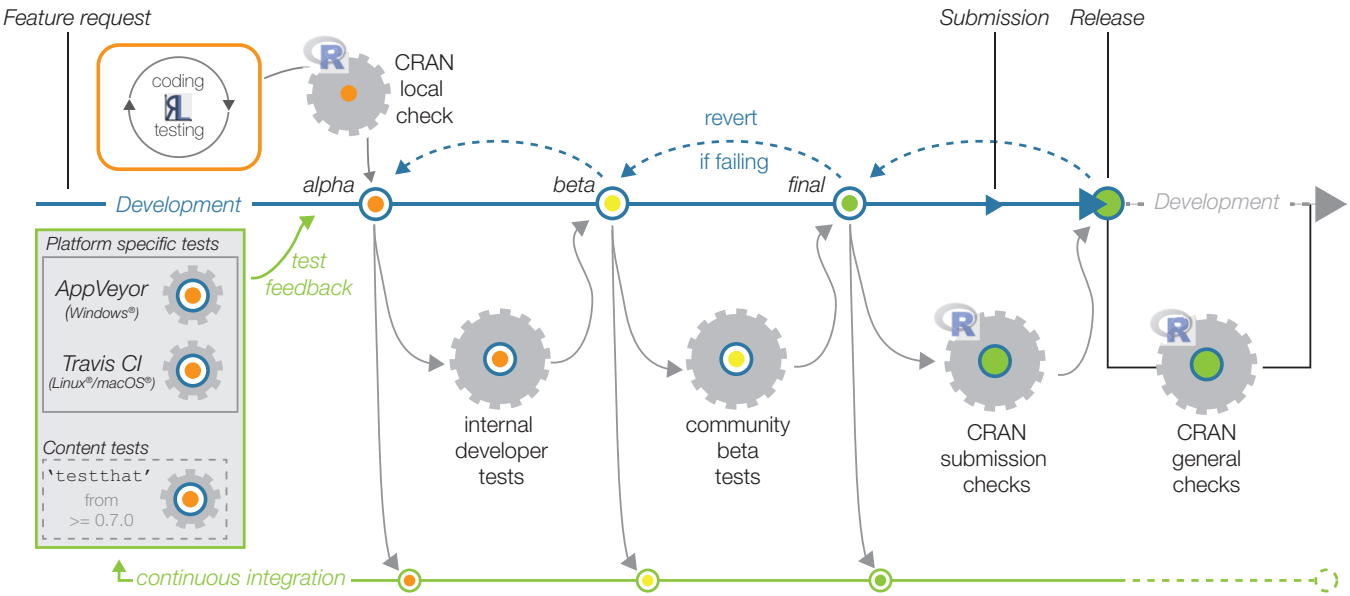

Figure 5. Development and testing process as implemented in the **R** package `'Luminescence'`. Once the development process has been initialised by a feature request (e.g., a new function), the new package version evolves over several development versions. Starting with an alpha version, stability and quality are improved until a final version, ready for submission to CRAN, is reached. The entire development process is supported by automatic platform and unit tests, which are run continuously.

age, local CRAN checks are performed, i.e., the same tests that are run by CRAN when submitting a package. If these tests were passed successfully, the entire package is send to two external resources, namely *AppVeyor*[8] and *Travis CI*[9], to conduct platform specific tests. Both resources are service platforms that provide continuous integration tests on virtual machines (virtual computers) for various platforms and are used in combination with GitHub. Currently, these services are free of charge for open-source projects.

The tests have the same intention as the local CRAN test, namely to run technical tests including the package examples, but they are run on different systems, newly set up, in a separate virtual machine for each test. On top of that, with version 0.7.0, special unit tests were defined and run using the package `'testthat'` (Wickham & RStudio, 2016; Wickham, 2011). In contrast to the tests before, complex test scenarios can be established and function output can be compared to predefined output values. For example, the function `calc_FiniteMixture()` can be run with predefined values while the output is compared against reference values. Any mismatch between calculated and pre-defined reference values causes an immediate test-error message.

Until this point, all tests (except in the first step, the developer test) run automatically. After passing, the new feature will be implemented in a first 'alpha' version. Now a test phase using "human resources" starts until the scheduled CRAN submission date. The CRAN submission can be compared with the submission of a scientific article for peer-review. The CRAN is volunteered by only a few members of the **R** community running further automated or semi-automated tests, though the review process only cares about technical aspects and takes usually not more than 24 h. After the package with the new feature is released on CRAN it is still continuously tested, i.e. as soon as a change in another package prevents the `'Luminescence'` package from functioning this would be recognised by the CRAN team.

6. Discussion

The previous section has demonstrated an increasingly complex system that is necessary to fulfil basic scientific standards, balancing transparency and reproducibility with enhanced tool functionality. The question is whether this effort is needed and justified.

Humans are imperfect, which justifies the established, peer-reviewed procedure in science. However, for software tools used in data analysis, this system appears to be underutilised. The required innovations and the dynamics of software development do not favour the long lasting peer-review procedures that every new version would require, and it would perhaps exhaust existing capacities. Take the package `'Luminescence'` as an example. It would have required a minimum of 25 publications and a minimum of up to twice as many reviewers within the last five years. Accordingly, to ensure basic scientific standards, we implemented the measures as discussed in Sec. 5.

Furthermore, tools of limited complexity may also only encounter problems of limited complexity. A pseudo LM-OSL curve conversion requires only a rather simple script, which can be easily validated by third parties. However, the

[8] https://www.appveyor.com
[9] https://travis-ci.org

additional benefit of such scripts remains limited. By contrast, a full equivalent dose determination routine requires a set of tools working together and thus becomes more complicated, but carries more overall value. The presented programming environment **R** favours simple scripts which can be combined to produce complex scenarios. Hence, the popularity of **R** within the scientific community might be partly explained by its package structure, which allows for aggregate packages to tackle rather complex tasks.

Nonetheless, **R** serves only as an example, and the drawbacks should not be overlooked. The nearly unlimited flexibility comes at the cost of lacking a native, easy-to-handle graphical user interface (GUI), which poses serious obstacles for beginners, as basic knowledge on the **R** environment is needed before packages can be used. And the advantage that **R** software is open for inspection by the user is of interest only to a small circle of **R** users. Even the package structure itself may partly cause a fragmentation of the system. Spreading needed functionalities across packages with limited compatibility gives no direct benefit to the user. Packages are not necessarily compatible with each other in terms of data exchange and functionality.

In contrast to the established peer-reviewed publishing procedure, software development is a far more agile and fast moving process, poorly suited to the established peer-review process. We may, therefore, advocate for a changed perception of scientific software developments. The correct and complete documentation of the applied tools would be an important first step. A minimum reporting standard for the tools used in luminescence dating studies should at least include the correct name of the tool, the version number (alternatively the release date) and an appropriate reference. If more complex procedures were applied (e.g., age models), used parameters might be provided as well to make the presented data comprehensible. To what extent such reporting is necessary depends on the particular case. For example, researchers may consider whether the raw data should be made available, or whether the computational work can be reproduced easily. Both discussions are beyond the scope of this article.

We furthermore suggest that every non-trivial piece of self-written software or script should be made freely accessible or published along with the study. Ideally, the source code itself would be open-source, provided under a commonly accepted open-source licence and available via platforms similar to those presented here (i.e., CRAN or GitHub).

7. Conclusions

The role of software for analysing luminescence data is increasingly important. In our article, we investigated the role of software in the luminescence dating community.

1. A literature screening was carried out, showing that only one-quarter of the screened articles reports on the software used for the data analysis. We argue for minimum reporting standards for the software applied to the data processing in a luminescence dating study, including the name of the tool, the version number and any relevant reference.

2. We listed software developed by the community to analyse luminescence data.

3. We explored the popularity of the statistical programming environment **R** and presented development concepts implemented for the **R** package `'Luminescence'`.

4. We explained how transparency, flexibility and reliability of the developed code and tools can be improved. To this end, the software development process for the `'Luminescence'` package was moved to an open repository and the software code is now largely tested automatically. The opening-up of the development process is believed to increase the transparency and reliability of the developed tools.

5. We suggest that the code of freely available, self-developed tools should be made accessible to the public.

Finally, we advocate for more attention to software developments, since they considerably influence the research from which scientific conclusions are drawn.

Acknowledgements

The manuscript benefitted considerably from suggestions by Rainer Grün and Nathan Brown. Johannes Friedrich is thanked for his help getting access to the *Boreas*' articles. Steve Grehl is thanked for fruitful discussions on object-based programming and questions on how to take advantage of this concept for the **R** package `'Luminescence'`. The work of Sebastian Kreutzer is financed by a programme supported by the ANR - n° ANR-10-LABX-52. Collaboration and personal exchange between the authors are gratefully supported by the DFG (SCHM 3051/3-1) in the framework of the programme Scientific Networks.

Appendix

*How do I cite an **R** package?*

R has an implemented functionality to get conclusive information on how a package should be cited and referenced. For the **R** package `'Luminescence'` this information will be shown by typing the following code line into the **R** terminal:

```
library(Luminescence)
citation("Luminescence", auto = TRUE)
```

References

Bailey, D J E. *Development of LM OSL Analysis Techniques for Applications to Optical Dating*. PhD thesis, Research Laboratory for Archæology and the History of Art Keble College, 2008.

Bailey, R M. *Towards a general kinetic model for optically and thermally stimulated luminescence of quartz*. Radiation Measurements, 33: 17–45, 2001.

Bluszcz, A and Adamiec, G. *Application of differential evolution to fitting OSL decay curves*. Radiation Measurements, 41(7-8): 886–891, 2006.

Boettiger, C. *An introduction to Docker for reproducible research*. ACM SIGOPS Operating Systems Review, 49(1): 71–79, 2015.

Brumby, S. *Regression analysis of ESR/TL dose-response data*. International Journal of Radiation Applications and Instrumentation. Part D. Nuclear Tracks and Radiation Measurements, 20 (4): 595–599, 1992.

Burow, C. *ESR: Package to analyse ESR data (under development)*. CRAN, version 0.1.0.9031, 2015. Developer version on GitHub: https://github.com/tzerk/ESR.

Burow, C, Kreutzer, S, Dietze, M, Fuchs, M C, Fischer, M, Schmidt, C, and Brückner, H. *RLumShiny - A graphical user interface for the R Package 'Luminescence'*. Ancient TL, 34: 22–32, 2016a.

Burow, C, Zens, J, Kreutzer, S, Dietze, M, Fuchs, M C, Fischer, M, Schmidt, C, and Brückner, H. *Exploratory data analysis using the R package 'Luminescence'. Towards data mining in OSL applications*. In *UK LED Liverpool, 2016-08-11 to 2016-08-13*, Liverpool, 2016b. Poster presentation.

Burow, C, Wolpert, U T, and Kreutzer, S. *RLumShiny: 'Shiny' Applications for the R Package 'Luminescence'*. CRAN, version 0.2.0, 2017. URL https://CRAN.R-project.org/package=RLumShiny. Developer version on GitHub: https://github.com/tzerk/RLumShiny.

Chacon, S and Straub, B. *Pro Git*. Everything you need to know about git. Apress, 2nd edition edition, 2014. web resource: https://git-scm.com.

Dietze, M, Kreutzer, S, Fuchs, M C, Burow, C, Fischer, M, and Schmidt, C. *A practical guide to the R package Luminescence*. Ancient TL, 31(1): 11–18, 2013.

Dietze, M, Kreutzer, S, Burow, C, Fuchs, M C, Fischer, M, and Schmidt, C. *The abanico plot: visualising chronometric data with individual standard errors*. Quaternary Geochronology, 31: 12–18, 2016.

Duller, G A T. *Assessing the error on equivalent dose estimates derived from single aliquot regenerative dose measurements*. Ancient TL, 25(1): 15–24, 2007.

Duller, G A T. *The Analyst software package for luminescence data: overview and recent improvements*. Ancient TL, 33(1): 35–42, 2015. URL http://users.aber.ac.uk/ggd/.

Durcan, J A, King, G E, and Duller, G A T. *DRAC: Dose Rate and Age Calculator for trapped charge dating*. Quaternary Geochronology, 28: 54–61, 2015. source code on GitHub: https://github.com/drac-calculator/DRAC-calculator.

Friedrich, J, Kreutzer, S, and Schmidt, C. *Solving ordinary differential equations to understand luminescence: 'RLumModel', an advanced research tool for simulating luminescence in quartz using R*. Quaternary Geochronology, 35(C): 88–100, 2016.

Friedrich, J, Kreutzer, S, and Schmidt, C. *RLumModel: Modelling Ordinary Differential Equations Leading to Luminescence*. CRAN, version 0.2.1, 2017. URL https://CRAN.R-project.org/package=RLumModel. Developer version on GitHub: https://github.com/R-Lum/RLumModel.

Fuchs, M C, Kreutzer, S, Burow, C, Dietze, M, Fischer, M, Schmidt, C, and Fuchs, M. *Data processing in luminescence dating analysis: An exemplary workflow using the R package 'Luminescence'*. Quaternary International, 362: 8–13, 2015.

Greilich, K-S, Harney, H L, Woda, C, and Wagner, G A. *AgesGalore—A software program for evaluating spatially resolved luminescence data*. Radiation Measurements, 41(6): 726–735, 2006.

Greilich, S. *AgesGalore: R routines for AgesGalore data*. 0.03, 2013. URL http://www.agesgalore.net.

Greilich, S, Gribenski, N, Mittelstraß, D, Dornich, K, Huot, S, and Preusser, F. *Single-grain dose-distribution measurements by optically stimulated luminescence using an integrated EMCCD-based system*. Quaternary Geochronology, 29(C): 70–79, 2015.

Grün, R. *The "AGE" program for the calculation of luminescence age estimates*. Ancient TL, 27(2): 45–46, 2009. URL to the *AGE* program: http://www.ecu.edu/cs-cas/physics/ancient-timeline/upload/ATL27-2_supplement_Grun.zip.

Grün, R and Macdonald, P D M. *Non-linear fitting of TL/ESR dose-response curves*. International Journal of Radiation Applications and Instrumentation. Part A. Applied Radiation and Isotopes, 40 (10-12): 1077–1080, 1989.

Hammer, Ø, Harper, D A T, and Ryan, P D. *PAST: Paleontological Statistics Software Package for Education and Data Analysis*. Palaeontologia Electronica, 4(1): 1–9, 2001. Software download: http://nhm2.uio.no/norlex/past/download.html.

Hornik, K and Zeilis, A. *Changes on CRAN*. The R Journal, 8(1): 402–403, 2016.

Howison, J and Bullard, J. *Software in the scientific literature: Problems with seeing, finding, and using software mentioned in the biology literature*. Journal of the Association for Information Science and Technology, 67(9): 2137–2155, 2015.

Kreutzer, S. *rxylib: Import XY-Data into R*. CRAN, 0.1.1, 2017. URL https://CRAN.R-project.org/package=rxylib. Developer version on GitHub: https://github.com/R-Lum/rxylib.

Kreutzer, S, Schmidt, C, Fuchs, M C, Dietze, M, Fischer, M, and Fuchs, M. *Introducing an R package for luminescence dating analysis*. Ancient TL, 30(1): 1–8, 2012.

Kreutzer, S, Burow, C, Dietze, M, Fuchs, M C, Schmidt, C, Fischer, M, and Friedrich, J. *Luminescence: Comprehensive Luminescence Dating Data Analysis*. CRAN, version 0.7.5, 2017. URL https://CRAN.R-project.org/package=Luminescence. Developer version on GitHub: https://github.com/R-Lum/Luminescence.

Kulig, G. *Erstellung einer Auswertesoftware zur Altersbestimmung mittels Lumineszenzverfahren unter besonderer Berücksichtigung des Einflusses radioaktiver Ungleichgewichte in der 238-U-Zerfallsreihe*. Master's thesis, Inst. F. Informatik, TU Bergakademie Freiberg, 2005.

Lanos, P, Philippe, A, Lanos, H, and Dufrense, P. *Chronomodel : Chronological Modelling of Archaeological Data using Bayesian Statistics*. version 1.5, 2015. URL http://www.chronomodel.fr.

Lapp, T, Jain, M, Ankjærgaard, C, and Pirtzel, L. *Development of pulsed stimulation and Photon Timer attachments to the Risø TL/OSL reader*. Radiation Measurements, 44: 571–575, 2009.

Lapp, T, Jain, M, Thomsen, K J, Murray, A S, and Buylaert, J P. *New luminescence measurement facilities in retrospective dosimetry*. Radiation Measurements, 47: 803–808, 2012.

Martin, L, Incerti, S, and Mercier, N. *DosiVox: Implementing Geant 4-based software for dosimetry simulations relevant to luminescence and ESR dating techniques* . Ancient TL, 33(1): 1–10, 2015.

Peng, J. *tgcd: Thermoluminescence Glow Curve Deconvolution*. CRAN, version 2.0, 2016. URL https://CRAN.R-project.org/package=tgcd.

Peng, J and Li, B. *numOSL: Numeric Routines for Optically Stimulated Luminescence Dating*. CRAN, version 2.3, 2017. URL https://CRAN.R-project.org/package=numOSL.

Peng, J and Pagonis, V. *Simulating comprehensive kinetic models for quartz luminescence using the R program KMS*. Radiation Measurements, 86: 63–70, 2016. URL https://github.com/pengjunUCAS/KMS.

Peng, J, Dong, Z B, Han, F Q, Long, H, and Liu, X J. *R package numOSL: numeric routines for optically stimulated luminescence dating*. Ancient TL, 31(2): 41–48, 2013.

Peng, J, Dong, Z, and Han, F. *tgcd: An R package for analyzing thermoluminescence glow curves*. SoftwareX, 5: 112–120, 2016.

Philippe, A and Vibet, M-A. *ArchaeoPhases: Post-Processing of the Markov Chain Simulated by 'ChronoModel', 'Oxcal' or 'BCal'*. CRAN, version 1.2, 2017a. URL https://CRAN.R-project.org/package=ArchaeoPhases.

Philippe, A and Vibet, M-A. *RChronoModel: Post-Processing of the Markov Chain Simulated by ChronoModel*. CRAN, version 0.4, 2017b. URL https://CRAN.R-project.org/package=RChronoModel.

Ramsey, C B. *Radiocarbon Calibration and Analysis of Stratigraphy: The OxCal Program*. Radiocarbon, 37(2): 425–430, 1995.

Strebler, D. *TLdating: Tools for Thermoluminescences Dating*. CRAN, version 0.1.3, 2016. URL https://CRAN.R-project.org/package=TLdating. Developer version on GitHub: https://github.com/dstreble/TLdating.

Strebler, D. *LumReader: TL/OSL Reader simulator (under development)*. CRAN, 0.1.0, 2017. URL https://CRAN.R-project.org/package=LumReader. Developer version on GitHub: https://github.com/dstreble/LumReader.

Strebler, D, Burow, C, Brill, D, and Brückner, H. *Using R for TL dating*. Quaternary Geochronology, pp. 1–27, 2016.

Stuiver, M, Reimer, P J, and Reimer, R. *CALIB: Radiocarbon Calibration*. 7.1, 2016. URL http://calib.org/calib/.

Tippmann, S. *Programming tools: Adventures with R*. Nature, 517 (7532): 109–110, 2014.

Tsakalos, E, Christodoulakis, J, and Charalambous, L. *The Dose Rate Calculator (DRc) for Luminescence and ESR Dating-a Java Application for Dose Rate and Age Determination*. Archaeometry, 58(2): 347–352, 2015. Software download: http://www.ims.demokritos.gr/download/.

Vermeesch, P. *RadialPlotter: A Java application for fission track, luminescence and other radial plots*. Radiation Measurements, 44(4): 409–410, 2009. URL http://www.ucl.ac.uk/~ucfbpve/radialplotter/.

Wickham, H. *ggplot2: Elegant Graphics for Data Analysis*. Springer-Verlag New York, 2009. ISBN 978-0-387-98140-6. URL http://ggplot2.org.

Wickham, H. *testthat: Get Started with Testing*. R Journal, 3(1): 5–10, 2011.

Wickham, H and RStudio. *testthat: Unit Testing for R*. 1.02, 2016. URL https://CRAN.R-project.org/package=testthat.

Reviewer

Nathan Brown

Ancient TL

Bleaching of quartz OSL signals under natural and laboratory light conditions

Alma Lindvall[1], Rebecka Stjern[1], Helena Alexanderson[1*]

[1] Department of Geology, Lund University, Lund, Sweden

*Corresponding Author: helena.alexanderson@geol.lu.se

Received: Sept. 27, 2017; in final form: Nov. 13, 2017

Abstract

Resetting or bleaching of the luminescence signal is a fundamental factor in luminescence dating. It must occur in nature during the event or process to be dated for an accurate age, but if it happens during sample processing in the laboratory it destroys the sample for dating purposes. In this study, we look into bleaching of quartz optically stimulated luminescence by light in nature and in the laboratory. Unsieved quartz-rich extracts and 180–250 μm quartz grains with known doses were exposed to outdoor light and laboratory light sources, respectively, and the change in dose with exposure time was measured. The outdoor conditions included direct sunlight, diffuse light from a cloud-covered sky and weak twilight, while indoor light sources were white fluorescent light, light from a computer screen and red darkroom light. Complete resetting took place only in daylight and was faster during sunny than cloudy conditions, and with bleaching rates that changed with exposure time. For all other light sources, including the darkroom lights, bleaching occurred to various degrees but was not complete after the longest exposure, which ranged from 15 min to 24 hours. The results show that some bleaching occurs even by low-intensity light with a limited spectrum. This implies that care should be taken in the laboratory not to expose samples to any light unnecessarily, but at the same time gives hope for bleaching in nature even in settings with limited or variable light conditions.

Keywords: quartz OSL, luminescence signals, resetting

1. Introduction

In luminescence dating, bleaching (zeroing, resetting) of the luminescence signal is a fundamental factor. To get an accurate luminescence age, the sediment must be effectively bleached at the time of deposition but it must not be bleached during field sampling or sample processing in the laboratory. Bleaching of the luminescence signal is mainly dependent on light intensity, light spectrum and duration of exposure (Spooner, 1994; Singarayer et al., 2005). Material properties such as grain size, grain coating and mineralogy may also influence bleaching efficiency (Jain et al., 2003; Sohbati et al., 2017). For sediments in nature, these characteristics are largely controlled by location and depositional environment, e.g. elevation of the sun, cloudiness, sediment transport process, sediment provenance, water turbidity and sedimentation rate.

In settings with limited or variable light exposure, sediments may not be sufficiently exposed to completely reset the luminescence signal at the time of deposition, resulting in incomplete bleaching and unwanted apparent age overestimation in luminescence dating. To quantify this effect, many studies have looked into bleaching in nature and the problem of incomplete bleaching, e.g. by investigating modern or known-age samples (e.g., Stokes et al., 2001; Alexanderson & Murray, 2012; King et al., 2013) or by analysing luminescence signals or dose distributions (e.g., Galbraith et al., 1999; Bailey, 2000; Singarayer et al., 2005). We thus now have a general knowledge of bleaching potential in various depositional environments (e.g., Jain et al., 2004; Fuchs & Owen, 2008), but also know that residual doses (apparent age overestimations) may vary greatly between sites and samples.

However, fewer studies have looked into the bleaching process and how fast bleaching takes place under various conditions. The approaches of the studies that have been

Lab.no	Site	Genesis	Age (ka)	Dose (Gy)	Preheat/ Cutheat (°C)	Out-door	In-door	Reference
13017	Starmoen, SE Norway	aeolian dune	10.0 ± 0.5	33.5 ± 0.7	260/240		x	Alexanderson & Henriksen (2015)
13028	Skattungheden, C Sweden	aeolian dune	10.7 ± 0.5	36.4 ± 0.6	220/200	x		Alexanderson & Bernhardson (2016)
13039	Orsa, C Sweden	glacifluvial delta	11.9 ± 0.6	47.9 ± 1.1	220/200	x	x	Alexanderson & Bernhardson (2016)
15001	Höllviken, S Sweden	beach sand	4.7 ± 0.3	4.9 ± 0.1	180/160	x		Alexanderson, unpublished data
15096	Zaskale, S Poland	fluvial terrace	19 ± 1.1	27.0 ± 0.7	260/220		x	Olszak, unpublished data

Table 1. Sample information.

made range from controlled (laboratory) to natural conditions for both sediments and illumination, and both 'dry' and underwater settings (e.g., Godfrey-Smith et al., 1988; Berger, 1990; Sommerville, 2003; Sanderson et al., 2007).

As important as full resetting is at the time of deposition, as important it is to avoid light exposure during processing of luminescence dating samples since any exposure would result in apparent age underestimation. Most luminescence laboratories use low-intensity darkroom light to minimise the risk of light exposure, and samples are normally exposed to such darkroom lights during preparation. However, in many laboratories there are also other, brighter light sources (e.g. white light, computer screens) that are not normally on but to which the samples could accidentally be exposed and which may have a large bleaching effect.

In this study, we will examine the bleaching process by exposing samples with known doses to various light conditions, both outdoors and indoors, and measure the change in dose with exposure duration. The light sources are selected to represent common natural conditions (outdoors) and typical laboratory light sources (indoors). We will determine the rate of bleaching of the quartz OSL signal and any residual dose for the different light sources (experimental set-ups), and the implications for bleaching in nature and for laboratory handling will be discussed.

2. Sample descriptions

Samples previously analysed (fully dated) at the Lund Luminescence Laboratory were used for these experiments. The samples were chosen to represent different sediment types (aeolian, (glaci)fluvial and beach) from different areas (Sweden, Norway, Poland), see Table 1. All samples were known to have good luminescence characteristics, including a fairly strong signal dominated by a fast component, and to have a limited spread in equivalent dose (Alexanderson & Henriksen, 2015; Alexanderson & Bernhardson, 2016; Olszak, unpublished data).

3. Experimental procedures

3.1. Sample preparation

To make the experiments as realistic as possible, the samples were prepared differently for the outdoor and indoor experiments, respectively. For the outdoor experiments, the sample should be as close to its original state as possible, but still allow us to measure a signal dominated by quartz. Untreated and unexposed sediment was therefore only put through density separation with heavy liquid (LST Fastfloat, 2.62 g/cm^3) to extract a quartz-rich fraction. The sediment thus largely retains its original (quartz) grain-size distribution but has lost most signal-contaminating feldspar grains ($\sim$ 50 % for samples 13028, 13039 and $\sim$ 5 % for 15001).

Although samples at all stages of preparation could be exposed to light indoors during preparation and measurement, we here chose to analyse fully processed samples. For the indoor experiments, we therefore used 180–250 µm quartz grains that had been extracted for previous dating analyses but had not been used. These samples had been through full preparation including wet sieving, density separation (at 2.62 g/cm^3) and chemistry (10 % HCl for 15 min, 10 % H_2O_2 for 15 min, 40 % HF for 60 min and 10 % HCl for 40 min). For more details see e.g. Alexanderson & Bernhardson (2016).

3.2. Outdoor experiments

The outdoor experiments took place in Lund, S Sweden (55.71° N, 13.20° E, ca. 67 m a.s.l.); experiments O-1 and O-2 outside the Department of Geology, Lund University and experiment O-3 in a residential quarter in Lund. Three experiments with different light conditions were carried out (Lindvall, 2017), as described below. Large (8 mm) aliquots of quartz grains were placed in shallow metal containers with lids and exposed to light by taking off the lids for set times. Three aliquots per exposure duration were used. Due to technical problems, the field spectrometer could not be used for the outdoor experiments and light intensities are based on modelled data from SMHI (2017) and no spectral distributions are available.

Experiment O-1 was done on a cloudy day (April 10, 2017, at 3–4 pm). The sky was almost completely covered by grey, medium-high level clouds. In addition, the experiment was carried out in the shadow of a building to avoid exposure to direct sunlight through occasional holes in the cloud cover. The global irradiance in Lund was during that afternoon declining from ca. 400 to ca. 260 W/m^2 (SMHI, 2017) but as the samples were placed in shadow they would only have been effected by diffuse light ($<$ 200–300 W/m^2), dominated by longer wavelengths. Samples were exposed for 5 s, 10 s, 30 s, 1 min, 2 min, 5 min, 10 min, 30 min and 1 hour.

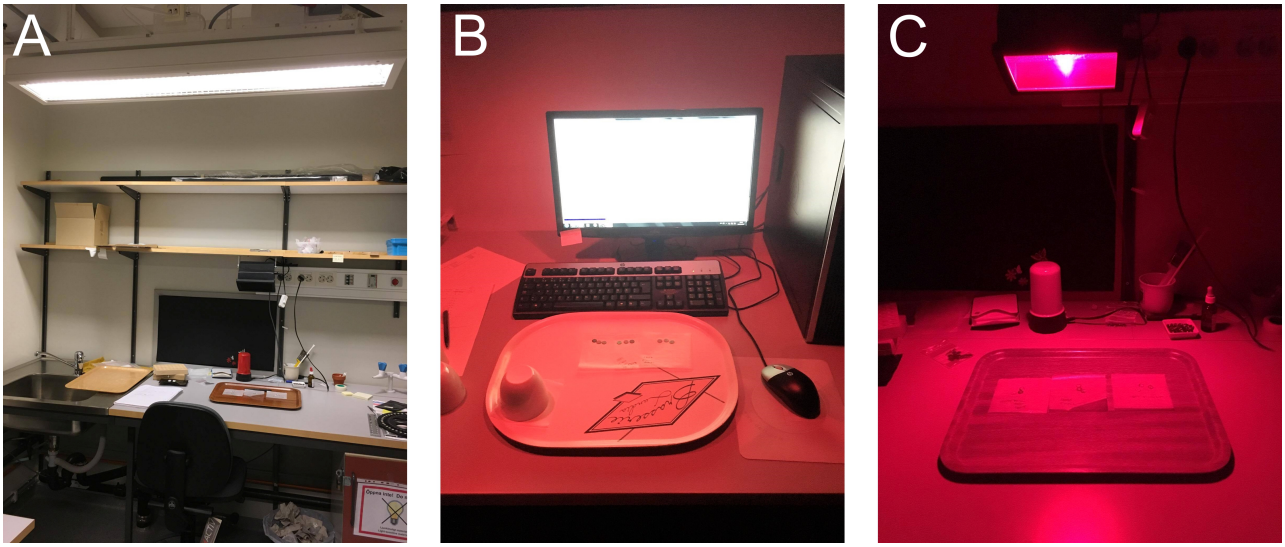

Figure 1. Indoor experiments. A. In experiment I-1, the samples were exposed to light from a fluorescent tube for 10 s to 15 min. B. In experiment I-3, samples were placed in front of a computer screen for 10 s to 15 min. C. In experiment I-4, the samples were exposed to red, darkroom light for 24 hours.

Experiment O-2 took place on a sunny day (April 11, 2017, at 1–2 pm) with only a few clouds in the sky. The global irradiance in Lund was then 650 W/m^2, of which ca. 410 W/m^2 was direct irradiance (SMHI, 2017). Samples were exposed to direct sunlight for the same durations as in experiment O-1.

Experiment O-3 was carried out in the late evening of April 19, 2017, starting at 9 pm. The sky was clear with scattered clouds. The light changed from twilight to night during the experiment with global irradiance from $<$ 20 W/m^2 to zero (SMHI, 2017). However, in addition to the natural light, there was also some light from surrounding houses and street lamps; the closest was 10 m away. Samples were exposed for 15 s, 30 s, 1 min, 5 min, 15 min, 30 min, 1 hour and 3 hours.

3.3. Indoor experiments

The indoor experiments were carried out in the Lund Luminescence Laboratory, Lund University, Sweden. Three different light sources typically found in any luminescence laboratory were used in four different set-ups (Stjern, 2017); these are described below. Large (8 mm) aliquots of quartz grains were placed on trays below or in front of the light source and exposed for set times. Outside the set exposure times, aliquots were covered by porcelain or metal containers. Three aliquots per exposure duration were used.

In experiment I-1, samples placed on a bench were exposed to white light from a fluorescent tube hanging from the ceiling directly above (Figure 1A). The light source was 140 cm from the samples and was of the type T5 ECO SAVER HE with 32 W effect (AuraLight, 2014). The light from the source was dominated by wavelengths around 540 and 620 nm with irradiance of 0.06 and 0.08 W/m^2/nm at the bench level, respectively, according to measurements with a spectrometer (ASD FieldSpec FR), corresponding to ca. 2.6 W/m^2 for the measured spectrum. This matches data given in the technical data sheet (AuraLight, 2014). Samples were exposed for 10 s, 30 s, 60 s, 5 min and 15 min.

The same light source was used in experiment I-2, but instead of illumination from above, the light reached the samples through a partly open door. The samples were placed on a bench 80 cm from the door and were exposed for 10 s, 30 s, 60 s and 5 min.

In experiment I-3, samples were placed 30 cm in front of an active computer screen, which mainly showed white (a full window of Risø SequenceEditor) (Figure 1B). The screen was of the type Fujitsu L20T-3 LED with a typical light intensity of 250 cd/m^2 (Fujitsu, 2012), which can be converted to ca. 0.4 W/m^2 at the source. Due to technical problems it was not possible to use the spectrometer to measure the light spectrum and irradiance at the samples' location for this experiment. Instead dominating wave lengths and corresponding spectral irradiance were assumed to be around 460, 530 and 650 nm and 0.01, 0.008 and 0.016 W/sr/m^2/nm, respectively, based on data from another study with a similar screen (Cajochen et al., 2011). Samples were exposed for 10 s, 30 s, 60 s, 5 min and 15 min.

Darkroom light was used in experiment I-4, where samples were placed on a bench 53 cm below a wall-mounted lamp (Figure 1C). The light source was a 15 W tungsten light bulb behind a red transparent glass filter (Fotokemika C-15). The light was too weak to be measured by the spectrometer so no wavelength or irradiance values are available. The samples were exposed for 24 hours.

3.4. Dose measurements and calculations

Dose measurements were carried out in a Risø OSL/TL reader model DA-20 with a ^{90}Sr/^{90}Y beta radiation source by following a single aliquot regeneration (SAR) protocol

(Murray & Wintle, 2000, 2003). Stimulation was by blue light (470 ± 30 nm; $\sim$ 50 mW/cm^2) at 125 °Cfor 40 s, and detection was through a 7 mm U340 glass filter. For sample 15001, post-IR blue stimulation was used due to some remaining feldspar contamination. The same preheat and cutheat temperature settings as in original dating analyses were used (Table 1; Alexanderson & Henriksen, 2015; Alexanderson & Bernhardson, 2016; Olszak, unpublished data). Since the previous analyses had shown that no or very few aliquots were rejected due to poor recycling ratios or high recuperation for the selected samples (ibid.), shortened SAR-protocols with three regenerative doses only were used for some measurements.

Equivalent doses were calculated in Risø Analyst v. 4.31.9, using exponential curve fitting. Aliquots were accepted if test dose error was < 15 %. A few aliquots gave doses much higher ($> +2\sigma$) than the natural dose; these were rejected.

Initial bleaching rates were calculated by linear interpolation between the zero-exposure equivalent dose and the dose measured at the shortest exposure time. Exponential curve fitting was done for the data from experiments O-1, O-2 and I-1, and surface power density dependent bleaching rates were calculated for these three data sets.

4. Results

4.1. Outdoor experiments

The samples that were exposed to daylight (O-1 cloudy, O-2 sunny) were bleached relatively rapidly; after 10 s the dose was 20 % or less of the natural dose (Figure 2, Figure 3). The initial bleaching was more rapid in direct sunlight than under cloud cover with average bleaching rates of 15 %/s and 9 %/s, respectively, for the first 5 s of exposure. After 1–2 min. there was no further change in dose with exposure time and the dose stabilised at 0.7–2.5 Gy (Table 2). This final dose corresponds to 3–7 % of the original dose for the older samples (13028, 13039) and 14–16 % for the younger sample (15001), cf. Table 1.

During the evening-night experiment (O-3), samples initially lost 20–40 % of their natural dose with a rate of 2 %/s for the first 30 s. With further exposure the average dose did not change much (70-80 % of the natural dose), but there was much variability between individual values (Figure 2, Figure 3).

The bleaching related to approximated surface power density (i.e. irradiance $\times$ exposure time) could not be well fitted to a single exponential curve (Figure 3B) as the slope (rate) changes with exposure. The slope is also lower for cloudy conditions than for sunny, and very low for the night experiment. For the initial part of the curves, decay constants were calculated to -4.0 and -0.8 for the sunny and cloudy conditions, respectively.

4.2. Indoor experiments

In both experiments with fluorescent light (I-1, I-2), doses were reduced to $\sim$ 90 % of the natural dose after 10 s of exposure (Figure 4), corresponding to initial bleaching rates of 0.1–1.8 %/s. In the experiment with light from directly above, further bleaching to $\sim$ 50 % had occurred after 5 min (300 s) and after 15 min (900 s) the doses were $\sim$ 20 % of the natural (Figure 4A, Table 3). When light came through a partly open door, there was no further significant change in dose after 10 s, although there was some variability between samples and aliquots (Figure 4B).

The doses in samples exposed to light from a computer screen (experiment I-3) were reduced to $\sim$ 80 % on average, but with much variability between samples, aliquots and exposure time (Figure 4C). One sample (15096) showed further reduction after 15 min to $\sim$ 40 % of the natural dose.

After 24 hours of exposure to darkroom light (experiment I-4), the doses had been reduced to 32.1 ± 1.2 Gy (13017), 42.1 ± 1.7 Gy (13039) and 21.4 ± 1.8 Gy (15096) (Table 3). This corresponds to 79–97 % of the natural dose remaining, and yields bleaching rates of 0.1–0.9 %/hour.

Due to the lower irradiance for the indoor light sources, the rate of bleaching related to approximated surface power density does not show a very clear pattern, but the shape of the curve for experiment I-1 seems to follow those of the outdoor experiments (Figure 3B) and a decay constant of 0.3 was calculated.

5. Discussion

5.1. Experimental sources of error

Although there is an overall decrease in remaining dose with exposure time, particularly for the daylight experiments, there are some values that break the steady decrease (Figure 2). An example is the 10 s measurement in experiment O-1, where values for all three samples are higher than expected and for two of the samples even higher than the preceding value (Figure 2). Since this appears systematic for all aliquots in all samples for this particular exposure time, we suspect that it is due to something that occurred during the experiment, e.g. an error in the exposure time when opening/closing the containers. Particularly for the very short exposure times and the more intense light sources a small error in timing may have a relatively large effect.

There is also inter-aliquot variability for the different experiments and samples (Figure 2, Figure 4). This variability is largest for the indoor experiments I-2-4 and the night-time outdoor experiment (O-3). For the indoor experiments, particularly I-3 (computer screen), part of the variability could be due to a directional component to the light, which may have yielded slightly different intensities depending on a particular aliquots location. The fluorescent light from above, as well as the daylight, on the other hand provided evenly distributed light to all exposed aliquots, resulting in less variability.

Another factor, which likely explains some of the inter-

Sample	Experiment Exposure (s)	O-1 cloudy Mean dose (Gy)	O-2 sunny Mean dose (Gy)	O-3 night Mean dose (Gy)
13039	0	47.9 ± 1.1	47.9 ± 1.1	47.9 ± 1.1
	5	28.54 ± 0.94	14.3 ± 1.1	
	10	30.8 ± 6.4	6.89 ± 0.80	
	15			28.5 ± 7.5
	30	10.96 ± 0.36	4.2 ± 1.4	35.5 ± 3.9
	60	7.49 ± 0.67	2.72 ± 0.16	42.7 ± 1.5
	120	3.22 ± 0.74	1.96 ± 0.53	
	300	2.04 ± 0.69	0.98 ± 0.32	35.2 ± 1.1
	600	1.93 ± 0.36	2.317 ± 0.091	
	900			37.0 ± 3.4
	1800	1.10 ± 0.55	1.85 ± 0.45	36.5 ± 2.6
	3600	1.45 ± 0.13	2.01 ± 0.40	29.8 ± 2.7
	10800			28.8 ± 9.2
13028	0	36.37 ± 0.64	36.37 ± 0.64	36.37 ± 0.64
	5	21.4 ± 1.2	8.20 ± 0.32	
	10	20.2 ± 1.9	4.67 ± 0.74	
	15			30.3 ± 2.4
	30	7.79 ± 0.74	1.53 ± 0.41	28.6 ± 2.5
	60	4.97 ± 0.46	1.66 ± 0.44	29.4 ± 1.4
	120	3.06 ± 0.21	1.01 ± 0.28	
	300	2.09 ± 0.50	0.830 ± 0.092	30.05 ± 0.85
	600	2.24 ± 0.39	1.28 ± 0.17	
	900			32.2 ± 1.9
	1800	2.52 ± 0.27	2.45 ± 0.12	29.96 ± 0.93
	3600	2.02 ± 0.18	2.47 ± 0.26	36.3 ± 5.8
	10800			30.4 ± 1.6
15001	0	4.92 ± 0.10	4.92 ± 0.10	4.92 ± 0.10
	5	2.07 ± 0.21	1.257 ± 0.012	
	10	2.62 ± 0.19	0.89 ± 0.13	
	15			3.68 ± 0.24
	30	1.270 ± 0.086	0.723 ± 0.094	4.00 ± 0.14
	60	0.71 ± 0.22	0.757 ± 0.084	3.94 ± 0.27
	120	0.850 ± 0.091	0.827 ± 0.052	
	300	0.837 ± 0.020	0.680 ± 0.053	3.73 ± 0.71
	600	0.800 ± 0.017	0.563 ± 0.077	
	900			3.14 ± 0.55
	1800	0.840 ± 0.035	0.89 ± 0.15	3.83 ± 0.87
	3600	0.77 ± 0.19	0.710 ± 0.066	3.47 ± 0.33
	10800			3.5967 ± 0.0033

Table 2. Equivalent doses measured after exposure to outdoor light. The dose is the mean of three aliquots and the uncertainty represented by the standard error of the mean. Exception is the zero exposure dose, which is based on ca. 24 aliquots (Alexanderson & Bernhardson, 2016; Alexanderson, unpublished data).

aliquot variability, is the inherent variation in (natural) dose as well as sensitivity between aliquots, as shown by the ranges of measured equivalent doses during dating analyses (Alexanderson & Henriksen, 2015; Alexanderson & Bernhardson, 2016; Alexanderson and Olszak, unpublished data). Although these samples were selected based on their limited spread of equivalent doses, occasional outliers still occurred. Such outliers may also explain some of the very high doses

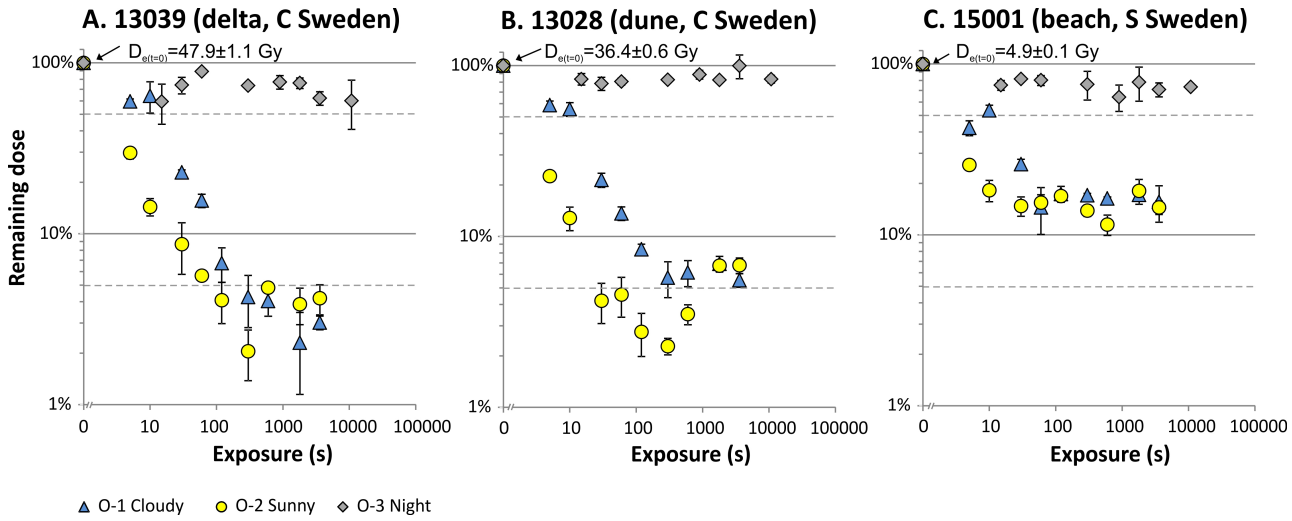

Figure 2. Remaining doses in % of the initial (zero exposure) equivalent dose (D_e) after exposure to outdoor light for the three samples and the three different outdoor experiments. The mean of three aliquots and the standard error of the mean for each exposure is shown. The value of the natural (equivalent) dose for the specific sample is given in each diagram. For values in Gy for the various exposures, see Table 2. A. Sample 13039 from a glacifluvial delta in central Sweden. B. Sample 13028 from an aeolian dune in central Sweden. C. Sample 15001 from Holocene beach sediments in southern Sweden.

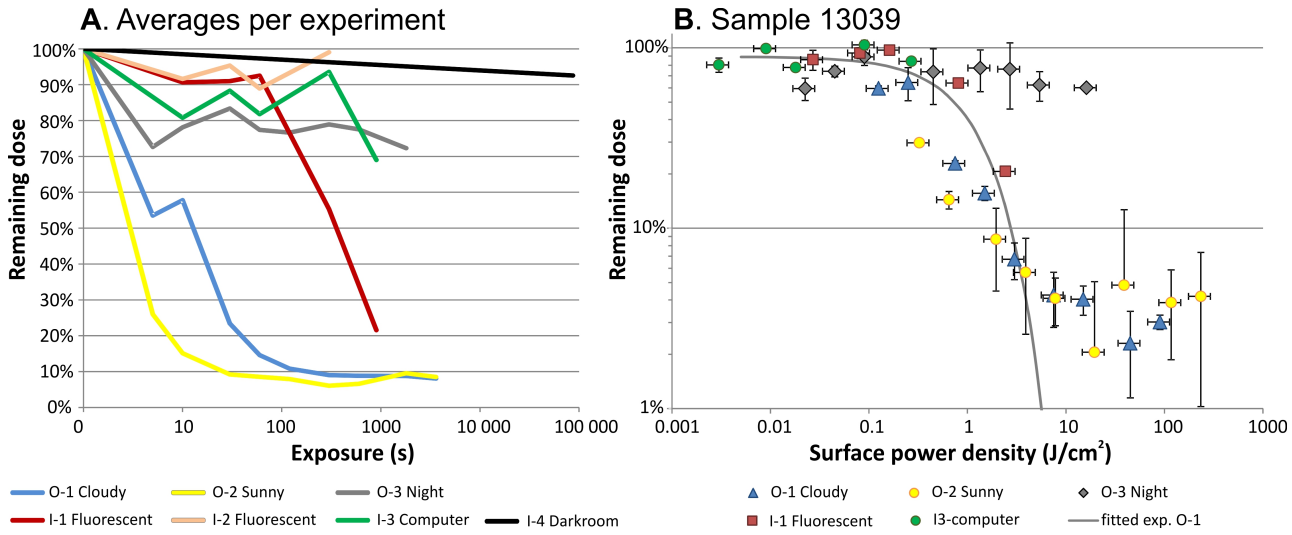

Figure 3. A. Averages of the remaining dose plotted against exposure time for all experiments and samples. B. Remaining doses for sample 13039 plotted against approximated surface power density (irradiance × exposure time) for five of the experiments and a single exponential function fitted to experiment O-1 data. See Table 2, Table 3, Figure 2 and Figure 4 for data points and values.

measured for a few aliquots and that were rejected.

For all experiments, bleaching rates were calculated for the initial part of the decay and by linear interpolation, both of which are simplifications. The dose (signal) decreases exponentially and bleaching rates change with exposure time and with the amount of energy received (surface power density), suggesting the presence of more than one component (cf. Aitken, 1998). However, for the purpose of this study and given the resolution of our data this level of simplification was deemed sufficient.

5.2. Bleaching under natural light

The bleaching rate of our samples in daylight is not as fast as that shown by Godfrey-Smith et al. (1988), where the quartz OSL signal was < 1 % after 10 s of exposure, but is similar to that of other samples from central Sweden (Alexanderson & Bernhardson, 2016) and Scotland (Sommerville, 2003). The difference in bleaching rate may be related to differences in light intensity and spectrum between the studies, or to the characteristics of the quartz (e.g., Jeong & Choi, 2012). In our own dataset, with samples of different depositional and geographic/geologic origin, there is some variation between samples but they generally follow the same

Sample	Experiment Exposure (s)	I-1 fluorescent Mean dose (Gy)	I-2 fluorescent Mean dose (Gy)	I-3 computer Mean dose (Gy)	I-4 darkroom Mean dose (Gy)
13017	0	33.53 ± 0.68	33.53 ± 0.68	33.53 ± 0.68	33.53 ± 0.68
	10	32.4 ± 1.8	27.5 ± 3.0	31.6 ± 6.3	
	30	30.3 ± 2.0	31.1 ± 6.8	29.3 ± 5.2	
	60	31.76 ± 0.39	30.27 ± 0.81	31.2 ± 5.0	
	300	18.3 ± 1.2	33.80 ± 0.40	31.4 ± 2.0	
	900	6.77 ± 0.92		27.7 ± 2.4	
	24 hrs				32.4 ± 1.2
13039	0	47.9 ± 1.1	47.9 ± 1.1	47.9 ± 1.1	47.9 ± 1.1
	10	41.2 ± 5.2	45.0 ± 2.0	38.5 ± 3.5	
	30	44.8 ± 3.1	47.1 ± 3.7	47.4 ± 1.8	
	60	46.5 ± 2.2	48.9 ± 6.4	37.26 ± 0.63	
	300	30.54 ± 0.70	39 ± 11	49.7 ± 3.0	
	900	9.90 ± 0.22		40.4 ± 1.6	
	24 hrs				42.1 ± 1.7
15096	0	27.02 ± 0.72	27.02 ± 0.72	27.02 ± 0.72	27.02 ± 0.72
	10	24.13 ± 0.29	26.68 ± 0.25	18.2 ± 6.0	
	30	24.1 ± 5.4	25.6 ± 3.5	21.2 ± 5.9	
	60	23.1 ± 2.5	20.1 ± 1.5	20.1 ± 5.1	
	300	12.9 ± 1.8	31.3 ± 2.5	22.43 ± 0.43	
	900	6.4 ± 1.4		10.85 ± 0.56	
	24 hrs				21.4 ± 1.8

Table 3. Equivalent doses measured after exposure to indoor light. The dose is the mean of three aliquots and the uncertainty represented by the standard error of the mean. Exception is the zero exposure dose, which is based on ca. 24 aliquots (Alexanderson & Henriksen, 2015; Alexanderson & Bernhardson, 2016; Olszak and Alexanderson, unpublished data).

pattern (Figure 2 - Figure 4) and do not allow us to draw any conclusions on bleaching potential related to sample origin.

Our results show that bleaching is slower with overcast conditions than in sunshine but that the signal (dose) is nevertheless eventually (close to) completely reset after 1–2 min of exposure irrespective of daylight conditions (Figure 2). The intensity of the light was also lower during the cloudy day (< 300 W/m^2) than during the sunny day (ca. 650 W/m^2). The findings are in agreement with previous studies that have shown that bleaching of luminescence signals occurs also by lower intensity light and longer wavelengths such as from diffuse light and underwater light, although it takes longer time (e.g., Godfrey-Smith et al., 1988; Berger, 1990; Sommerville, 2003).

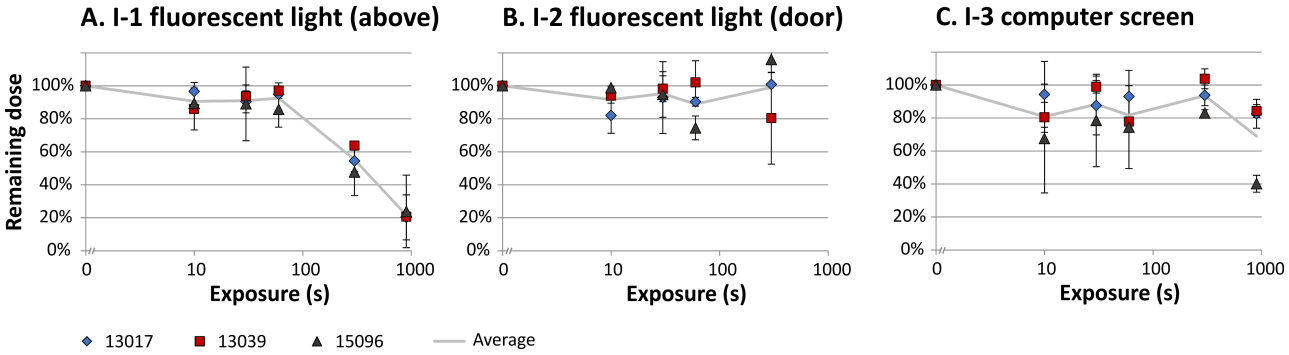

Figure 4. Remaining doses in % of the initial (zero exposure) equivalent dose (D_e) after exposure to indoor light for the three samples and experiments I-1, I-2 and I-3. The mean of three aliquots and the standard error of the mean is shown. For values in Gy for the various exposures, see Table 2. A. Experiment I-1 where samples were exposed to fluorescent light from above. B. Experiment I-2 where samples were exposed to fluorescent light coming through a partly open door. C. Experiment I-3 where samples were placed in front of a computer screen.

The remaining dose after 1 hour exposure to daylight is at face value not consistent with zero within error (0.7–2.5 Gy; Table 2). However, for sample 15001, there is no peak in the OSL signal remaining after 1 min exposure and the residual dose value is an artefact of the background noise; this sample has been completely reset. In contrast, for the two other samples (13028, 13039), there is still a small peak in the OSL signal showing that some signal is there even after 1 hour (3600 s) exposure to daylight. This could be due to a small thermal transfer effect, as shown by Alexanderson & Bernhardson (2016) for samples from the same area. A residual dose of this size – similar to that of some modern fluvial sediments (e.g., Jain et al., 2003) – would likely give rise to some apparent age overestimation for very young (low-dose) samples, while it is insignificant for older (higher-dose) samples.

During night time there was only moderate bleaching of the OSL signal (ca. 20 % on average), and only a slow, or no, continued reduction of dose with exposure time (Figure 2). The intensity of the natural light, and any nearby artificial light, was clearly not strong enough to completely reset the signal, and any sedimentary material that would have been deposited under such conditions would have suffered from incomplete bleaching. Our data are thus in line with the observations of Gemmell (1999), who noted that infrared stimulated luminescence (IRSL) signals and doses were much higher in fine-grained glacifluvial sediments transported during the night than in those transported during the day.

5.3. Bleaching during laboratory work

Our observations show that initially the light from the computer screen is the most efficient of the three artificial light sources in bleaching the OSL signal, but with longer exposure the fluorescent light from above bleaches more (Figure 4) and the shape of the decay is similar to that from the outdoor, daytime experiments (Figure 3B). An explanation may be that the light from the computer screen is dominated by somewhat shorter wavelengths than the fluorescent light, and should thus bleach quicker since shorter (higher energy) wavelengths are more efficient in bleaching the luminescence signal than longer wavelengths (Spooner, 1994), but since we unfortunately do not have accurate data on intensity (irradiance) for the computer screen we cannot draw any conclusions about this.

However, the bleaching from either light source did not occur as fast or as extensively as expected: the signal was not reset completely even after the longest exposure time (15 min). Compared to the daylight experiments, where the signal was reset completely, the artificial light has much lower intensity (< 0.4 W/m^2) and emits in fewer wavelengths, which would lead to slower bleaching rates (Spooner, 1994). Still, from a laboratory risk assessment point of view, there is an effect even after a short exposure (< 10 s) and precautions to avoid accidental white light exposure during sample preparation and measurement must be taken.

Ideally, the laboratory lights required for safe working in a luminescence laboratory should not have any effect on the luminescence signal. However, although the Lund Luminescence Laboratory, like most other luminescence laboratories, uses low-intensity red-orange lights to minimize any unintentional bleaching, these lights do have an effect on the luminescence signal (Figure 3, Table 3). The bleaching rate is slow (0.1–0.5 %/h) but after 24 hours the dose has been reduced by up to 21 %.

It is rare that samples are exposed to darkroom lights for this long, so in practice the risk is fairly small. Nevertheless, samples should not be exposed to the red light unnecessarily. If lengthier exposures are required, a change in light source may be useful. As recently shown by Sohbati et al. (2017), low-intensity, orange LEDs have a small effect on the samples and provide better visibility for laboratory staff than red light from light bulbs with filters.

6. Conclusions

- Samples of quartz-rich extracts from unsieved and unexposed samples exposed to daylight are rapidly reset; after 10 s the dose was 20 % or less of the natural dose. The bleaching rate was slower during cloudy than sunny conditions, likely related to differences in light intensity and spectrum.
- Samples exposed to evening-night light showed some reduction in dose (up to 4 %), but remaining doses varied between aliquots and exposure time but with on average a stable or slightly decreasing dose with exposure time.
- Red darkroom light in the laboratory does cause some bleaching of the luminescence signal in 180–250 μm quartz grains during long exposures. Doses were reduced by 3–21 % after a 24-hour exposure.
- White fluorescent light and bright light from computer screens bleaches samples by up to 20 % within less than 10 s, but then require longer exposures to reduce the luminescence signal further.
- The bleaching rates change with exposure time as well as with surface power density for those experiments for which such data were available, and the curves do not fit with a single exponential function. This suggests that more than one OSL component is present.

Acknowledgments

We appreciate the help from Maria Tagle Casapia and Lars Eklundh with the spectrometer. The STRÅNG data used in this paper are from the Swedish Meteorological and Hydrological Institute (SMHI), and were produced with support from the Swedish Radiation Protection Authority and the Swedish Environmental Agency. The reviewer David Sanderson provided constructive comments on the manuscript.

References

Aitken, M.J. *An Introduction to Optical Dating*. Oxford University Press, 1998.

Alexanderson, H. and Bernhardson, M. *OSL dating and luminescence characteristics of aeolian deposits and their source material, Dalarna, central Sweden*. Boreas, 45: 876–893, 2016.

Alexanderson, H. and Henriksen, M. *A short-lived aeolian event during the Early Holocene in southeastern Norway*. Quaternary Geochronology, 30: 175–180, 2015.

Alexanderson, H. and Murray, A.S. *Luminescence signals from modern sediments in a glaciated bay, NW Svalbard*. Quaternary Geochronology, 10: 250–256, 2012.

AuraLight. *Technical Data Sheet T5 ECO SAVER HE.*, 2014.

Bailey, R.M. *The interpretation of quartz optically stimulated luminescence equivalent dose versus time plots*. Radiation Measurements, 32(2): 129–140, 2000.

Berger, G.W. *Effectiveness of natural zeroing of the thermoluminescence in sediments*. Journal of Geophysical Research: Solid Earth, 95(B8): 12375–12397, 1990.

Cajochen, C., Frey, S., Anders, D., Späti, J., Bues, M., Pross, A., Mager, R., Wirz-Justice, A., and Stefani, O. *Evening exposure to a light-emitting diodes (LED)-backlit computer screen affects circadian physiology and cognitive performance*. Journal of Applied Physiology, 110(5): 1432–1438, 2011.

Fuchs, M. and Owen, L.A. *Luminescence dating of glacial and associated sediments: review, recommendations and future directions*. Boreas, 37(4): 636–659, 2008.

Fujitsu. *Data Sheet Fujitsu Display L20T-3 LED Display*, 2012.

Galbraith, R F., Roberts, R.G., Laslett, G.M., Yoshida, H., and Olley, J.M. *Optical dating of single and multiple grains of quartz from Jinmium rock shelter, northern Australia. Part I: experimental design and statistical models*. Archaeometry, 41(2): 339–364, 1999.

Gemmell, A.M.D. *IRSL from fine-grained glacifluvial sediment*. Quaternary Science Reviews, 18(2): 207–215, 1999.

Godfrey-Smith, D.I., Huntley, D.J., and Chen, W.-H. *Optical dating studies of quartz and feldspar sediment extracts*. Quaternary Science Reviews, 7: 373–380, 1988.

Jain, M., Murray, A.S., and Bøtter-Jensen, L. *Characterisation of blue-light stimulated luminescence components in different quartz samples: implications for dose measurement*. Radiation Measurements, 37(4-5): 441–449, 2003.

Jain, M., Murray, A.S., and Bøtter-Jensen, L. *Optically stimulated luminescence dating: How significant is incomplete light exposure in fluvial environments?* Quaternaire, 15: 143–157, 2004.

Jeong, G.Y. and Choi, J.-H. *Variations in quartz OSL components with lithology, weathering and transportation*. Quaternary Geochronology, 10: 320–326, 2012.

King, G.E., Robinson, R.A.J., and Finch, A.A. *Apparent OSL ages of modern deposits from Fåbergstølsdalen, Norway: implications for sampling glacial sediments*. Journal of Quaternary Science, 28(7): 673–682, 2013.

Lindvall, A. *Hur snabbt påverkas och nollställs luminiscenssignaler under naturliga ljusförhållanden?* BSc. thesis, 501, Department of Geology, Lund University, Lund, 2017. URL http://lup.lub.lu.se/luur/download?func=downloadFile&recordOId=8916161&fileOId=8916170.

Murray, A.S. and Wintle, A.G. *Luminescence dating of quartz using an improved single-aliquot regenerative-dose protocol*. Radiation Measurements, 32(1): 57–73, 2000.

Murray, A.S. and Wintle, A.G. *The single aliquot regenerative dose protocol: potential for improvements in reliability*. Radiation Measurements, 37(4-5): 377–381, 2003.

Sanderson, D.C.W., Bishop, P., Stark, M., Alexander, S., and Penny, D. *Luminescence dating of canal sediments from Angkor Borei, Mekong Delta, Southern Cambodia*. Quaternary Geochronology, 2(1): 322–329, 2007.

Singarayer, J.S., Bailey, R.M., Ward, S., and Stokes, S. *Assessing the completeness of optical resetting of quartz OSL in the natural environment*. Radiation Measurements, 40(1): 13–25, 2005.

SMHI. *STRÅNG data*, 2017.

Sohbati, R., Murray, A., Lindvold, L., Buylaert, J.-P., and Jain, M. *Optimization of laboratory illumination in optical dating*. Quaternary Geochronology, 39: 105–111, 2017.

Sommerville, A.A. *Luminescence dating of wind blown sands from archaeological sites in northern Scotland*. Phd thesis, College of Science and Engineering, University of Glasgow, 2003. URL http://theses.gla.ac.uk/id/eprint/2934.

Spooner, N.A. *On the optical dating signal from quartz*. Radiation Measurements, 23(2): 593–600, 1994.

Stjern, R. *Hur påverkas luminiscenssignaler från kvarts av ljusexponering under laboratorieförhållanden?* BSc. thesis, 519, Department of Geology, Lund University, Lund, 2017. URL http://lup.lub.lu.se/luur/download?func=downloadFile&recordOId=8916682&fileOId=8916718.

Stokes, S., Bray, H.E., and Blum, M.D. *Optical resetting in large drainage basins: tests of zeroing assumptions using single-aliquot procedures*. Quaternary Science Reviews, 20(5): 879–885, 2001.

Reviewer

David Sanderson

Ancient TL

Les sables de Fontainebleau: A Natural Quartz Reference Sample and its Characterisation

Sebastian Kreutzer,[1*] Johannes Friedrich,[2] David Sanderson,[3]
Grzegorz Adamiec[4], Alicja Chruścińska[5], Mauro Fasoli[6,7],
Marco Martini[6,7], George S. Polymeris[8], Christopher I. Burbidge[9] & Christoph Schmidt[2]

[1] IRAMAT-CRP2A, Université Bordeaux Montaigne, Pessac, France
[2] Chair of Geomorphology & BayCEER, University of Bayreuth, Bayreuth, Germany
[3] SUERC, Scottish Enterprise and Technology Park, East Kilbride, Scotland, UK
[4] Institute of Physics CSE, Silesian University of Technology, Gliwice, Poland
[5] Institute of Physics, Faculty of Physics, Astronomy and Informatics, Nicolaus Copernicus University, Torun, Poland
[6] Dipartimento di Scienza dei Materiali, Università degli Studi di Milano Bicocca, Milano, Italy
[7] INFN, Sezione di Milano Bicocca, Piazza della Scienza 1, I-20126 Milano, Italy
[8] Ankara University, Institute of Nuclear Sciences, Ankara, Turkey
[9] Office of Radiation Protection and Environmental Monitoring, Environmental Protection Agency, Dublin, Ireland

[*]Corresponding Author: sebastian.kreutzer@u-bordeaux-montaigne.fr

Received: November 2, 2017; in final form: December 6, 2017

Abstract

Fundamental studies on luminescence production in natural quartz require samples which can be studied by groups of laboratories using complementary methods. In the framework of a European collaboration studying quartz luminescence, a sample originating from the Fontainebleau Sandstone Formation in France was selected for characterisation and distribution to establish a starting point for interlaboratory work. Here we report on the preparation and characterisation work undertaken before distribution with the aim of ensuring that each laboratory received comparable material. Material was purified to enrich the quartz concentration, followed by mineralogical screening by SEM and ICP-MS analyses. Luminescence screening measurements were undertaken at a single laboratory (SUERC) to verify the suitability of the sample for use within the study, and to establish the level of homogeneity of subsamples prepared for distribution. The sample underwent minimal non-chemical pre-treatment by multiple cycles of magnetic separation and annealing. SEM analysis showed that the sample consists mainly of SiO_2. The luminescence characterisation confirmed a dose sensitivity of ca. 22,000–160,000 cts K^{-1} Gy^{-1} per 260–290 grains for the 110 °C UV TL peak, well developed low (here: 100–300 °C) temperature (pre-dose) TL signals and high OSL sensitivities. The grain to grain OSL response varies by more than one order of magnitude. No significant IRSL signal was observed. In summary, the results from luminescence characterisation confirm the suitability of the sample for the luminescence experiments envisaged and have established a basis for comparability in studies conducted by a network of laboratories.

Keywords: OSL, TL, Characterisation, Fundamental research

1. Introduction

Fundamental studies on quartz luminescence characteristics dedicated to dosimetric applications quickly reach a

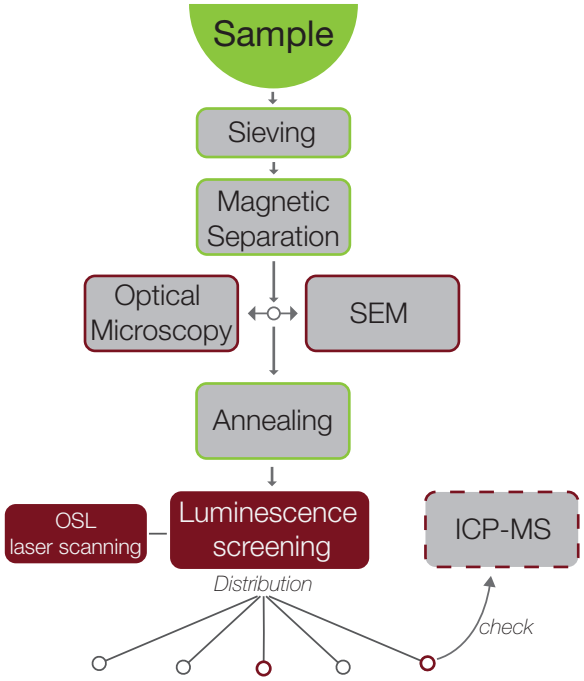

Figure 1. Flowchart of the sample treatment and applied screening procedures. The ICP-MS analysis was carried out on one subsample only.

point where (natural) reference samples are needed. Such samples ideally would (1) enable reproducible experiments to be conducted within individual laboratories to help set up procedures, (2) provide material which could be used as a control sample for work with a range of different samples, and (3) provide a traceable means of assimilating data from different laboratories, providing the homogeneity has been adequately established. The requirements for such materials were discussed in the framework of a European collaboration at meetings in Bayreuth, Torun and Glasgow, where it was concluded that natural quartz samples of high purity were needed to establish interlaboratory comparability. Materials with high dose sensitivity (110 °C single grain peak intensity > 100 cts K^{-1} Gy^{-1}), good signal reproducibility (e.g., TL peak shape), minimal preceding chemical treatment and availability in large quantities (> 500 g) were required, and the importance of characterisation in a single laboratory and careful partition and distribution were recognised. In the longer term, it may be necessary to develop a series of such materials from different natural settings, to reflect a broader range of quartz luminescence characteristics as well.

Some previous studies have used samples initially obtained from dating studies as model systems (e.g., Wintle & Murray, 1997; Bailey, 2000; Gong et al., 2014), others have used commercially available bulk material (e.g., Keleş et al., 2016), quartz extracted from the bedrock (e.g., Friedrich et al., 2017) or a mixture of such samples (e.g., Adamiec, 2005). However, the information on origin, pre-treatment and mineralogical characterisation and homogeneity differ in these examples, and basic luminescence characteristics appear to be only rarely reported, or if given, spread over several articles. Here we report the characterisation and preparation of a quartz derived from the Fontainebleau sands, undertaken at the Scottish Universities Environmental Research Centre (SUERC) prior to distribution to the working group. This material has subsequently been used in an interlaboratory study of the kinetic parameters of the 110 °C TL signal, and it is intended that it should also be used for future experiments on luminescence production of quartz within the group.

Chemical composition screening using a scanning electron microscope (SEM) was used to ensure the purity of the quartz sand and inductively coupled plasma mass spectrometry (ICP-MS) analyses were conducted to obtain information on trace elements. We furthermore present a brief and easily to apply luminescence pre-characterisation routine using thermally stimulated luminescence (TL) and optically stimulated luminescence (OSL) measurements. Additional OSL laser scanning investigates the grain to grain variation in luminescence response.

The characterisation and homogeneity testing reported here have been used in formal interlaboratory validation studies (e.g., Sanderson et al., 2003a,b,c,d), but do not seem to have been adopted to the same extent, so far, in geochronological applications of luminescence methods. However, we believe that such (pre-) characterisation is indispensable to avoid ambiguities later in the research project. It is furthermore a cornerstone to combine research results from different labs, without worrying about the sample to sample differences biasing the conclusions. We structured the manuscript as a workflow paper, with information on the equipment used given in the corresponding sections. The general preparation and characterisation workflow is shown in Fig. 1.

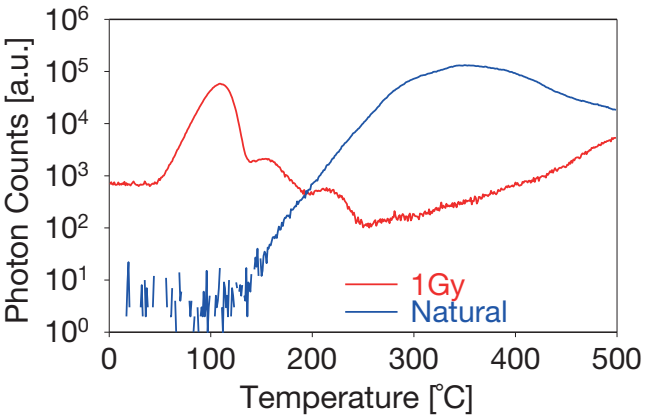

Figure 2. Thermoluminescence glow curves from the quartz fraction before annealing. Net curves after reheat subtraction recorded at 5 K s^{-1} using a SUERC manual TL reader from the natural signal and a 1 Gy regenerated signal.

2. Sample origin and description

The material selected originates from the Oligocene Fontainebleau Sandstone Formation (Formation des Sables de Fontainebleau) in France. These sediments were de-

posited during the time of the last marine intrusion into the Paris Basin (the Stampian Sea, or Sea of Estampes) ca. 35 Ma ago (e.g., Grisoni & Thiry, 1988). The sand itself is usually extracted in large quantities by surface mining from a coastal palaeo-dune system, which reaches a mean thickness of ca. 50 m (max. 100 m; Thiry & Marechal 2001). Thiry & Marechal (2001) distinguish three diagenetic facies: (1) plateau sands and sands at the edge of valleys, which are almost composed of pure quartz, (2) sands beneath the plateaus containing clays and traces of feldspars and (3) sands from below the water-table containing, amongst others, feldspar, carbonates and organic matter. For more detailed information see El Bied et al. 2002; Thiry & Marechal 2001; Robin & Barthélemy 2000; Grisoni & Thiry 1988. Due to its high purity (quartz concentration $> 99\,\%$; e.g., Saadi et al. 2017; Thiry et al. 1985; Bourbie & Zinszner 1985), Fontainebleau sand is preferred in industrial glass production. After mining, the sand for this purpose undergoes a pre-treatment, consisting mainly of chemical washing and density separation (cf. Bouniol, 2013).

Five kilograms of the 'Sable de Fontainebleau' were purchased in 2005 by SUERC from Merck Eurolab (nowadays: *VWR*). The material was characterised together with a series of other commercial quartz samples, to select materials which could be sensitised for use as OSL-D materials. This preliminary screening work confirmed that the material had high sensitivity TL and OSL with well-defined low temperature ($< 300\,°C$) and high-temperature TL ($> 300\,°C$) peaks. Both OSL and the low-temperature TL signals exhibit pre-dose sensitisation. A retained portion of 800 g of the sieved 150–250 μm fraction was available at SUERC, and this was selected for this study. The supplier label of the material did not include specific batch numbers or give details of the Merck processing of the product before purchase.

However, TL and OSL analysis of the raw input material, as well as the sieved fractions, shows the presence of geological residual signal. The presence of this residual geological signals in the material had been noted in the exploratory work conducted by Burbidge in 2005 (unpublished). Figure 2 shows the TL signals associated with this geological dose, and the shape of a 1 Gy regenerated response recorded with a manual TL reader at SUERC. It displays the high temperature residual signal (equivalent dose approximately 400–500 Gy based on the 340–360 °C signal integral) and the response to a 1 Gy dose read without preheat. The curves are net curves following reheat. The natural curve confirms that the sample had not been significantly heated prior to receipt, gives an indication of the shape of the high temperature TL signals, and suggests that deeper trap signals above 500 °C may also be present. The regenerated curve shows initial phosphorescence, the post irradiation delay being approximately 300 s and the low temperature peaks corresponding to nominal 110 °C , 150 °C and 210 °C signals. All of these peaks respond to pre-dose sensitisation, whereas the sensitisation of the higher temperature (e.g., 325 °C) peaks is minimal and hardly visible.

Additionally, high-resolution γ-ray spectrometry analysis

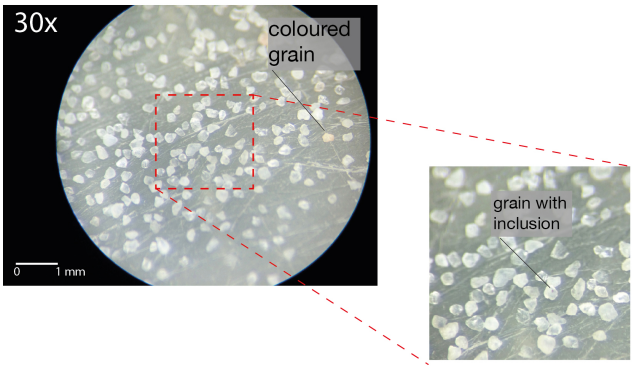

Figure 3. Pan view through an optical microscope with a magnification of 30 x. Note the grains with inclusions and coloured grains.

was conducted on the raw material, but not published so far. For this, 100 g were counted for 50 ks on a shielded (50 % relative efficiency) Ortec Gamma-X spectrometer at the SUERC. Weighted analysis of the main U and Th series γ-lines were used to obtain activity per mass and concentration data (Table 1). See Sec. 8 for a discussion of these results.

Table 1. High-resolution γ-ray spectrometry analysis results (bulk sample).

Source	Activity [Bq kg^{-1}]	Concentration [ppm]
K	5.979 ± 4.413	190 ± 140
U	0.757 ± 0.202	0.061 ± 0.016
Th	1.369 ± 0.227	0.337 ± 0.056

Net data were derived after background subtraction and quantified relative to the SUERC Shap granite standard presented in a matched geometry. Quoted uncertainties combine sample, background and standard measurements, plus the uncertainties of the reference data. Sample counting statistics dominates the stated errors.

3. Magnetic separation

Our sample preparation design for the Fontainebleau (FB) quartz aimed to avoid any chemical treatments. In particular, we did not treat the samples with HF, since we wanted to avoid modifications of the surface condition of quartz grains, or other malign effects on the grain shape (e.g., Porat et al., 2015). Visual inspection under low power optical microscopy revealed mainly milky and clear quartz grains, a few coloured grains and potentially some opaque heavy minerals. The latter contamination was hardly visible using optical microscopy (cf. Fig. 3). To remove heavy minerals without applying heavy liquids for density separation and to roughly quantify their abundance, a magnetic separator (Frantz, LB-1) was used to purify the sample further. Porat (2006) gives details on this method. The magnetic separation was performed using a current of 1.5 A for the magnetic field (ca. 2 T), a slope of 7 ° and a tilt of 5 ° for the chute. After

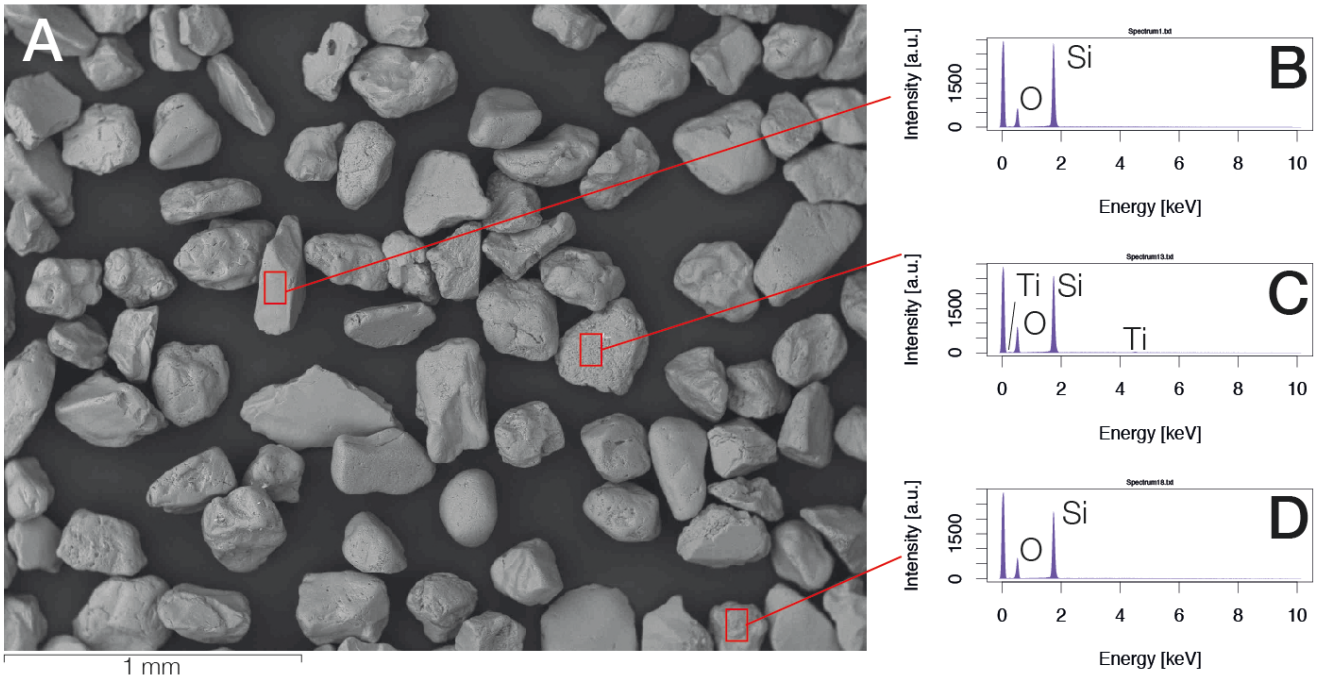

Figure 4. SEM pan view (A) and selected example spectra for three grains (B, C, D). No major impurities were observed.

four runs with half of the available material, visual inspection showed that black or dark grains were slightly enriched (supposedly heavy minerals) in the separated magnetic fraction. Both fractions ('magnetic' and 'non-magnetic') were subsequently analysed using backscattered electron microscopy to see whether heavy minerals were present. The magnetic separation procedure was later repeated at least ten times, following a first SEM inspection using the fraction enhanced in magnetic grains.

4. SEM inspection

We used scanning electron microscopy in backscatter mode (using the Hitachi S-3400N SEM in the SUERC luminescence lab, electron beam: 20 keV), coupled to X-ray spot analysis (Oxford instruments INCA system) to manually analyse the magnetic fraction (suspected to be enriched in heavy minerals) and the purified non-magnetic fraction. However, no differences were found between the two fractions, and therefore they were not further separated for following analyses. Figures 4 and 5 summarise the results of the SEM inspection. We found mainly pure quartz grains with rounded and sub-rounded shapes, although diverse forms and surface textures (sub-angular) were observed (cf. Powers, 1953, for a roundness scale). The observed grade of rounding is likely to reflect the diverse origin of the sample material. There was no substantial indication of effects from any prior chemical treatment by the supplier (cf. Figs. 4 and 5). The major elemental composition of the inspected grains was dominated by SiO_2. A small minority of grains showed Zr and Ti-bearing inclusions (Figs. 5A, 5C). We also found fragments of Ca and S (Fig. 5B), which are believed to remain from the sample pre-treatment by the supplier. Considering the constraints of the subsampling by SEM, qualitatively it can be said that the sieved sand is a high-purity quartz-dominated sample, as expected. The minor impurities and potentially diverse quartz textures are generally consistent with other work on the Fontainebleau Sandstone Formation (e.g., El Bied et al., 2002). No quantitative mineralogical analysis was performed.

5. Annealing and packing

After SEM inspection, the sample material was annealed, in air, in a muffle furnace to remove residual luminescence signal. The material was annealed in a zirconium crucible, with closed lid, placed on a metal plate on ceramic pillars in the centre of the preheated furnace. The temperatures of both the metal plate and the sample material were monitored using separate logged thermocouples. Figure 6 shows the temperature of the plate below the zirconium crucible and the temperature of the thermocouple embedded in the quartz sand sample. The furnace had been preheated to 470 °C before introducing the material. It took ca. 50 min before the sample temperature converged with the temperature recorded by the oven itself. In total, the sample was annealed for 82 min, while the temperature of the quartz itself was held at 490 °C for 30 min (indicated by the vertical lines in Fig. 6). Subsequently, the crucible was allowed to cool rapidly to room temperature outside the oven. This annealing cycle aimed to remove the geological TL and OSL signals without crossing the quartz α- to β-phase transition, and without fully depleting deep traps that might have de-sensitised the luminescence.

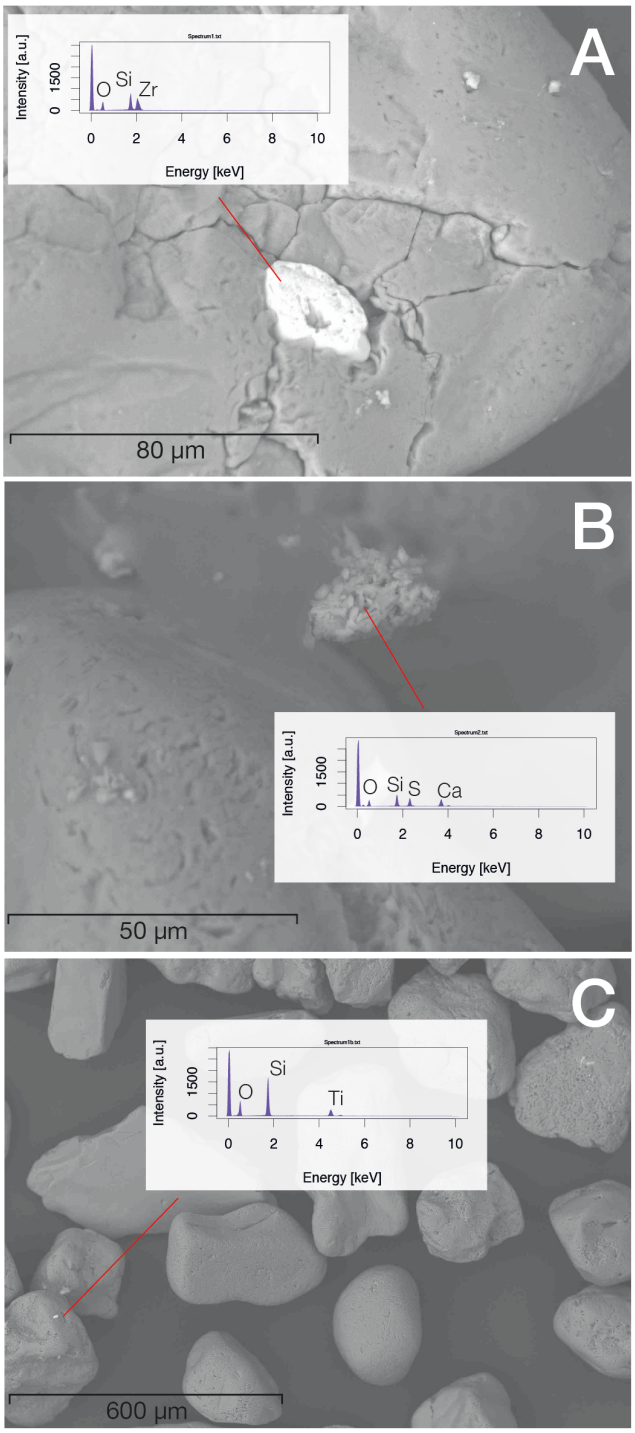

Figure 5. SEM close up. Three grains were exemplarily selected; detected major elements are indicated in the inset graphs. The following impurities were verified: Zr (A), Ca, S (B) and Ti (C). The majority (ca. 99 %) of the inspected grains consisted only of Si and O.

After annealing, the sample material was homogeneously divided into ten batches packed into two tubes (A and B) of ca. 4 g each (in total twenty subsamples). While tubes labelled 'A' were distributed amongst the collaboration partners, tubes labelled with 'B' were retained at SUERC in case of loss in transit and for a later cross-check. A further quantity of unpacked annealed material has also been retained. Each of the 40 subsamples was then subject to luminescence screening to determine the extent of homogeneity prior to distribution.

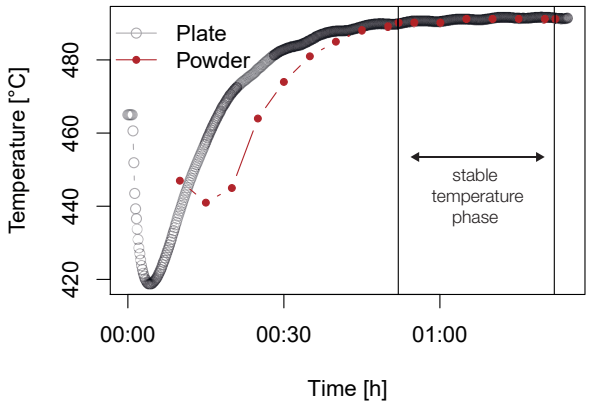

Figure 6. Temperatures recorded during annealing of the Fontainebleau quartz. Vertical lines indicate the time while the metal plate and the sample were held at similar temperatures for 30 min. The oven had been preheated to ca. 470 °C before loading. The sudden temperature decrease at the beginning was caused by the loading process.

6. Luminescence screening

6.1. Equipment

Before distribution, the luminescence properties of the annealed quartz samples were investigated. Two aliquots were prepared from each 'A' and 'B' subsample of the packed material, making a set of 40 aliquots in total. The grains were dispensed onto 9.6 mm diameter and 0.25 mm thick cleaned stainless steel discs using Electrolube Silicone Grease. It is estimated that the weighed aliquots comprised ca. 260–290 grains (estimated using the function `calc_AliquotSize()`; Burow 2017 from the **R** package 'Luminescence'). Measurements were done using a Risø DA-15 TL/OSL reader equipped with a ^{90}Sr/^{90}Y β-source delivering ca. 0.1 Gy s^{-1} to quartz coarse grains (100–250 μm). Luminescence was recorded through a 7.5 mm Hoya U340 filter, while stimulating the sample either with blue LEDs (470 $\pm$ 5 nm at ca. 24 mW cm^{-2}) or an infrared laser (830 nm at ca. 90 mW cm^{-2}). The data analysis presented here was carried out using the **R** (R Core Team, 2017) package 'Luminescence' (Kreutzer et al., 2012, 2017). The **R** script used for analysing the luminescence measurements is provided as supplementary data.

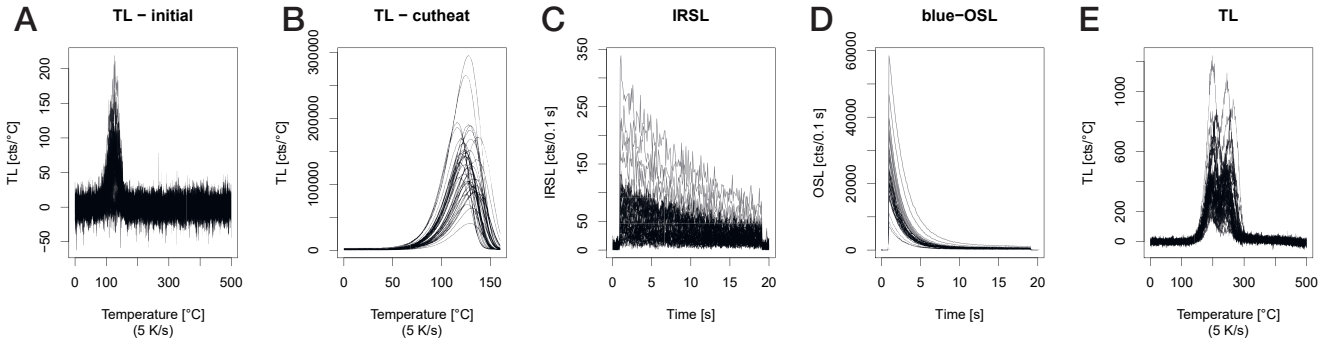

Figure 7. Luminescence screening results of the Fontainebleau quartz. Shown is a comprehensive plot comprising the signals of all measured aliquots (40 in total). The horizontal order of the plots follow the screening sequence (Sec. 6.1). The initial TL peak in (A) is believed to be induced by irradiation cross-talk within the luminescence reader. For further details see main text.

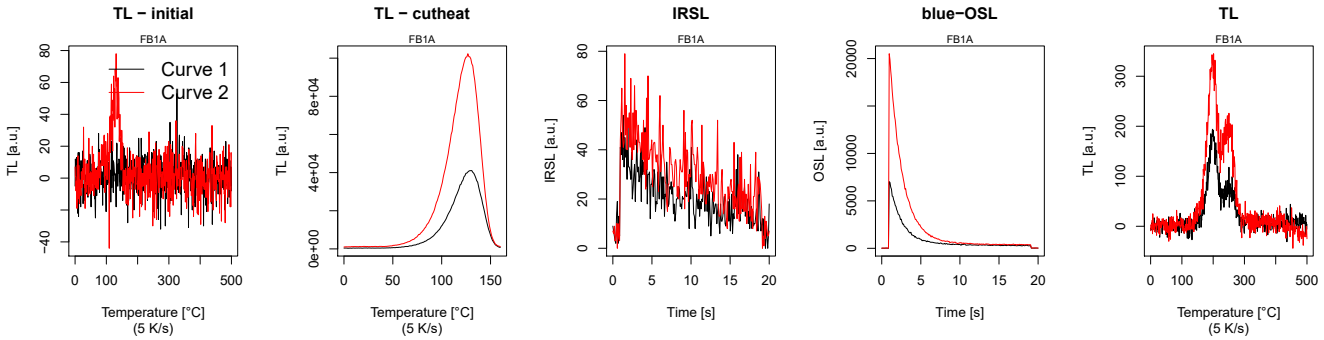

Figure 8. Luminescence screening results for one sub-sample (the first two aliquots measured). These results further emphasise that the small TL peak in Fig. 7A is likely resulting from cross-irradiation within the reader, since the first curve ever measured is unaffected. Intensity differences are believed to be usual inter-aliquot scatter.

6.2. Sequence

Two aliquots were prepared from each batch ('A' and 'B', 40 aliquots in total). Our rapid luminescence screening sequence comprised the following steps:

A. TL to 500 °C with 5 K s^{-1} (reader background subtraction)

   β-irradiation for 20 s ($\sim$ 2 Gy)

B. TL to 160 °C with 5 K s^{-1} (reader background subtraction)

C. IRSL at 50 °C for 20 s (60 % LED power)

D. OSL at 125 °C for 20 s (60 % LED power)

E. TL to 500 °C with 5 K s^{-1} (reader background subtraction)

6.3. Results

The summary of all measured curves is shown in Figs. 7A–E. The horizontal order follows the screening sequence (steps A to E). Each plot shows the results of all measured 40 aliquots. After annealing, first a TL residual measurement up to 500 °C was conducted. Fig. 7A reveals a small initial low-temperature TL signal at ca. 150 cts K^{-1} for 32 out of 40 measured aliquots. In contrast, the aliquot on position 1 (first measured aliquot) did not show this signal (Fig. 8, TL-initial, black curve). Thus, we conclude that irradiation cross-talk induced these small TL signals within the luminescence reader (e.g., Bray et al., 2002). The relative irradiation cross-talk of this signal is 0.045 $\pm$ 0.025 % and corresponds to the findings by Bray et al. (2002) (0.0055 $\pm$ 0.012 %).

In Fig. 7B the response of the so-called 110 °C UV TL peak following irradiation with a dose of ca. 2 Gy is shown. Exact peak positions vary from aliquot to aliquot, reflecting variations in thermal contact from disc to disc in the reader. The mean nominal temperature for this peak was 127 °C (range: 116 °C to 137 °C). The results show a 110 °C UV TL peak sensitivity of the material from ca. 22,000–160,000 cts Gy^{-1} for the ca. 260–290 grains (roughly 30,400 cts Gy^{-1} mg^{-1}) placed on each disc, if measured with a heating rate of 5 K s^{-1}. Further TL peaks (step E) were found at 200 °C (range: 187 °C to 219 °C) and 250 °C (mean: 248 °C, range: 230 °C to 276 °C). No further UV TL signal, e.g., at ca. 325 °C was found, presumably due to its lower sensitivity in comparison to the peaks at lower temperature.

All aliquots showed a weak IRSL signal in the UV-band (Fig. 7C). The weak correlation between the integrated OSL and IRSL signal of $r = 0.21$ (cf. Fig. S3, supplement) suggests that the IRSL signal is caused by mineral phases other than quartz. However, the IRSL signal is in 39 out of 40 cases $< 1\,\%$ (mean: 0.4 %; extreme value: 1.5 %) of the corresponding blue-OSL signal (Fig. 7D) and with this considered being negligible. The signal integration range was similar for IRSL and OSL.

6.4. Further analysis

The presented measurement data were used to further characterise the Fontainebleau quartz by post-processing. Of particular interest are: (A) TL peak position distribution, (B) TL peak intensity distribution, (C) TL peak intensity vs. IRSL intensity and (D) TL peak intensity vs. OSL intensity. The TL peak position was determined semi-automatically, selecting the intensity maximum of each peak in a given temperature range (1–220 °C and 230–500 °C). The peak intensity was derived from the sum of the intensity of the ±5 channels (1 channel := 1 K) around the maximum. The intensity values for the IRSL and blue-OSL signal were obtained from the full shine-down curves (no background subtraction) and plotted against the TL peak intensities on a logarithmic scale. The above described analysis was performed for all identified UV TL peaks (110 °C, 200 °C and 250 °C). The full analysis is given in the supplement.

Figure 9 shows the results for 110 °C TL peak. The peak intensities are slightly positively skewed, but without any extreme value. IRSL signal and 110 °C TL peak intensities are not correlated ($r = 0.132$), while a positive correlation ($r = 0.945$) was observed for blue-OSL and 110 °C TL peak intensity, as expected from previous investigations (e.g., Aitken & Smith, 1988; Murray & Roberts, 1998; Kiyak et al., 2008). In contrast, for UV TL peaks at higher temperatures (200 °C and 250 °C), IRSL and blue-OSL are positively correlated with the corresponding TL peak intensities (Figs. 10 and 11). Mineral phases other than quartz may cause this signal correlation, although the TL peaks show no obvious contamination by, e.g., K or Na-feldspar.

7. OSL laser scanning

To give a preliminary view of the extent of homogeneity at grain to grain level, a pattern of grains was dispensed on a stainless steel disc, β-irradiated with approximately 20 Gy dose, preheated for 30 min at 50 °C and than subjected to OSL laser scanning using the system described by Sanderson et al. (2004). An area of 1 cm^2 was scanned with 1 s OSL data recorded on a 100 μm matrix. Figure 12A shows the resulting colour coded image in pixellated form, Fig. 12B shows a backscattered electron image of the sample disc, indicating the positions of individual grains within the pattern, and Fig. 12C shows the log frequency distribution of the 4,250 pixels containing the pattern FBQ (Fontainebleau Quartz). Empty pixels form the histogram background peak at ca. 50–100 photon counts, with the distribution from approximately 100 counts to 5,000 counts containing data from grains. Figure 12D shows a 3D view of the same data. The data imply that there is a variation of luminescence response from grain to grain of slightly more than one order of magnitude. Additional studies using single grain readers would be needed to characterise this further.

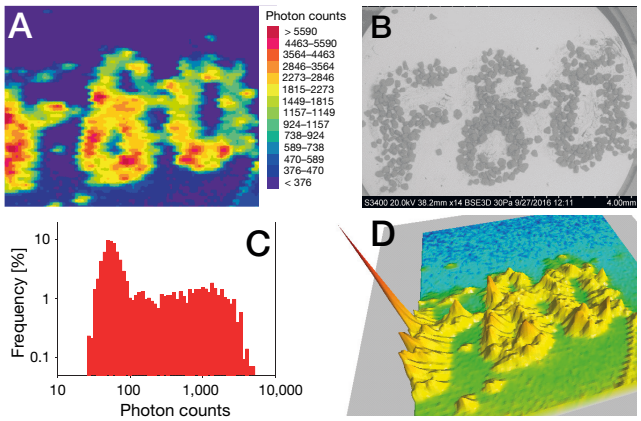

Figure 12. (A) OSL scan of a pattern of Fontainebleau quartz irradiated with a 20 Gy β-dose, (B) a backscatter SEM image of the object, (C) Histogram of the 4,280 pixels containing the grain image FBQ, (D) 3D view of the scanned image.

8. ICP-MS analysis

Along with the luminescence screening, for one subsample (FB2A) ICP-MS analyses were carried out at the IRAMAT-CRP2A in Bordeaux. The analyses aimed at identifying and quantifying trace elements in the sample. The 1.38 g of sample material were conditioned for the ICP-MS measurement applying HCl (12 mol/l) and HNO_3 (16 mol/l). The solution was further prepared using 3 cycles of treatment with HF (40 %, 3 ml) and $HClO_4$ (72 %, 1 ml).

Table 2. ICP-MS results sample FB2A

Element	Concentration [ppm]
K	35.0 ± 1.2
Th	0.333 ± 0.015
U	0.149 ± 0.007

The results of the ICP-MS analysis are listed in Table 2. In contrast to the previously carried out high-resolution γ-ray spectrometry (100 g), the amount of investigated material is small and variations due to the subsampling are likely. Th concentrations are in agreement with the findings from the γ-ray spectrometry (0.337 ± 0.056 ppm), but still circa twice as high as the average value reported by Vandenberghe et al. (2008) for purified quartz. The U concentration obtained by ICP-MS for the sample (not to be mixed up with internal trace element concentration of 'pure' quartz grains) is an order of magnitude higher than reported by Vandenberghe et al.

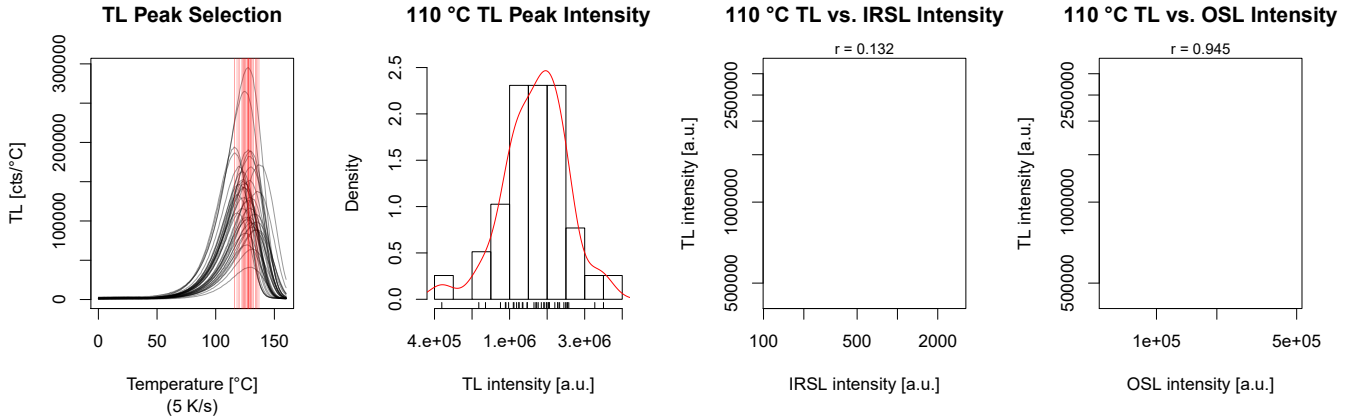

Figure 9. 110 °C TL peak intensity plots. Shown are (left to right): (1) all measured 110 °C TL peaks (cf. Fig. 7B) with identified peak positions marked with red vertical lines, (2) histogram of the logarithmised intensity of the 110 °C peak (peak ± 5 channels), (3) scatter plot of the logarithmised TL peak intensity vs the logarithmised IRSL intensity, (4) scatter plot of the logarithmised 110 °C TL peak intensity vs the logarithmised OSL intensity. The 110 °C TL peak intensity correlates positively with the OSL intensity ($r = 0.95$), while no correlation was found between 110 °C TL peak intensity and the IRSL intensity ($r = 0.13$).

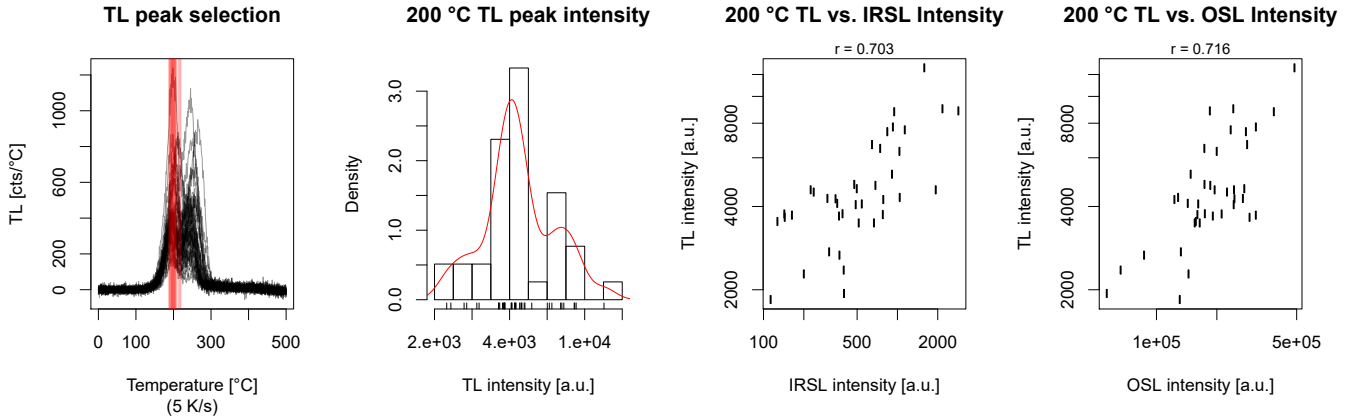

Figure 10. 200 °C TL peak intensity plots. The figure has a similar structure as Fig. 9 and the TL curves (first plot) refer to the results presented in Fig. 7E. It appears that the logarithmised TL peak intensities positively correlate with the logarithmised IRSL and OSL intensities (r values given as subtitles). However, the partly automatic peak selection algorithm might have biased the results since the peak search range was preset and thus the peaks manually predefined.

(2008). However, similar or even higher U concentrations for chemically untreated and treated samples were found by Mejdahl (1987), De Corte et al. (2006) and Steup (2015). Furthermore, the γ-ray spectrometry results (Table 1) indicate that the U concentration for larger sample sizes is an order of magnitude lower (0.061 ± 0.016 ppm). Thus, it appears likely that the few zircon inclusions contribute to the U concentration found by the ICP-MS analysis, which could perhaps be verified by sequential digestion or spatially resolved analysis if needed in the future. The K concentration is consistent with the observations from SEM analysis. The γ-ray spectrometry results (Table 1) list a larger K concentration (190 ± 140 ppm), which appears to be more robust and consistent with XRF data on Fontainebleau Sandstone by Saadi et al. (2017) (K_2O: 140 ± 4 ppm). Nevertheless, our findings confirm the high purity of the quartz sample and suggest that the sample does not contain significant quantities of K-feldspar.

9. Conclusions

A workflow to check purity and appropriate luminescence behaviour of a natural reference quartz sample from the Fontainebleau Sandstone Formation was presented. The preparation and analyses comprised sieving, magnetic separation, optical microscopy, SEM, ICP-MS, γ-ray spectrometry and luminescence screening.

The Fontainebleau quartz is composed of Si and O, since it consists mainly of quartz. No significant contamination by other minerals was found in SEM analysis apart from some microinclusions of zircon and rutile and in a few grains some surficial calcium-bearing phases. The bulk K concentrations of only 35 ± 1.2 ppm (ICP-MS) and 190 ± 140 ppm (γ-ray spectrometry on 100 g) indicates no apparent contamination with K-feldspar. However, observed IRSL signals suggest negligible (IRSL/OSL ratio < 1 % in 39 out of 40 cases) UV signal contribution by mineral phases other than quartz (e.g.,

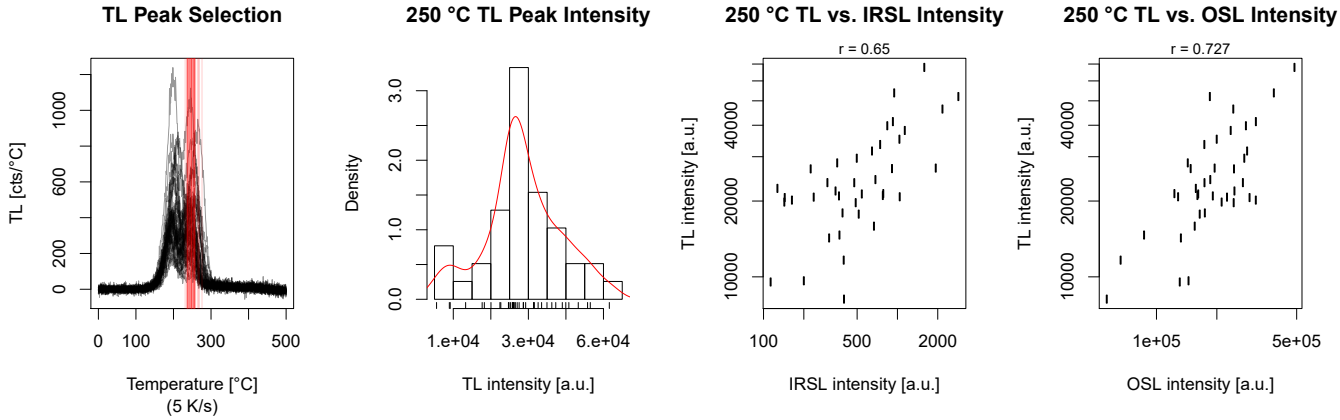

Figure 11. 250 °C TL peak intensity plots. The figure has a similar structure as Fig. 9 and the TL curves (first plot) refer to the results presented in Fig. 7E. As in the previous figure the TL peak intensity appears to correlate with the IRSL and OSL peak intensities. However, also in this case the observed correlation could be an artefact of the partly pseudo-automatic peak selection.

zircon). Luminescence screening confirmed the high luminescence sensitivity for the 110 °C TL peak for low doses (here: 2 Gy) expected from the preselection work, as well as the presence of the other two low-temperature pre-dose sensitivity peaks. Two further UV TL peaks at 200 °C and 250 °C were identified. Glow curve shapes are generally well reproduced, with peak position variations observed in rapid screening measurements on the Risø reader attributed to thermal contact variations. OSL sensitivities are in the order of 10^5 (cts s^{-1}) Gy^{-1} after a TL preheat to 160 °C and IRSL stimulation for 20 s.

The intensity variations from aliquot to aliquot have been defined here and provide a baseline for future assessments of interlaboratory variations. Sensitivity variations at single grain level have yet to be determined in detail but are implicit in the results of preliminary luminescence scanning work, which suggests grain to grain variations covering at least one order of magnitude. Grain textural (rounded, sub-rounded, sub-angular) differences have been noted in the SEM data, but they appear to be consistent with other work published on the Fontainebleau Sandstone Formation. Overall we conclude that the reference sample is well suited for further analyses within the collaborative group, and we have started looking at the 110 °C TL peak characteristics, as well as at individual examinations of other properties.

Acknowledgements

We are thankful to André Sawakuchi for his constructive and thoughtful review. We acknowledge the support of the Bavarian Research Alliance (BayFor) for financing the project meeting in Bayreuth (BayIntAn_UBT_2016_74). JF is gratefully supported by the DFG (2015–2018, "Modelling quartz luminescence signal dynamics relevant for dating and dosimetry", SCHM 3051/4-1). The work of SK is financed by a programme supported by the ANR - n° ANR-10-LABX-52. SUERC provided the material and supported the characterisation and purification work.

References

Adamiec, G. *Investigation of a numerical model of the pre-dose mechanism in quartz*. Radiation Measurements, 39 (2): 175–189, 2005.

Aitken, M. J. and Smith, B. W. *Optical dating: recuperation after bleaching*. 7: 387–393, 1988.

Bailey, R. M. *The slow component of quartz optically stimulated luminescence*. Radiation Measurements, 32(3): 233–246, 2000.

Bouniol, M. *Les sables de Fontainebleau*. mines et carrières, 199: 16–20, 2013.

Bourbie, T. and Zinszner. *Hydraulic and acoustic properties as a function of porosity in Fontainebleau Sandstone*. Journal of Geophysical Research, 90(B13): 11524–11532, 1985.

Bray, H. E., Bailey, R. M., and Stokes, S. *Quantification of cross-irradiation and cross-illumination using a Risø TL/OSL DA-15 reader*. Radiation Measurements, 35(3): 275–280, 2002.

Burow, C. *calc_AliquotSize(): Estimate the amount of grains on an aliquot. In: Kreutzer, S., Dietze, M, Burow, C, Fuchs, M C, Schmidt, C, Fischer, M, Friedrich, J (2017). Luminescence: Comprehensive Luminescence Dating Data Analysis. R package version 0.7.5.* CRAN, version 0.3.1, 2017. URL https://CRAN.R-project.org/package=Luminescence.

De Corte, F., Vandenberghe, D., Buylaert, J. P., Van den haute, P., and Kučera, J. *Relative and k0-standardized INAA to assess the internal (Th, U) radiation dose rate in the "quartz coarse-grain protocol" for OSL dating of sediments: Unexpected observations*. Nuclear Instruments and Methods in Physics Research Section A: Accelerators, Spectrometers, Detectors and Associated Equipment, 564 (2): 743–751, 2006.

El Bied, A., Sulem, J., and Martineau, F. *Microstructure of shear zones in Fontainebleau sandstone*. International Journal of Rock Mechanics and Mining Sciences, 39(7): 917–932, 2002.

Friedrich, J., Pagonis, V., Chen, R., Kreutzer, S., and Schmidt, C. *Quartz radiofluorescence: a modelling approach*. Journal of Luminescence, 186: 318–325, 2017.

Gong, Z., Sun, J., Lü, T., and Tian, Z. *Investigating the optically stimulated luminescence dose saturation behavior for quartz grains from dune sands in China*. Quaternary Geochronology, 22: 137–143, 2014.

Grisoni, J.-C. and Thiry, M. *Réparation des grès dans les sables de Fontainebleau: Implications géotechniques des études récentes*. Bulletin des laboratoires des ponts et chaussées, 157, 1988.

Keleş, Ş. K., Meriç, N., and Polymeris, G. S. *Dose response on the 110°C thermoluminescence peak of un-heated, synthetic Merck quartz*. Physica B: Physics of Condensed Matter, pp. 1–30, 2016.

Kiyak, N. G., Polymeris, G. S., and Kitis, G. *LM-OSL thermal activation curves of quartz: Relevance to the thermal activation of the 110∘C TL glow-peak*. Radiation Measurements, 43(2-6): 263–268, 2008.

Kreutzer, S., Schmidt, C., Fuchs, M. C., Dietze, M., Fischer, M., and Fuchs, M. *Introducing an R package for luminescence dating analysis* . Ancient TL, 30(1): 1–8, 2012.

Kreutzer, S., Burow, C., Dietze, M., Fuchs, M. C., Schmidt, C., Fischer, M., and Friedrich, J. *Luminescence: Comprehensive Luminescence Dating Data Analysis*. CRAN, version 0.7.5, 2017. URL https://CRAN.R-project.org/package=Luminescence. Developer version on GitHub: https://github.com/R-Lum/Luminescence.

Mejdahl, V. *Internal radioactivity in quartz and feldspar grains*. Ancient TL, 5(2): 10–17, 1987.

Murray, A. S. and Roberts, R. G. *Measurement of the equivalent dose in quartz using a regenerative-dose single-aliquot protocol*. Radiation Measurements, 29(5): 503–515, 1998.

Porat, N. *Use of magnetic separation for purifying quartz for luminescence dating*. Ancient TL, 24(2): 33–36, 2006.

Porat, N., Faerstein, G., Medialdea, A., and Murray, A. S. *Re-examination of common extraction and purification methods of quartz and feldspar for luminescence dating*. Ancient TL, 33(1): 22–30, 2015.

Powers, M. C. *A New Roundness Scale for Sedimentary Particles*. Journal of Sedimentary Petrology, 23(2): 117–119, 1953.

R Core Team. *R: A Language and Environment for Statistical Computing*. Vienna, Austria, 2017. URL http://www.r-project.org.

Robin, A.-M. and Barthélemy, L. *Essai de chronologie – depuis 2300 ans – de dépôts sableux, pédogénisés, en foret de Fontainebleau (France)*. Comptes Rendus de l'Académie des Sciences - Series IIA - Earth and Planetary Science, 331(5): 359–366, 2000.

Saadi, F. A., Wolf, K.-H., and Kruijsdijk, C. v. *Characterization of Fontainebleau Sandstone: Quartz Overgrowth and its Impact on Pore-Throat Framework*. Journal of Petroleum & Environmental Biotechnology, 08(03): 1–12, 2017.

Sanderson, D. C. W., Carmichael, L. A., and Fisk, S. *Thermoluminescence Detection of Irradiated Fruits and Vegetables: International Interlaboratory Trial*. Journal of AOAC International, 86(5): 971–975, 2003a.

Sanderson, D. C. W., Carmichael, L. A., and Fisk, S. *Thermoluminescence Detection of Irradiated Shellfish: International Interlaboratory Trial*. Journal of AOAC International, 86(5): 976–982, 2003b.

Sanderson, D. C. W., Carmichael, L. A., and Fisk, S. *Photostimulated Luminescence Detection of Irradiated Shellfish: International Interlaboratory Trial*. Journal of AOAC International, 86(5): 983–989, 2003c.

Sanderson, D. C. W., Carmichael, L. A., and Fisk, S. *Photostimulated Luminescence Detection of Irradiated Herbs, Spices, and Seasonings: International Interlaboratory Trial*. Journal of AOAC International, 86(5): 990–997, 2003d.

Sanderson, D. C. W., Carmichael, L. A., Murphy, S. D., Whitley, V. H., Scott, E. M., and Cresswell, A. J. *Statistical And Imaging Methods For Luminescence Detection Of Irradiated Ingredients*. Food Standards Agency Research Report, Reference CSA 5240: 40p, 2004.

Steup, R. *Charakterisierung von natürlichen Quarz-Präparaten unterschiedlicher Genese und Herkunft unter Anwendung von Techniken zur Elementanalyse*, 2015. unpublished Bachelor's thesis (in German), University of Gießen.

Thiry, M. and Marechal, B. *Development of Tightly Cemented Sandstone Lenses in Uncemented Sand: Example of the Fontainebleau Sand (Oligocene) in the Paris Basin*. Journal of Sedimentary Research, 71(3): 473–483, 2001.

Thiry, M., Ayrault, M. B., and Grisoni, J.-C. *Groundwater silicification and leaching in sands: Example of the Fontainebleau Sand (Oligocene) in the Paris Basin*. Geological of America Bulletin, 100: 1283–1290, 1985.

Vandenberghe, D., De Corte, F., Buylaert, J. P., Kučera, J., and Van den haute, P. *On the internal radioactivity in quartz*. Radiation Measurements, 43(2-6): 771–775, 2008.

Wintle, A. G. and Murray, A. S. *The relationship between quartz thermoluminescence, photo-transferred thermoluminescence, and optically stimulated luminescence*. Radiation Measurements, 27(4): 611–624, 1997.

Reviewer

André Oliveira Sawakuchi

Ancient TL

Single-aliquot Regenerative-Dose (SAR) and Standardised Growth Curve (SGC) Equivalent Dose Determination in a Batch Model Using the R Package 'numOSL'

Jun Peng[1] and Bo Li[2*]

[1]School of Resource Environment and Safety Engineering,
Hunan University of Science and Technology, Xiangtan 411201, China

[2]Centre for Archaeological Science, School of Earth and Environmental Sciences,
University of Wollongong, Wollongong, NSW 2522, Australia

*Corresponding Author: bli@uow.edu.au

Received: November 1, 2017; in final form: December 12, 2017

Abstract

The single-aliquot regenerative-dose (SAR) protocol is widely used for determining equivalent dose (D_e) in optically stimulated luminescence (OSL) dating of Quaternary sediments. The standardised growth curve (SGC) method has been used as an efficient procedure to save measurement time for OSL measurements. The analysis of OSL signals and SAR data to determine D_e estimates and to establish SGC, however, usually involves a large amount of tedious work and is very time consuming, especially when a large number of aliquots or grains are measured and analysed. Here we present transparent and easy-to-use R functions to analyse OSL data sets obtained using SAR procedures in a batch model under the framework of the R package 'numOSL'. These functions allow users to: (1) import and select data records from single or multiple BIN (or BINX) file; (2) analyse OSL signals and determine their standard errors, based on either a Poisson distribution or a non-Poisson (over-dispersed) distribution in counting statistics; (3) establish dose response curves (DRC) with a range of fitting functions, including a general order kinetic (GOK) function; (4) calculate SAR D_e and associated error using either a Monte Carlo simulation or a simple transformation method; (5) select reliable SAR D_e estimates based on a variety of rejection criteria; (6) select well-behaved DRCs to establish SGC using a least-square normalisation (LS-normalisation) procedure and calculate SGC D_e; (7) graphically summarise and report the results. Worked examples are provided to demonstrate the above functions using experimentally obtained data sets. The relevant R code templates are provided.

Keywords: OSL dating; SAR; SGC; Batch model; R package numOSL

1. Introduction

The single-aliquot regenerative-dose (SAR) protocol (Galbraith et al., 1999; Murray & Wintle, 2000) has been successfully applied to determining equivalent dose (D_e) of sediments from a wide variety of Quaternary environments (Murray & Olley, 2002; Roberts et al., 2015). A standard SAR procedure involves the measurement of natural signals and a series of regenerative-dose signals, together with their corresponding test-dose signals, to establish dose response curves (DRC) using the sensitivity-corrected signals. SAR data analysis usually involves a number of processes, including calculating signal intensities and their associated errors, fitting DRC, determining D_e estimates and their associated errors based on natural signals and DRCs, with application of a number of rejection criteria to select reliable D_e (e.g., Wintle & Murray, 2006; Jacobs et al., 2003, 2006).

SAR D_e analysis is routinely performed using the popular and user-friendly software package *Analyst* (Duller, 2015). In *Analyst*, D_e analysis can be performed interactively by the user with real-time and visual adjustment of parameters and manually choosing analysing methods. For single-grain analysis, *Analyst* provides a simple way for automatically analysing SAR data through the function menu "Analyse All Grains". The interactive process, on the other hands, may be tedious and time-consuming if the user wants to compare

D_e values selected using different rejection criteria settings. Moreover, it is difficult to integrate and graphically report the results of large numbers of aliquots (grains), and only a brief statistical report of data manipulation is provided. There is also an **R** package called 'Luminescence' (Kreutzer et al., 2012) that provides many functions for SAR D_e calculation. However, only a limited number of rejection criteria are provided to select D_e estimates in this package.

The standardised growth curve (SGC) procedure (Roberts & Duller, 2004) has been proposed to save instrument time for D_e determination, because this method requires solely the measurements of the sensitivity-corrected natural signal (L_n/T_n). This method has been successfully applied to date sedimentary samples from different regions (Burbidge et al., 2006; Lai, 2006; Stevens et al., 2007; Telfer et al., 2008; Long et al., 2010; Yang et al., 2011; Shen & Mauz, 2011). The original SGC method was recently improved by Li et al. (2015a,b), by incorporating an additional regenerative dose for normalising the natural signals from different aliquots (grains), the so-called "re-normalisation" procedure. Based on this new method, it is possible to establish common SGCs not only for samples from the same site but also for samples from different regions. The re-normalisation procedure was subsequently further improved using a more generalised procedure that involves multiple iterative scaling and fitting processes, the so-called "least-squares normalisation" (LS-normalisation) procedure (Li et al., 2016). An increasing number of studies have successfully applied the improved SGC methods (e.g., Guo et al., 2016; Hu et al., 2016; Jacobs et al., 2017; Fu et al., 2017). The process for selecting reliable growth curves and applying the LS-normalisation procedures to establish SGCs and calculate SGC D_e, however, is non-trivial and involves a large amount of data handling.

In this study, we present easy-to-use standardised programmes for analysing, summarising, and reporting single-grain or single-aliquot SAR data in a batch model, and selecting well-behaved DRCs and applying the LS-normalisation procedure to establish SGCs and calculate D_e values. In contrast to manual operation, in batch processing, jobs are queued and processed internally one after the other without manual intervention. It thus provides an easier and more convenient way to analyse and report large SAR data sets. Our functions have already been released under the framework of the **R** package 'numOSL' (version 2.3) (https://cran.r-project.org/package=numOSL) (Peng et al., 2013). These functions are self-contained and do not depend on any external **R** packages. Codes were programmed using the Fortran 90 programming language and were wrapped by **R** using an interface to improve efficiency and running speed. We presented here detailed implementation of SAR and SGC D_e analysis using simple **R** code templates. The report for these templates was automatically generated using the **R** package 'knitr' (Xie, 2015) and an example is provided in the supplementary materials.

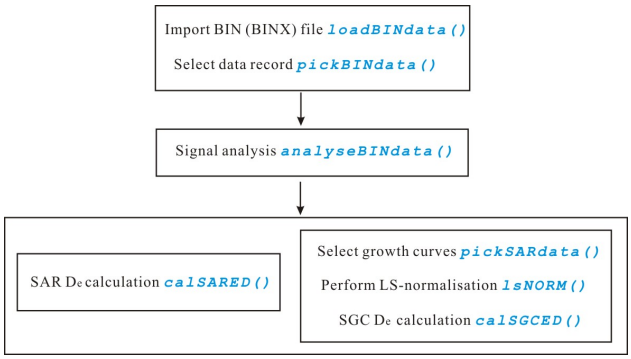

Figure 1. Workflows of SAR and SGC D_e analysis using functions in **R** package 'numOSL'.

2. D_e analysis using the 'numOSL' package

SAR and SGC D_e analysis can be separated into three major steps: (1) data import and selection; (2) signal analysis; and (3) D_e calculation and summarising. These steps and relevant functions are described graphically using the workflow shown in Fig. 1, and are elaborated as follows.

2.1. Data import and selection

The function `loadBINdata()` loads standard luminescence data stored in files with extension ".BIN" or ".BINX" into **R**. It can load a single file or multiple files simultaneously. The output of this function is an object of S3 class "loadBIN" containing loaded data records (`$records`) and a summary table (`$tab`). The summary table showing the attributions of each record can be visualized by setting argument `view=TRUE`.

Once the data are loaded, the function `pickBINdata()` can be used to select data records stored in the object "loadBIN" according to various attributions of each signal record, such as position number (`Position`), grain number (`Grain`), run number (`Run`), set number (`Set`), data type (`DType`), irradiation time (`IRRTime`), etc. The selected records are summarised in a table as shown in Fig. 2. The selected records can also be further filtered by setting argument `manual.select=TRUE` and modifying logical values (`TRUE` or `FALSE`) in the second column (with column name `Selected`) of Fig. 2. This function re-orders the selected records according to their `Position` and `Grain`. To improve visibility and clarity, data records with different combination of `Position` and `Grain` are separated by two rows of blanks in the summary table (see Fig. 2). The output of function `pickBINdata()` is an object of S3 class "pickBIN".

2.2. Signal analysis

Data records stored in object "pickBIN" can be analysed using the function `analyseBINdata()`. A number of arguments are available to suit different types of data analysis.

2.2.1 Net OSL calculation

The first step of signal analysis is to select appropriate time integrals (or channels) to calculate the net OSL

Selected Records

File

	row.names	Selected	Position	Grain	Run	Set	DType	IRRTime	NPoints	LType	Low	High	Rate	Temperature	Delay	On	Off	LightSource	AnTemp	TimeSinceIrr	Time
1	6	TRUE	1	1	1	3	Natural	0	100	TRPOSL	0	2	5	0	5	90	5	GreenLaser	125	-1	82156
2	511	TRUE	1	1	1	6	Dose	100	100	TRPOSL	0	2	5	0	5	90	5	GreenLaser	125	-1	93021
3	1016	TRUE	1	1	2	3	Bleach+dose	600	100	TRPOSL	0	2	5	0	5	90	5	GreenLaser	125	-1	112308
4	1521	TRUE	1	1	2	6	Dose	100	100	TRPOSL	0	2	5	0	5	90	5	GreenLaser	125	-1	123142
5	2026	TRUE	1	1	3	3	Bleach+dose	1200	100	TRPOSL	0	2	5	0	5	90	5	GreenLaser	125	-1	31442
6	2531	TRUE	1	1	3	6	Dose	100	100	TRPOSL	0	2	5	0	5	90	5	GreenLaser	125	-1	114439
7	3036	TRUE	1	1	4	3	Bleach+dose	1800	100	TRPOSL	0	2	5	0	5	90	5	GreenLaser	125	-1	32543
8	3541	TRUE	1	1	4	6	Dose	100	100	TRPOSL	0	2	5	0	5	90	5	GreenLaser	125	-1	43640
9	4046	TRUE	1	1	5	3	Bleach+dose	2400	100	TRPOSL	0	2	5	0	5	90	5	GreenLaser	125	-1	90250
10	4551	TRUE	1	1	5	6	Dose	100	100	TRPOSL	0	2	5	0	5	90	5	GreenLaser	125	-1	101133
11	5056	TRUE	1	1	6	3	Bleach+dose	3200	100	TRPOSL	0	2	5	0	5	90	5	GreenLaser	125	-1	34153
12	5561	TRUE	1	1	6	6	Dose	100	100	TRPOSL	0	2	5	0	5	90	5	GreenLaser	125	-1	45022
13	6066	TRUE	1	1	7	3	Bleach+dose	0	100	TRPOSL	0	2	5	0	5	90	5	GreenLaser	125	-1	55258
14	6571	TRUE	1	1	7	6	Dose	100	100	TRPOSL	0	2	5	0	5	90	5	GreenLaser	125	-1	70152
15	7076	TRUE	1	1	8	3	Bleach+dose	600	100	TRPOSL	0	2	5	0	5	90	5	GreenLaser	125	-1	85437
16	7581	TRUE	1	1	8	6	Dose	100	100	TRPOSL	0	2	5	0	5	90	5	GreenLaser	125	-1	100323
17	8091	TRUE	1	1	10	3	Bleach+dose	600	100	TRPOSL	0	2	5	0	5	90	5	GreenLaser	125	-1	120220
18	8596	TRUE	1	1	10	6	Dose	100	100	TRPOSL	0	2	5	0	5	90	5	GreenLaser	125	-1	11059
19	-9																				
20	-10																				
21	7	TRUE	1	2	1	3	Natural	0	100	TRPOSL	0	2	5	0	5	90	5	GreenLaser	125	-1	82201
22	512	TRUE	1	2	1	6	Dose	100	100	TRPOSL	0	2	5	0	5	90	5	GreenLaser	125	-1	93026
23	1017	TRUE	1	2	2	3	Bleach+dose	600	100	TRPOSL	0	2	5	0	5	90	5	GreenLaser	125	-1	112312
24	1522	TRUE	1	2	2	6	Dose	100	100	TRPOSL	0	2	5	0	5	90	5	GreenLaser	125	-1	123147
25	2027	TRUE	1	2	3	3	Bleach+dose	1200	100	TRPOSL	0	2	5	0	5	90	5	GreenLaser	125	-1	31447
26	2532	TRUE	1	2	3	6	Dose	100	100	TRPOSL	0	2	5	0	5	90	5	GreenLaser	125	-1	114444
27	3037	TRUE	1	2	4	3	Bleach+dose	1800	100	TRPOSL	0	2	5	0	5	90	5	GreenLaser	125	-1	32547
28	3542	TRUE	1	2	4	6	Dose	100	100	TRPOSL	0	2	5	0	5	90	5	GreenLaser	125	-1	43644
29	4047	TRUE	1	2	5	3	Bleach+dose	2400	100	TRPOSL	0	2	5	0	5	90	5	GreenLaser	125	-1	90254
30	4552	TRUE	1	2	5	6	Dose	100	100	TRPOSL	0	2	5	0	5	90	5	GreenLaser	125	-1	101138
31	5057	TRUE	1	2	6	3	Bleach+dose	3200	100	TRPOSL	0	2	5	0	5	90	5	GreenLaser	125	-1	34158
32	5562	TRUE	1	2	6	6	Dose	100	100	TRPOSL	0	2	5	0	5	90	5	GreenLaser	125	-1	45026
33	6067	TRUE	1	2	7	3	Bleach+dose	0	100	TRPOSL	0	2	5	0	5	90	5	GreenLaser	125	-1	55302
34	6572	TRUE	1	2	7	6	Dose	100	100	TRPOSL	0	2	5	0	5	90	5	GreenLaser	125	-1	70156

Figure 2. Summary of the attributes of selected records using `pickBINdata()`, by setting the argument `view=TRUE`.

intensity. Two arguments `nfchn` and `nlchn` are used to specify the numbers of channels to be used for calculating initial signal and background, respectively. Two background subtraction methods, the "early" and "late" background subtraction, are available via setting the argument `bg='early'` or `bg='late'`, respectively. It is to be noted that this function automatically detects the start and end of signal based on the attributes `NPoints` (the total number of channels), `Delay` (the "light-off" channels before stimulation), and `Off` (the "light-off" channels after stimulation) of the corresponding signal record. This is useful when some channels have been allocated before or/and after stimulation; a "light-off" (or delay) period is commonly used to monitor any residual thermal signal after preheat (e.g., Fu et al., 2012). In this case, the signal channels are calculated as `(Delay+1):(Delay+nfchn)`, and the background channels for the "early" and "late" background subtraction methods are calculated as `(Delay+nfchn+1):(Delay+nfchn+nlchn)` and `(NPoints-Off-nlchn+1):(NPoints-Off)`, respectively.

2.2.2 Signal error estimation

The counting error of luminescence signal can be estimated using two methods. For the argument `distp='p'`, the variance of photon counts is assumed to follow a Poisson distribution. In this case, the relative standard error of the net OSL response (L) is estimated using the formula described by Galbraith (2002):

$$\mathrm{rse}(L) = \frac{\sqrt{I_f + \frac{t_f^2}{t_l^2} I_l}}{I_f - \frac{t_f}{t_l} I_l} \qquad (1)$$

where I_f is the total number of counts over the first few channels of total duration t_f of the decay curve. I_l is the total number of counts over the last few channels of total duration t_l. However, recent studies (e.g., Li, 2007; Adamiec et al., 2012) suggest that the variation in photon counts are dispersed more than would be expected from the assumed Poisson distribution. In this case, the user can set the argument `distp='op'` to calculate the relative standard error following the equation provided by Bluszcz et al. (2015):

$$\mathrm{rse}(L) = \frac{\sqrt{k_{ph}^2 I_f + (k_{dc}^2 - k_{ph}^2)\dot{B} t_f + \frac{t_f^2}{t_l^2}(k_{ph}^2 I_l + (k_{dc}^2 - k_{ph}^2)\dot{B} t_l)}}{I_f - \frac{t_f}{t_l} I_l} \qquad (2)$$

where k_{ph} and k_{dc} are the square root of variance to mean ratio (Adamiec et al., 2012) for the photon and dark counts, respectively, and $\dot{B}$ denotes the dark count rate (unit in cts/s). It is noted that, to be able to use this method, the user need to provide the values of k_{ph}, k_{dc}, and $\dot{B}$ (through arguments `kph`, `kdc`, and `dcr`, respectively), which should be measured independently for individual readers or measurement systems (see Adamiec et al. 2012 for details), as argument inputs for the function `analyseBINdata()`. Then the relative standard error of sensitivity-corrected OSL (L/T) is estimated as:

$$\mathrm{rse}\left(\frac{L}{T}\right) = \sqrt{\mathrm{rse}^2(L) + \mathrm{rse}^2(T) + 2\sigma_{ins}^2} \qquad (3)$$

where σ_{ins} is the instrumental irreproducibility for each individual OSL measurement (L or T) that can be set using the argument `me` in function `analyseBINdata()`.

2.2.3 Signal type selection

Apart from extracting the sensitivity-corrected signals (L/T), a default setting for the SAR procedure, user can also set the argument `signal.type` to extract the results of "L", or "T". This is useful for analysing the data from a procedure different from SAR, such as the pre-dose MET-pIRIR procedure for K-feldspar (Li et al., 2013, 2014), where the sensitivity-corrected (L/T), test dose (T) and sensitivity-uncorrected (L) signals can be used for D_e estimation.

2.2.4 Fast ratio of the signal

In the function `analyseBINdata()`, the user can also set the arguments `FR.fchn`, `FR.mchn` and `FR.lchn`, denoting the channels for fast component, medium component and background, respectively, to estimate the "fast ratio" (Durcan & Duller, 2011) for quantifying the dominance of the fast component in the initial test-dose response for the natural dose (T_n). Since the fast ratio will vary depending on the power density and wavelength of stimulation source being used for OSL measurements, the channel integrals used to determine it (i.e., `FR.fchn`, `FR.mchn`, `FR.lchn`) are set to `NULL` by default. So the fast ratio will not be calculated unless the values of `FR.fchn`, `FR.mchn`, `FR.lchn` are specified by the user.

2.2.5 Output signal analysis results

The function `analyseBINdata()` returns an invisible list of S3 class object "analyseBIN". The SAR data related quantities (such as the position and grain numbers, SAR cycles, doses, signals and backgrounds for each aliquot or grain, etc) can be output into a named CSV file via the argument `outfile`. Figure 3 shows an example of the quantities saved in a CSV file.

2.2.6 Comparing results of signal analysis with *Analyst*

Figure 4 compares sensitivity-corrected natural signal L_n/T_n and associated standard errors estimated using `'numOSL'` (version 2.3) and *Analyst* (version 4.31.9), using the single-grain data from sample HF11 from Haua Fteah (Cyrenaica, northeast Libya) (Douka et al., 2014; Li et al., 2016; Jacobs et al., 2017). The Pearson correlation coefficient $R^2 = 1$ indicates that L_n/T_n and associated standard errors (based on Poisson distribution) calculated using the two software packages are identical (Fig. 4A–B). However, since the counting statistics of the reader used to measure this sample does not follow a Poisson distribution (i.e., $k_{ph} = 1.37$ and $k_{dc} = 1.92$), the standard errors of L_n/T_n estimated using eqn. (2) are systematically larger than those estimated using eqn. (1) (Fig.4C); this suggests that the uncertainty of the sensitivity-corrected signal determined using eqn. (1) is likely to be underestimated when photon count numbers do not follow a Poisson distribution.

2.3. SAR D_e analysis

Function `calSARED()` calculates a series of SAR D_e values for different aliquots (grains) in a batch model using the data stored in the object "analyseBIN". Both D_e determination and rejection of unreliable D_e estimates can be achieved using this function.

2.3.1 Growth curve fitting

Fitting of the regenerative-dose data is implemented internally according to the Levenberg-Marquardt algorithm (Moré, 1978). In the function `calSARED()`, five models can be chosen for growth curve fitting via the argument `model`, including:

$$f(x) = ax + b \tag{4}$$

$$f(x) = a[(1 - exp(-bx)]) + c \tag{5}$$

$$f(x) = a[1 - exp(-bx)] + cx + d \tag{6}$$

$$f(x) = a[1 - exp(-bx)] + c[1 - exp(-dx)] + e \tag{7}$$

$$f(x) = a[1 - (1 + bcx)^{-1/c}] + d \tag{8}$$

Eqn. (4)–(8) describe the linear (LINE, `model='line'`), single saturation exponential (EXP, `model='exp'`), single saturation exponential plus linear (LEXP, `model='lexp'`), double saturation exponential (DEXP, `model='dexp'`), and general order kinetic model (GOK, `model='gok'`) (Guralnik et al., 2015), respectively. Where x and $f(x)$ denote regenerative dose and corresponding dose response signal, respectively, and a, b, c, d, e are parameters to be optimised. It is vitally important that the number of data points (N) to be fitted should at least be equal to the number of model parameters (n). The optimal parameters are obtained through "trial-and-error". Argument `weight` is a logical value indicating if the growth curve should be fitted using a weighted procedure (weighted by the inverse variance of individual data point). Argument `trial` is a logical value indicating if the growth curve should be fitted using other models if the given model fails. Growth curves can be fitted with more flexibility during the batch process by setting `trial=TRUE`. For example, if the fitting model is specified as LEXP, then a number of models (i.e., LEXP, GOK, EXP, LINE) will be tried one after another until the fit succeeds when `trial=TRUE`. In contrast, only the LEXP model will be tried if `trial=FALSE`.

The GOK model (Guralnik et al., 2015) is used by default in the function `calSARED()`. This model is highly recommended for batch analysis given its generality and robustness. In the GOK model, a denotes the maximum signal level, b is the reciprocal of the saturation dose D_0, c is a kinetic order modifier, and d is an offset accounting for potential "recuperation" effects. For $c \to 0$, the GOK model

A	B	C	D	E	F	G	H	I	J	K	L	M	N	O	P
	NO	Position	Grain	SAR.Cycle	Dose	Init	BG	Lx	seLx	TInit	TBG	Tx	seTx	LxTx	seLxTx
1	1	1	1	N	0	22642	524.5	22117.5	467.523	4258	127.5	4130.5	105.5754	5.354679	0.177605
2	1	1	1	R1	600	15736	340.5	15395.5	332.7384	3864	114.5	3749.5	97.69724	4.106014	0.139001
3	1	1	1	R2	1200	21926	532.5	21393.5	453.0618	4361	101	4260	108.0303	5.021948	0.16592
4	1	1	1	R3	1800	28159	687	27472	574.7928	5185	143	5042	124.1983	5.448631	0.176096
5	1	1	1	R4	2400	28918	809.5	28108.5	587.6716	5503	147.5	5355.5	130.573	5.24853	0.168571
6	1	1	1	R5	3200	34665	970	33695	699.4935	5989	171	5818	140.0505	5.791509	0.184095
7	1	1	1	R6	0	299	88.5	210.5	18.99932	6256	170	6086	145.4536	0.034588	0.003229
8	1	1	1	R7	600	20979	408	20571	436.4051	5726	197	5529	134.3594	3.720564	0.120019
9	1	1	1	R8	600	20843	426	20417	433.3562	5776	155.5	5620.5	135.977	3.632595	0.116912
10	2	1	2	N	0	51206	572.5	50633.5	1037.783	7136	150	6986	163.5013	7.247853	0.225481
11	2	1	2	R1	600	30530	349.5	30180.5	628.5299	6345	132	6213	147.8227	4.857637	0.153596
12	2	1	2	R2	1200	46353	555.5	45797.5	941.0607	7198	170.5	7027.5	164.431	6.516898	0.202937
13	2	1	2	R3	1800	57639	778	56861	1162.453	8425	191.5	8233.5	188.7775	6.906055	0.212145
14	2	1	2	R4	2400	67979	868.5	67110.5	1367.458	9165	213	8952	203.29	7.496705	0.228727
15	2	1	2	R5	3200	69506	986.5	68519.5	1395.696	9291	266	9025	204.9494	7.592188	0.231607
16	2	1	2	R6	0	566	120	446	26.5625	9419	210	9209	208.4377	0.048431	0.003086
17	2	1	2	R7	600	38278	454	37824	781.5158	8311	221.5	8089.5	186.0047	4.675691	0.144539
18	2	1	2	R8	600	37346	533	36813	761.3746	8651	199	8452	193.1968	4.355537	0.134264
19	3	1	3	N	0	13345	465	12880	282.7282	2556	128.5	2427.5	70.55035	5.30587	0.193246
20	3	1	3	R1	600	9780	351	9429	213.3493	2446	133	2313	68.20915	4.076524	0.151524
21	3	1	3	R2	1200	13021	495	12526	275.7332	2636	139.5	2496.5	72.10239	5.017424	0.182202
22	3	1	3	R3	1800	13904	597.5	13306.5	291.5955	2795	175.5	2619.5	75.01641	5.079786	0.183178
23	3	1	3	R4	2400	14878	630.5	14247.5	310.467	2894	179.5	2714.5	77.01399	5.248665	0.187766
24	3	1	3	R5	3200	15211	771	14440	314.6457	3001	230	2771	78.65988	5.211115	0.186483
25	3	1	3	R6	0	239	67.5	171.5	16.86757	2857	202.5	2654.5	76.00525	0.064607	0.006618
26	3	1	3	R7	600	9965	442	9523	215.5482	2682	172.5	2509.5	72.71373	3.79478	0.139527
27	3	1	3	R8	600	9448	450	8998	205.0819	2491	152	2339	68.95918	3.846943	0.143356
28	4	1	4	N	0	134804	503.5	134300.5	2711.034	17954	161.5	17792.5	380.3472	7.548152	0.221928

Figure 3. An example of the CSV file output by function `analyseBINdata()`. `Init` and `BG` denote the initial and background signals, respectively. `Lx=Init-BG`, `Tx=TInit-TBG`, `LxTx=Lx/Tx`, `seLx`, `seTx`, and `seLxTx` are the standard errors of `Lx`, `Tx`, and `LxTx`, respectively.

reduces to the EXP model, but as c increases, the GOK model progressively deviates from first-order behaviour and approximates the LEXP or DEXP model. Guralnik et al. (2015) demonstrated that the GOK model can successfully capture the behaviours of different materials and experimental conditions using a minimum number of model parameters.

The performance of the GOK model was tested and compared to other models using a large number of single-grain data sets from sample HF11, as shown in Fig.5. A total of 665 growth curves were fitted using different models. It turns out that the numbers of grains that fail in fitting are 0, 0, 310, and 237 for the EXP, GOK, LEXP, and DEXP models, respectively. This suggests that the universality and flexibility of EXP and GOK models are significantly better than the LEXP and DEXP models. The goodness-of-fit (see the next section) of the GOK model is marginally better than the EXP model (Fig. 5A–B) and comparable to the LEXP and DEXP models (Fig. 5C–F). Based on this comparison, we use GOK as a default fitting model for a batch analysis.

2.3.2 Goodness of fit

Two criteria are employed to measure the goodness-of-fit, i.e., the reduced chi-square (RCS) and figure-of-merit (FOM). The RCS is routinely provided in *Analyst* to measure the quality of fit of growth curves, which is defined as follows:

$$RCS = \frac{1}{N-n} \times \Sigma \frac{(y_i^o - y_i^f)^2}{\sigma_i^2} \tag{9}$$

where y_i^o and y_i^f denote the $i-th$ observed and fitted values, respectively, N and n denote the number of data points and the number of model parameters, respectively, and σ_i denotes the standard error for the $i-th$ observation. The value of RCS approximates unity if the fitting model is a good approximation of the observations (Bevington & Robinson, 2002). RCS greater than 1 indicates that the fitting function is not appropriate for describing the data points. However, a RCS less than 1 does not necessarily indicate a high-quality fit. A value of RCS that is very small may indicate overestimation of the uncertainties of observations (Bevington & Robinson, 2002) or an inappropriate assignment of fitting model.

The FOM is widely used to measure the goodness-of-fit in thermoluminescence (TL) glow curve deconvolution (Bos et al., 1994; Pagonis & Kitis, 2002). According to Balian & Eddy (1977), the FOM is defined as follows:

$$FOM = 100\% \times \frac{\Sigma |y_i^o - y_i^f|}{\Sigma y_i^f} \tag{10}$$

Balian & Eddy (1977) considered a good fit to have a FOM value of less than 2.5 %. Horowitz & Yossian (1995) suggested that a FOM value on the order of a few percent indicates an accurate fit for their computerized glow curves. According to our experience, the upper limit on FOM should not exceed 10%.

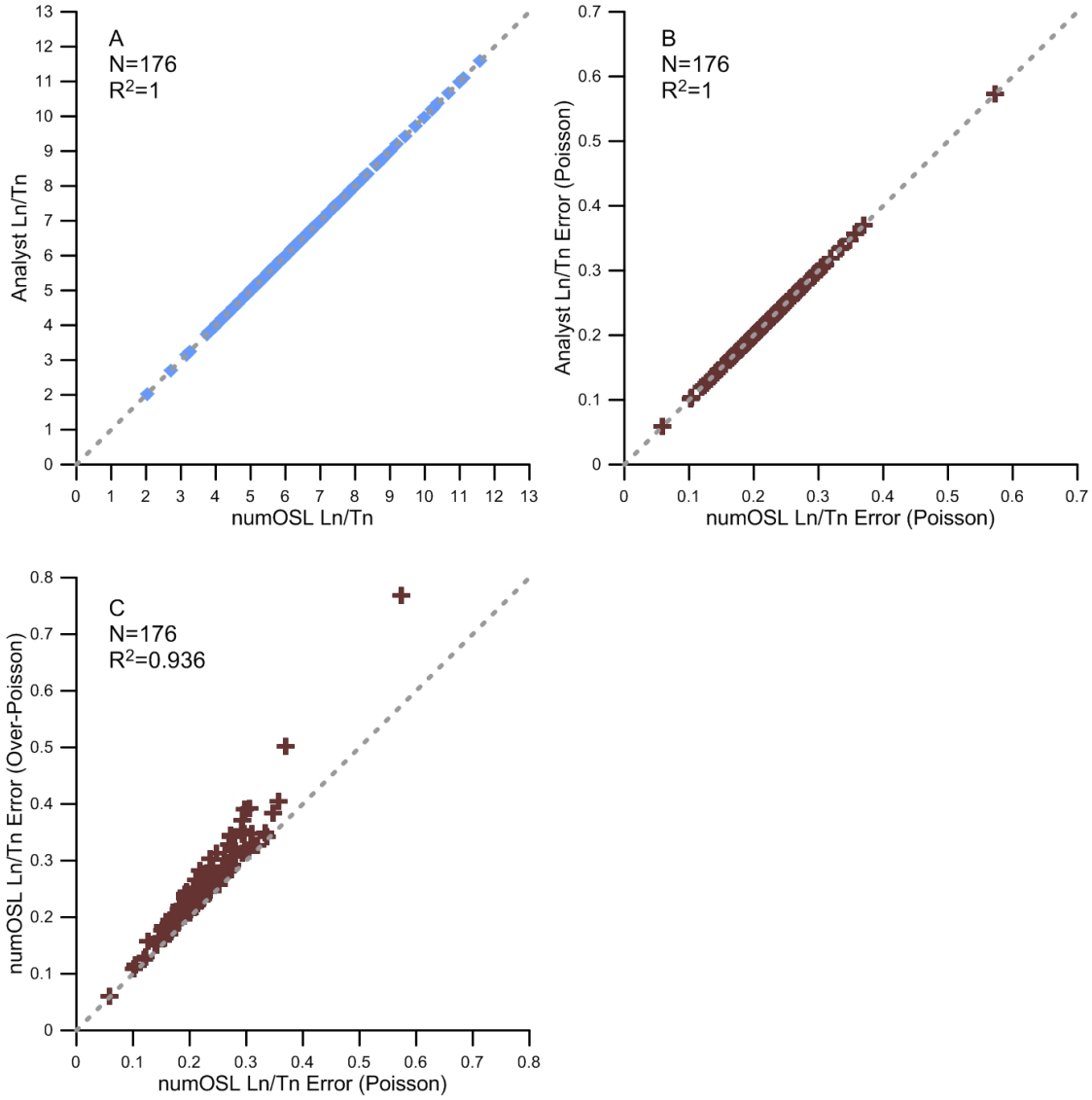

Figure 4. Comparison of L_n/T_n (A) and its standard error (B) calculated using '`numOSL`' and *Analyst*, using 176 grains from sample HF11. The net OSL was calculated using the "late" background subtraction method. The numbers of channels used for signal and background integration are 5 and 10, respectively. A relative standard error of 2% per measurement was combined in quadrature with the uncertainty of the net OSL by setting argument `me=2` in function `analyseBINdata()`. The dashed line indicates $y = x$. (C) Comparison of standard error of L_n/T_n estimated using Poisson and over Poisson distributions of photon counts. Correction factors were set as $k_{ph} = 1.37$ and $k_{dc} = 1.92$, and the dark count rate was set equal to 70 cts/s.

Both RCS and FOM have their own advantages and disadvantages as a measurement of goodness-of-fit of growth curves. Firstly, the RCS takes the standard errors of observations into consideration, while the FOM takes only the differences between observed and fitted data into account. For dim samples where large counting uncertainties are associated with the measured signals, large scatter may be expected for their growth curves. In this case, the growth curve under analysis may yield small RCS but large FOM. On the contrary, a bright sample may have well-behaved growth curves that can yield small fitting residuals (or FOM values) but high RCS values (due to the small error in signal). Secondly, the differences between the observed and fitted data are normalised using the fitted data in FOM, but this is not the case for RCS. Such a normalisation has an advantage to avoid the problem that the difference between the observed and fitted values increases with the size of observed values. As a result, FOM is more appropriate for comparing the quality of fit between growth curves that have significantly different magnitudes in signal intensity. Finally, according to Eqn. (9), RCS is only suitable for cases where the numbers of data points N is larger than the number of model parameters n. According to our experience, most of the growth curves with a RCS value below 5 and a FOM value below 10 may have an satisfactory fit; the user can, however, set a more stringent criterion by using smaller RCS and FOM values.

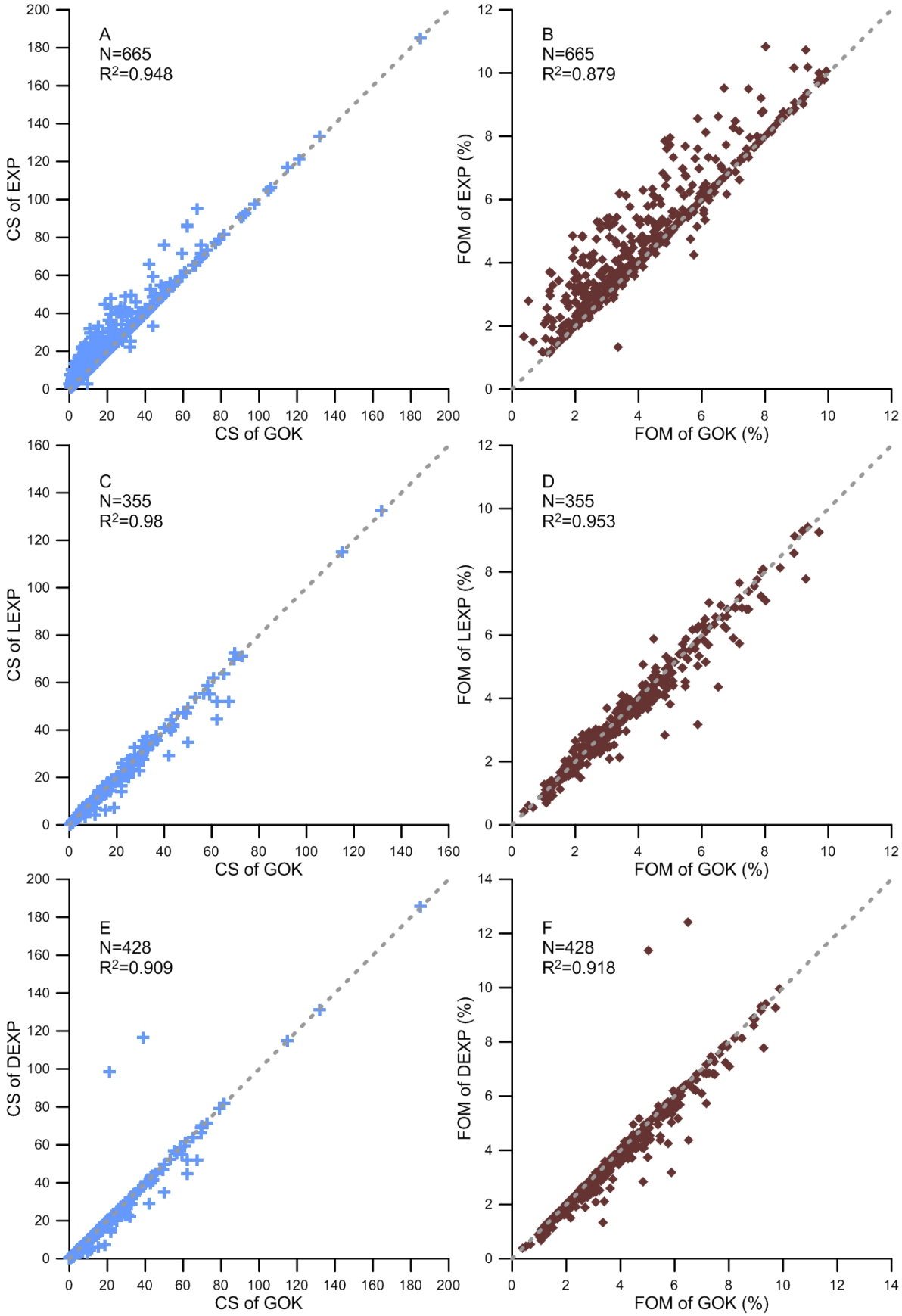

Figure 5. Comparison of goodness-of-fits between the GOK model and the EXP, LEXP, DEXP models. CS and FOM are short for chi-square and figure-of-merit values, respectively. The dashed line indicates $y = x$.

2.3.3 Error estimation in D_e

The function `calSARED()` employs two methods proposed by Duller (2007) to estimate the standard error of D_e estimate, i.e., simple transformation and Monte Carlo simulation (also called a "parameter bootstrap" method) by specifying the argument `errMethod`. For the simple transformation method used in *Analyst*, the standard error of the natural signal is combined in quadrature with the uncertainty of the fitted growth curve (i.e., the average deviation between observed and fitted data) (Duller, 2007):

$$avgDev = \frac{\sqrt{\Sigma_{i=1}^{i=N}(y_i^0 - y_i^f)^2}}{N} \quad (11)$$

This combined error is then propagated through interpolation on the growth curve to calculate the lower and upper limits on the D_e estimate and associated error. The simple transformation method takes less calculation resource and is less time-consuming compared to the Monte Carlo method. It should be mentioned that a finite upper limit on D_e cannot be obtained if the natural signal (L_n/T_n) is statistically consistent with, or above, the saturation level of the growth curve, indicating that the natural signal of the aliquot (grain) may have been saturated. When the simple transformation method is used, the function `calSARED()` estimates D_e error as well as its 68 (one sigma) and 95% (two sigma) confidence intervals by assuming that the sampling distribution of D_e is approximately normal (Galbraith & Roberts, 2012).

For the Monte Carlo method, the assessment of standard error of D_e estimate involves calculating a number of D_e values by randomly generating natural and regenerative signals according to Gaussian distributions. The 68% and 95% confidence intervals of D_e are derived directly from the sampling distribution of randomly simulated D_e. This method provides more reliable confidence interval estimates, especially when the sampling distribution of D_e is not approximately normal. It must be pointed out, however, that, when the natural signal lies on the non-linear region of a saturating exponential growth curve, the distribution of randomly simulated D_e using the Monte Carlo method tends to have an asymmetric distribution. As a result, the distribution of randomly simulated D_e may be significantly truncated if $D_e > 2D_0$ (D_0 denotes the characteristic saturation dose in a saturating exponential function) (or L_n/T_n exceeds about 85% of the saturation level). This is because many of the randomly simulated natural signals may not intersect the corresponding growth curve. In this situation, both the mean random D_e and the D_e error are likely to be underestimated.

2.3.4 SAR D_e selection using rejection criteria

In OSL dating, it is important to select aliquots (grains) that are suitable for D_e determination. Potential rejection criteria can be divided into several categories, including (1) signal-related criteria, such as whether the test-dose response for the natural dose (T_n) is more than 3 sigma above the background (BG) (Jacobs et al., 2006), ratio of initial signal to BG for T_n, relative standard error of T_n (Ballarini et al., 2007), and fast ratio of T_n (Madsen et al., 2009; Durcan & Duller, 2011; Duller, 2012); (2) growth-curve-related criteria, such as recycling ratio (Wintle & Murray, 2006), OSL-IR depletion ratio (Duller, 2003), recuperation (Wintle & Murray, 2006), and goodness of fit; (3) D_e-related criteria, such as the methods used for D_e determination (interpolation or extrapolation), relative standard error of D_e, etc.

We have incorporated a range of rejection criteria for extracting reliable D_e estimates in the function `calSARED()`, including (a) `Tn.above.3BG`: if the net test-dose OSL response for the natural dose (T_n) is 3 sigma above the background; (b) `TnBG.ratio.low`: lower limit on the ratio of initial signal to background for T_n; (c) `rseTn.up`: upper limit on the relative standard error of T_n; (d) `FR.low`: lower limit on the fast ratio of T_n; (e) `rcy1.range`, `rcy2.range`, and `rcy3.range`: lower and upper limits on recycling ratios (note that only the first three identical doses are taken into account); (f) `rcp1.up` and `rcp2.up`: upper limits on recuperation (note that `rcp1` and `rcp2` are the ratios of the sensitivity-corrected zero-dose signal to natural signal and to the signal from the maximum regenerative dose, respectively); (g) `fom.up`: upper limit on the FOM of fitted growth curve; (h) `rcs.up`: upper limit on the RCS of fitted growth curve; (i) `calED.method`: the method used for D_e determination (interpolation or extrapolation); (j) `rseED.up`: upper limit on the relative standard error of D_e. Among the rejection criteria listed above, (a)–(d) are signal-related, (e)–(h) are growth-curve-related, and (i)–(j) are D_e-related. Argument `use.se` is a logical value indicating if standard errors (two sigma) are taken into consideration during application of rejection criteria. Note that the user does not have to specify arguments for all the rejection criteria listed above. If the user does not want to consider a particular rejection criterion then they can simply leave the argument out of the function.

It should be noted that if the sensitivity-corrected signals for the first, second, and third repeated regenerative doses are L_{r_1}/T_{r_1}, L_{r_2}/T_{r_2}, and L_{r_3}/T_{r_3}, respectively, then the first, second and third recycling ratios are calculated as $[L_{r_2}/T_{r_2}]/[L_{r_1}/T_{r_1}]$, $[L_{r_3}/T_{r_3}]/[L_{r_1}/T_{r_1}]$, and $[L_{r_3}/T_{r_3}]/[L_{r_2}/T_{r_2}]$ (similar to *Analyst*). The lower and upper limits on recycling ratios can be specified directly by the user to apply recycling ratio criteria. In contrast, the application of the OSL-IR depletion ratio criterion is not straightforward. For example, if three duplicate regenerative doses are administrated and OSL responses from the first two regenerative doses are measured without infrared stimulation while only the 3rd one is measured after being exposed to infrared stimulation, then the OSL-IR depletion ratio will be calculated using the third recycling ratio (i.e., $[L_{r_3}/T_{r_3}]/[L_{r_2}/T_{r_2}]$. In this case, the user needs to specify argument `rcy3.range` to apply the OSL-IR depletion ratio criterion.

The function `calSARED()` calculates two recuperation ratios: the first ("recuperation-1") is the ratio of the sensitivity-corrected zero-dose to natural signals ($[L_0/T_0]/[L_n/T_n]$), which is commonly adopted as a measure of extent of thermal transfer (Murray & Wintle, 2000). However, for young

samples whose natural doses are close to zero or sensitivity-corrected natural signals are close to background, applying a low limit on "recuperation-1" may result in many grains (aliquots) being rejected. This may bias the results towards acceptance of older grains or aliquots whose natural signal are higher, and, hence, may overestimate the final D_e results. In this case, therefore, it is more reasonable to use "recuperation-2", the ratio of the zero-dose signal to that of the maximum regenerative dose ($[L_0/T_0]/[L_{max}/T_{max}]$), as an indicator of the extent of thermal transfer.

The function `calSARED()` was designated according to the principle that calculation resources should be saved as much as possible. For this purpose, signal-related rejection criteria (a–d) are applied firstly, and those aliquots (grains) rejected by these criteria will not be considered during the next step of analysis. The growth-curve-related criteria (e–h) are then applied to the culled data set, before the D_e-related criteria (i–j) are applied to any remaining aliquots (grains). The function returns a summary table (as shown in Fig. 6) showing the numbers of aliquots (grains) rejected by each of the specified rejection criterion and the number of aliquots (grains) that cannot be successfully calculated using function `calED()` (such as, improper input arguments, failure in growth curve fitting, saturation in natural signal, failure in D_e calculation or D_e error estimation, etc). Providing such a summary table is crucial, as it reveals the variability of luminescence behaviours of different grains or aliquots, and it has been widely used as the standard output information in single-grain dating (e.g. Feathers, 2003; Jacobs et al., 2006, 2015; Armitage et al., 2011; Arnold et al., 2012).

2.3.5 Output SAR D_e analysis results

The function `calSARED()` provides two arguments to output SAR D_e analysis results. The results of SAR D_e determination obtained through the batch process can be output graphically into a named PDF file via the argument `outpdf`. The SAR D_e related quantities (such as the position and grain numbers, values of rejection criteria, natural signal and associated standard error, standard error and confidence intervals of each accepted D_e estimate, etc.) can be output into a named CSV file via the argument `outfile`.

2.3.6 Comparing results of SAR D_e determination with *Analyst*

Figure 7 shows comparison between the D_e estimates and their associated standard errors determined using `'numOSL'` and*Analyst*, for single grains of sample HF11. The results obtained using the simple transformation method are indistinguishable ($R^2 = 1$) between the two software packages (Fig.7A–B). The D_e errors estimated using the Monte Carlo method are also consistent with each other ($R^2 = 0.974$) (Fig. 7C).

2.4. SGC D_e analysis

2.4.1 Select growth curves to establish SGC

SGC should be established using only those aliquots (grains) considered to be well-behaved so that reliable growth curves are produced (Li et al., 2016). Accordingly, poorly-behaved grains (aliquots) should be identified and rejected beforehand. In order to achieve this, function `pickSARdata()` uses rejection criteria similar to (but with exclusion of the D_e-related criteria) those used in function `calSARED()` to enable the user to select well-behaved grains or aliquots to establish SGC. The input of the function is an object "analyseBIN" produced by function `analyseBINdata()`. In order to save calculation resources, the design of function `pickSARdata()` is similar to the function `calSARED()`.

It is noted that, for single-grain quartz, different grains may have considerably different growth curve shapes (Li et al., 2016), which may prevent the establishment of a common SGC for all the grains. For such samples, Li et al. (2016) found that growth curves from different grains for their samples from Haua Fteah (Cyrenaica, northeast Libya) can be divided into three broad groups (i.e., "early", "medium" and "later"), with each group saturating at a different dose level. Each group of grains, however, share a common SGC, and the SGCs from different groups are identical up to a dose of 50 Gy after which they start to significantly deviate. Therefore, it is necessary to characterise the growth curves from different aliquots (grains) to check whether it is appropriate to establish a common SGC for the samples under consideration.

2.4.2 LS-normalisation

In comparison to the original SGC method from Roberts & Duller (2004) and the re-normalisation method from Li et al. (2015a,b), the LS-normalisation method of Li et al. (2016) can further reduce the variation of growth curves between aliquots (grains) measured from the same or different samples. This has been validated not only experimentally using natural sedimentary samples (Li et al., 2016) but also confirmed theoretically by modeling and simulation (Peng et al., 2016).

According to Li et al. (2016), the LS-normalisation procedure for SGC optimization involves the following steps: (1) fit regenerative-dose signals from all aliquots (grains) using a best-fit model (e.g., single saturating exponential function); (2) re-scale regenerative-dose signals from each aliquot (grains) using scaling factors determined in a way such that the difference between the re-scaled sensitivity-corrected regenerative-dose signals and the fitted common growth curve is minimised through an optimization procedure; each aliquot (grain) is treated individually, and different scaling factors are determined for different aliquots (grains); (3) repeat the fitting (step 1) and re-scaling (step 2) procedures iteratively. The iteration is performed repeatedly until there is negligible change in the relative standard deviation of re-scaled regenerative-dose signals.

	Description	N
1	Total number of analyzed aliquots (grains)	500
2	Rejection criterion: Tn below 3 sigma BG	0
3	Rejection criterion: ratio of Tn to BG below 3	0
4	Rejection criterion: RSE of Tn exceeds 30%	0
5	Rejection criterion: recycling ratio 1 outsides [0.9,1.1]	37
6	Rejection criterion: recycling ratio 3 outsides [0.9,1.1]	18
7	Rejection criterion: recuperation 2 exceeds 5%	0
8	Rejection criterion: FOM of growth curve exceeds 10%	80
9	Rejection criterion: RCS of growth curve exceeds 5	70
10	Rejection criterion: ED not calculated by Interpolation	7
11	Function calED(): improper input argument	0
12	Function calED(): failed in growth curve fitting	52
13	Function calED(): saturated in Ln/Tn	92
14	Function calED(): failed in ED calculation	0
15	Function calED(): failed in ED error estimation	0
16	Total number of rejected aliquots (grains)	356
17	Total number of accepted aliquots (grains)	144

Figure 6. A summary of results of SAR D_e analysis for 500 grains of sample HF11 reported from function `calSARED()`. Numbers of grains rejected according to user-supplied criteria and numbers of grains that cannot be successfully analysed using function `calED()` are summarised.

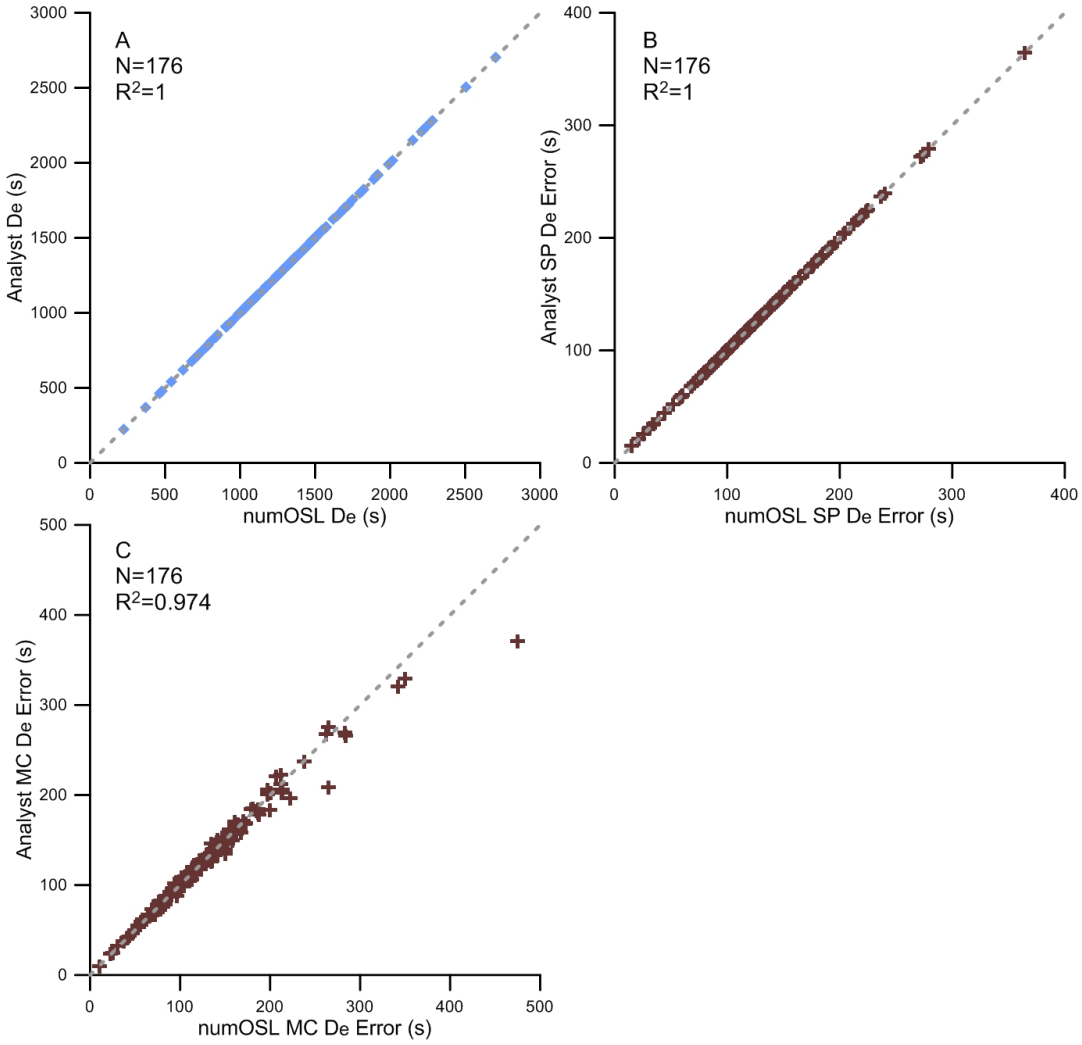

Figure 7. Comparison between SAR D_e values and associated standard errors obtained using '`numOSL`' and *Analyst*, using 176 single grains from sample HF11. The dashed line indicates $y = x$. Note that the unit of D_e is in irradiation time (second) rather than in Gy.

Li et al. (2016) found that the re-scaled regenerative-dose signals for the "early" group of their samples were best fitted using the EXP model, whereas those for the "medium" and "later" groups were best described using the DEXP model. They proposed that the best-fit model can be chosen on the basis of a chi-squared statistical test. However, during the application of this method, one needs to apply all possible models (such as LINE, EXP, LEXP, and DEXP) one after the other to the data to find out the best-fit model that yields the lowest chi-square value. For large data sets, the process is tedious and time-consuming. The function `lsNORM()` avoids the problem by applying the GOK model to fitting the data during the LS-normalisation process by default. The kinetic order modifier c in the GOK model (see eqn. (8)) automatically adjusts its magnitude to capture the variation pattern of the data during the fitting process.

We tested the performance of the function `lsNORM()` using randomly simulated growth curve data according to the kinetic model of Bailey (2001). The simulation was implemented using the **R** program KMS (Peng & Pagonis, 2016). The simulation steps are similar to those summarised in the Table 2 of Peng et al. (2016). The experimentally observed variability in OSL characteristics of quartz grains was simulated by allowing trap concentrations to vary randomly within $\pm 60\,\%$ of the original kinetic parameters of Bailey (2001), using uniformly distributed random numbers. Growth curves were simulated using regenerative doses of $0.4D_n$, $0.8D_n$, $1.2D_n$, $1.6D_n$, 0, and $0.4D_n$ Gy, where D_n stands for the natural dose and was simulated uniformly between 0 Gy and 200 Gy. The test dose was simulated uniformly from discrete numbers $[0.1D_n, 0.15D_n, 0.2D_n, 0.25D_n]$. The natural and laboratory dose rates were simulated uniformly from discrete numbers $[1\times10^{-3}, 1\times10^{-5}, 1\times10^{-7}, 1\times10^{-9}, 1\times10^{-11}]$ and $[0.2, 0.4, 0.6, 0.8, 1.0]$ Gy/s, respectively. The pre-heat and cut-heat temperatures were simulated uniformly from discrete numbers $[240, 250, 260]$ and $[200, 210, 220]\,^{\circ}$C, respectively.

The simulation result using 300 versions of model variants is shown in Fig.8A. It demonstrates that growth curve data simulated using various series of regenerative doses, test doses, natural and laboratory dose rates, and pre-heat and cut-heat temperatures show significantly difference in their shapes and magnitudes. The scatter of the data reduced significantly after being standardised using their test doses (Fig.8B). The variability of the data further decreased after being re-normalised using the sensitivity-corrected regenerative-dose signal at 200 Gy (Fig. 8C). The growth curve data re-scaled using the function `lsNORM()` demonstrate the lowest variability and best quality of fit (Fig. 8D).

It should be pointed out that, though the re-normalisation procedure of Li et al. (2015a,b) further reduces the scatter of growth curve data compared to the original SGC method of Roberts & Duller (2004), the application of the re-normalisation requires administration of a common regenerative dose (200 Gy in Fig. 8C) for different grains or aliquots. As a result, it is inapplicable if the growth curves used for SGC establishment do not share one common regenerative dose. In contrast, the LS-normalisation procedure of Li et al. (2016) does not require a common regenerative dose among all growth curves. This means that the normalisation can be implemented in a more flexible manner and it is possible to obtain more optimal results.

2.4.3 SGC D_e determination

Once a common SGC has been established, the sensitivity-corrected natural signal should be multiplied by a scaling factor, determined from the established SGC and an additional sensitivity-corrected regenerative-dose signal, to obtain the re-scaled natural signal in order to calculate a SGC D_e using the following formula:

$$\frac{L'_n}{T'_n} = \frac{L_n}{T_n} \times \frac{f(D_r)}{\frac{L_r}{T_r}} \tag{12}$$

where L'_n/T'_n denotes the re-scaled sensitivity-corrected natural signal, D_r and L_r/T_r denote the additional regenerative dose used for normalisation and the corresponding sensitivity-corrected signal, respectively, and $f(D_r)$ denotes the signal of D_r predicted using SGC established by LS-normalisation.

Function `calSGCED()` calculates D_e using the parameters (supplied using the argument `SGCpars`) of the SGC established externally through the function `lsNORM()` or `fitGrowth()`. D_e values can be calculated using the original SGC method proposed by Roberts & Duller (2004) (if argument `method='SGC'`) and the improved SGC method suggested by Li et al. (2016) (if argument `method='gSGC'`). Unlike function `calSARED()`, only signal-related rejection criteria can be used to select reliable D_e estimates in function `calSGCED()`.

The simple transformation method (rather than the Monte Carlo method) is implemented in function `calSGCED()` to assess error estimate of SGC D_e by default. During the application of the simple transformation method, the average deviation of established common SGC calculated according to eqn (11) is combined in quadrature with the uncertainty of the natural signal to account for the uncertainty of the SGC. This error term was taken into account via argument `avgDev`. The results of SGC D_e determination obtained through the batch process can also be output graphically into a named PDF file via the argument `outpdf`.

3. Worked examples

In this section, detailed examples for SAR and SGC D_e analysis are presented using **R** code templates. These templates are available from the supplementary and can be easily adapted by users for their own D_e analysis.

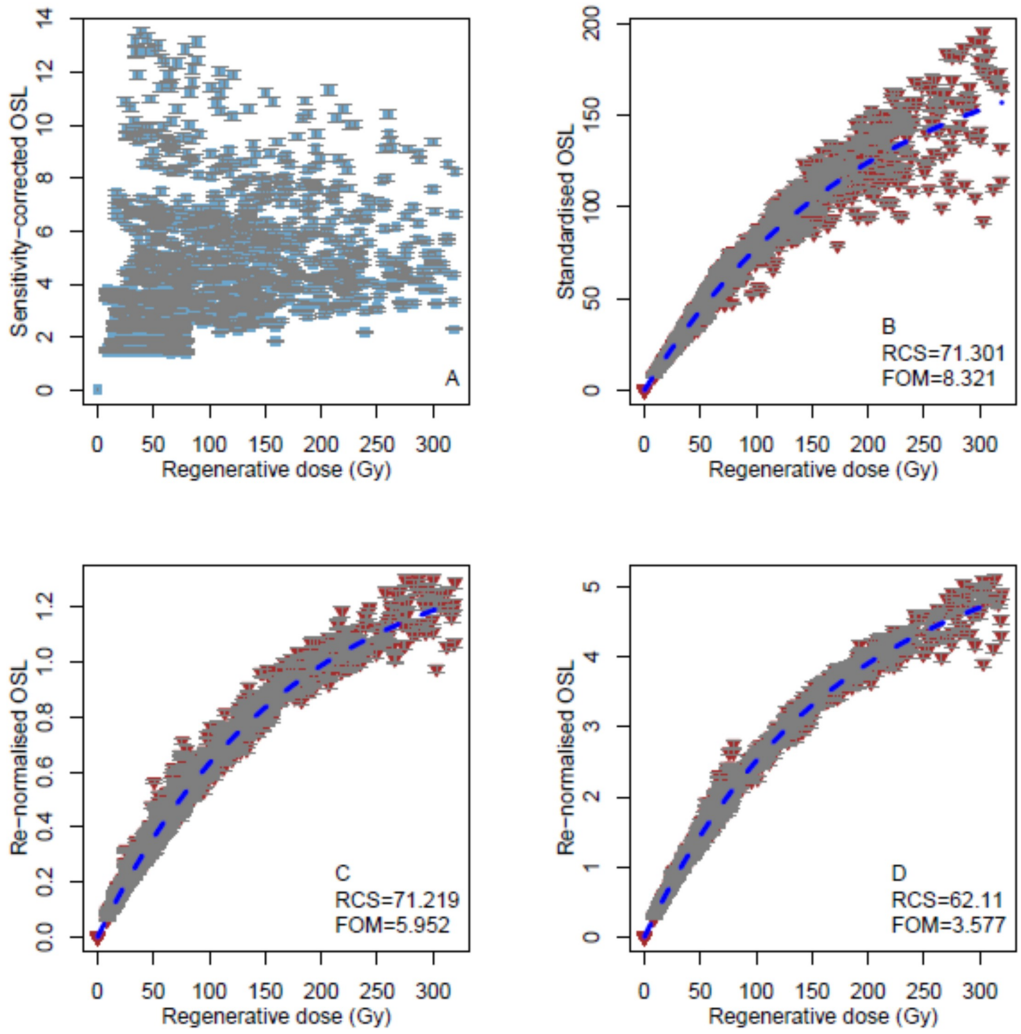

Figure 8. (A) Distribution of 300 randomly simulated growth curve data sets. Data shown in (B) was obtained by standardising the data from (A) using their corresponding test doses D_t. Data shown in (C) was obtained by re-normalising the data from (A) using sensitivity-corrected regenerative-dose signals at 200 Gy. Data shown in (D) was obtained by re-scaling the data from (A) using the LS-normalisation procedure. The dashed blue lines indicate the best-fit curves obtained using the GOK model.

3.1. SAR D_e determination and rejection criteria application

We first load package 'numOSL' into the **R** console using the first line of command (#1). BIN file "HF11(SG_Qtz_500_Grains).BIN" (available in the supplementary material) contains 500 grains of quartz OSL results for sample HF11. The file was loaded using function `loadBINdata()` and saved in object `res_loadBINdata` according to the commands in lines 2–3. The user needs to ensure that the BIN or BINX files to be imported are located in the current working directory. Imported single-grain data stored in `res_loadBINdata` with luminescence type of "TRPOSL" were selected using function `pickBINdata()` according to the commands in lines 4–6.

```
1 library(numOSL)
2 res_loadBINdata <- loadBINdata(
3  "HF11(SG_Qtz_500_Grains).BIN")
4 res_pickBINdata <- pickBINdata(
5  res_loadBINdata,
6  LType="TRPOSL")
```

Extracted data records stored in object `res_pickBINdata` were analysed using the function `analyseBINdata()` (the code in lines 7–13). The numbers of signal and background channels were set equal to 5 and 10, respectively (`nfchn=5, nlchn=10`). The "late" background subtraction method was used for net signal calculation (`bg='late'`). A measurement error of 2 % was given on each OSL measurement (i.e., L or T) (`me=2`). The photon counts were assumed to follow a Poisson distribution (`distp='p'`). Argument `signal.type='LxTx'` means that the sensitivity-corrected signal (L/T) was extracted. Results saved in a CSV file named "analyseBIN.csv" (available in the supplementary material) were output to the current work-

ing directory by using argument `outfile='analyseBIN'`.

```
res_analyseBINdata <-
 analyseBINdata(
 res_pickBINdata, nfchn=5,
 nlchn=10, bg="late",
 me=2, distp="p",
 signal.type="LxTx",
 outfile="analyseBIN")
```

Resultant data stored in object `res_analyseBINdata` were used to perform SAR D_e analysis using function `calSARED()` (code in lines 14–25). The GOK model was used and all growth curves were not forced to pass the origin (`model='gok'`, `origin=FALSE`). The Monte Carlo method was used for D_e error assessment and the desired number of simulation was set equal to 500 (`errMethod='mc'`, `nsim=500`), i.e., simulation will be performed repeatedly until 500 random D_e are generated. The acceptance rate of the Monte Carlo simulation is defined as the ratio of the number of obtained D_e to the total number of simulations. For example, if 1,000 simulations are performed and only 500 random D_e values are generated, then the acceptance rate of the simulation is 50 %. A low acceptance rate may imply that the model is not appropriate to fit the growth curve or the natural signal (L_n/T_n) is close to saturation; in the latter case a large number of simulated natural signals do not intersect with the simulated growth curves, so finite D_e cannot be obtained. Argument `trial=TRUE` ensures that other models will be tried if the given model fails in growth curve fitting.

Three signal-related rejection criteria (`Tn.above.3BG`, `TnBG.ratio.low`, and `rseTn.up`), five growth-curve-related criteria (`rcy1.range`, `rcy3.range`, `rcp2.up`, `fom.up`, and `rcs.up`), and one D_e-related criterion (`calED.method`) were then applied to select acceptable D_e values. Standard errors were taken into account during the application of rejection criteria (`use.se=TRUE`). The result of SAR D_e calculation was output to a PDF file named "calSARED.pdf" and a CSV file named "calSARED.csv" (`outpdf='calSARED'`, `outfile='calSARED'`) (available in the supplementary material). The SAR D_e analysis result for a grain of sample HF11 is shown in Fig. 9. A total of 356 grains were rejected according to these rejection criteria and 144 D_e values were obtained (as summarised in Fig. 6).

```
res_calSARED <- calSARED(
  res_analyseBINdata,
  model="gok", origin=FALSE,
  errMethod="mc", nsim=500,
  trial=TRUE, Tn.above.3BG=TRUE,
  TnBG.ratio.low=3, rseTn.up=30,
  rcy1.range=c(0.9,1.1),
  rcy3.range=c(0.9,1.1),
  rcp2.up=5, fom.up=10, rcs.up=5,
  calED.method="Interpolation",
  use.se=TRUE, outpdf="calSARED",
  outfile="calSARED")
```

The calculated SAR D_e distribution for the 144 grains was visualized using a simplified (pseudo) radial plot (Galbraith, 1988) implemented using function `psRadialPlot()` from the `'numOSL'` package (the code in lines 26–29) (Fig. 10). The lower and upper limits on the z-axis are controlled by the arguments `zmin` and `zmax`, respectively.

```
psRadialPlot(
  res_calSARED$sarED,
  zmin=450, zmax=2100,
  zlabel="De (s)")
```

3.2. Growth curve selection, LS-normalisation, and SGC D_e determination

BIN file "SA_Qtz_example.BIN" (available in the supplementary material) contains 24 multiple-grain aliquots of quartz OSL results for a fluvial sample from Shanxi province in China. The file was loaded and OSL data was selected using the commands in lines 30–31 and 32–33, respectively. Then we analysed the signal data using the **R** command in lines 34–38. We use function `pickSARdata()` to select well-behaved growth curves from data object `res_analyseBINdata1` using the commands in lines 39–47. Three signal-related criteria (`Tn.above.3BG`, `TnBG.ratio.low`, and `rseTn.up`) and four growth-curve-related criteria (`rcy1.range`, `rcp1.up`, `fom.up`, and `rcs.up`) were applied to select well-behaved growth curves. The results are output into a PDF file named "pickSARdata.pdf" (available in the supplementary material). Figure 11 shows results output by the function `pickSARdata()` for an aliquot of this sample.

```
res_loadBINdata1 <- loadBINdata(
 "SA_Qtz_example.BIN")
```

```
res_pickBINdata1 <- pickBINdata(
 res_loadBINdata1, LType="OSL")
```

```
res_analyseBINdata1 <-
  analyseBINdata(
  res_pickBINdata1, nfchn=10,
  nlchn=20, bg="late", me=2,
  distp="p", signal.type="LxTx")
```

```
res_pickSARdata <- pickSARdata(
  res_analyseBINdata1,
  model="gok", origin=FALSE,
  Tn.above.3BG=TRUE,
  TnBG.ratio.low=3, rseTn.up=30,
  rcy1.range=c(0.9,1.1),
  rcp1.up=10, fom.up=10,
  rcs.up=5, use.se=TRUE,
  outpdf="pickSARdata")
```

We use commands in lines 48–51 to optimise the selected growth curve data from well-behaved aliquots stored in `res_pickSARdata$SARdata` according to the LS-normalisation procedure using function `lsNORM()`. The allowed maximum number of iterations is set equal to 10 (`maxiter=10`). The automatically generated plot is shown in Fig. 12.

```
res_lsNORM <- lsNORM(
 res_pickSARdata$SARdata,
 model="gok", origin=FALSE,
 maxiter=10)
```

The commands in lines 52–61 were used to calculate SGC D_e according to the method of Roberts & Duller (2004). Objects `res_lsNORM$LMpars1[,1]` and

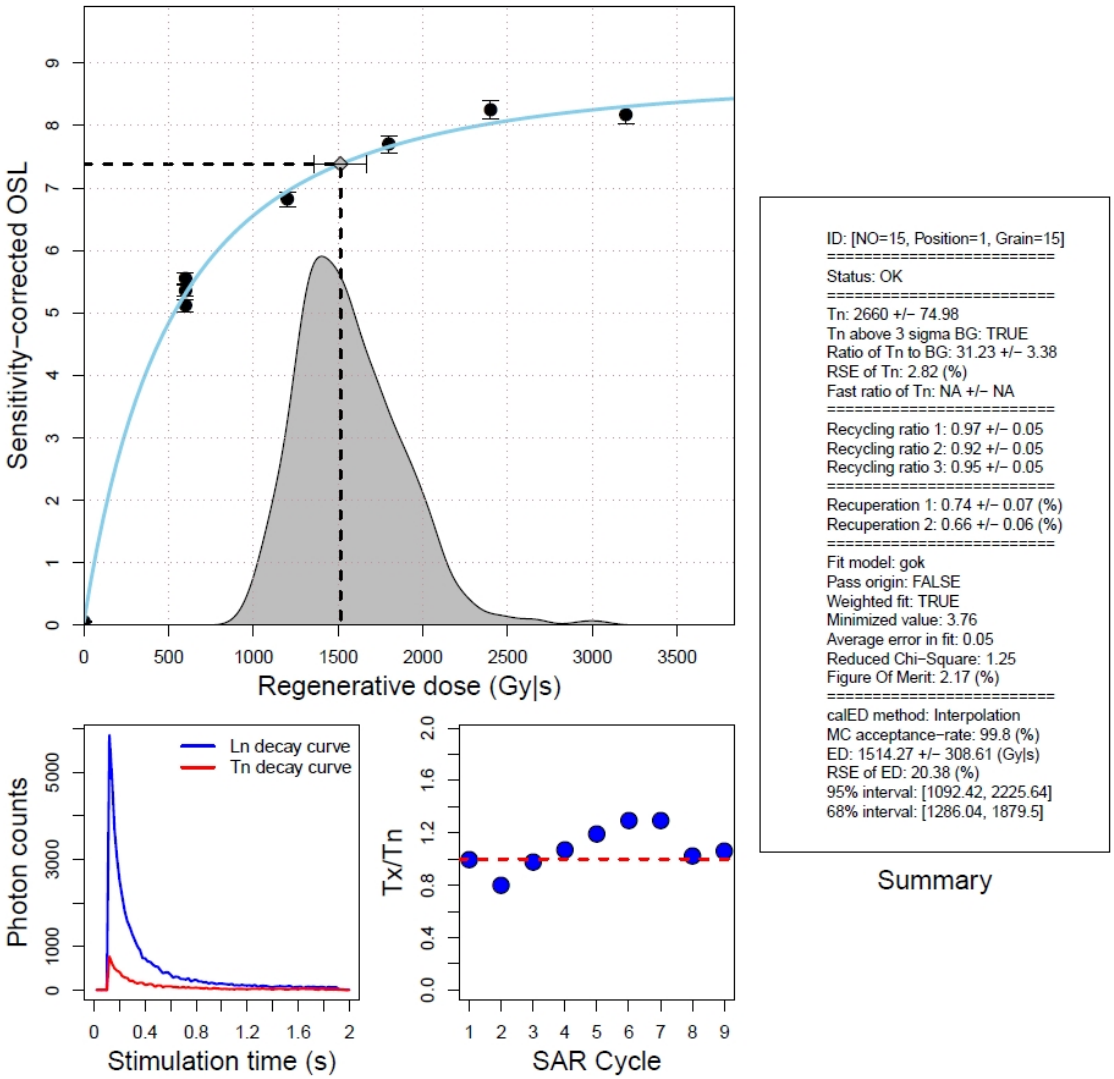

Figure 9. Results of SAR D_e calculation produced using function `calSARED()` for one of the grains of sample HF11.The upper plot shows results of growth curve fitting, D_e determination, and D_e error assessment using the Monte Carlo method. The distribution of the simulated D_e is shown in the grey area. The lower left plot shows the decay curves for the natural dose and its test dose. The lower right plot demonstrates the variation in the ratio of T_x to T_n for different SAR cycles. The right panel summarises the results of D_e calculation. The 68 % (one sigma) and 95 % (two sigma) confidence intervals of D_e were determined from the sampling distribution of randomly simulated D_e using the Monte Carlo method. Note that the unit of dose is in irradiation time (second) rather than in Gy.

`res_lsNORM$avg.error1` stand for the parameters and average deviation of the common SGC, respectively, established using growth curve data that have not been re-scaled by LS-normalisation. `res_lsNORM$LMpars1` is a two-column matrix in which SGC parameters and associated standard errors are stored in the first and second column, respectively. SGC parameters stored in the first column are accessed using `res_lsNORM$LMpars1[,1]`. The average deviation was used to account for uncertainty of the SGC, which was incorporated into the estimation of D_e error using the simple transformation method. It is of vital importance that arguments `model` and `origin` used in function `calSGCED()` are consistent with those used in function `lsNORM()`if the same parameters used in function `calSGCED()` are derived from the output of function `lsNORM()`. Three signal-related criteria (`Tn.above.3BG`, `TnBG.ratio.low`, and `rseTn.up`) were employed to select acceptable SGC D_e estimates (note that growth-curve-related criteria are inapplicable for the SGC method). The results of SGC D_e calculation were output into a PDF file named "SGCED.pdf" (available in the supplementary material).

```
52 res_SGCED <- calSGCED(
53   res_analyseBINdata1,
54   SGCpars=res_lsNORM$LMpars1[,1],
55   model="gok", origin=FALSE,
56   avgDev=res_lsNORM$avg.error1,
57   method="SGC", errMethod="sp",
58   SAR.Cycle="N",
59   Tn.above.3BG=TRUE,
60   TnBG.ratio.low=3, rseTn.up=30,
61   use.se=TRUE, outpdf="SGCED")
```

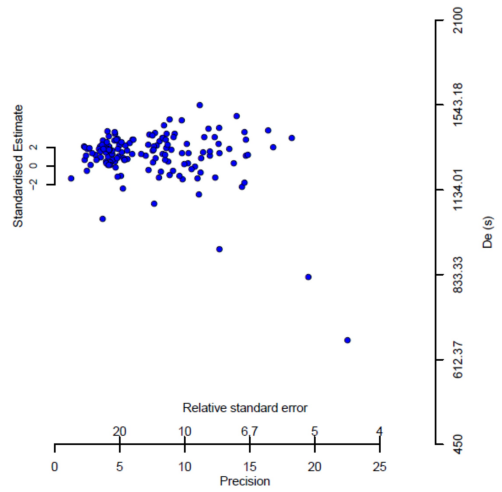

Figure 10. D_e distribution for 144 single grains from sample HF11 calculated using function `calSARED()` visualized using a pseudo radial plot.

The commands in lines 62–72 were used to calculate SGC D_e according to the method of Li et al. (2016). Objects `res_lsNORM$LMpars2[,1]` and `res_lsNORM$avg.error2` stand for the best-fit parameters and associated average deviation of the SGC established using LS-normalisation, respectively. Note that in order to calculate SGC D_e using the method of Li et al. (2016), the sensitivity-corrected natural signal and an additional sensitivity-corrected regenerative-dose signal need be specified (via argument `SAR.Cycle`). `SAR.Cycle=c("N","R2")` means that the second regenerative dose will be used to re-scale the natural signals for SGC D_e calculation. Figure 13 shows results of SGC D_e calculation for an aliquot of the fluvial sample.

```
62 res_gSGCED <- calSGCED(
63   res_analyseBINdata1,
64   SGCpars=res_lsNORM$LMpars2[,1],
65   model="gok", origin=FALSE,
66   avgDev=res_lsNORM$avg.error2,
67   method="gSGC", errMethod="sp",
68   SAR.Cycle=c("N","R2"),
69   Tn.above.3BG=TRUE,
70   TnBG.ratio.low=3,
71   rseTn.up=30, use.se=TRUE,
72   outpdf="gSGCED")
```

Finally, to test the reliability of SGC D_e determined above, we compared the SGC D_e values with those determined using the full SAR protocol. SAR D_e calculation using the data sets stored in object `res_analyseBINdata1` was implemented using the commands in lines 73–83. Here the fitting model and method used for D_e error assessment were chosen to be consistent with those used in SGC D_e calculation performed above. The commands in lines 84–87 used the **R** internal function `intersect()` to identify aliquots that succeed in both SAR and SGC D_e calculations.

```
73 res_SARED <- calSARED(
74   res_analyseBINdata1,
75   model="gok", origin=FALSE,
76   errMethod="sp",
77   Tn.above.3BG=TRUE,
78   TnBG.ratio.low=3,
79   rseTn.up=30,
80   rcy1.range=c(0.9,1.1),
81   rcp1.up=10, fom.up=10,
82   rcs.up=5, use.se=TRUE,
83   calED.method="Interpolation")

84 index <- intersect(intersect(
85   rownames(res_SARED$sarED),
86   rownames(res_SGCED$sgcED)),
87   rownames(res_gSGCED$sgcED))
```

The commands in lines 88–118 compare calculated D_e values between SAR and SGC using a scatter plot. The SAR D_e (lines 88–89) and SGC D_e calculated using the method of Li et al. (2016) (lines 90–91) were used as the x and y coordinates, respectively. To compare SAR D_e with SGC D_e calculated using the method of Roberts & Duller (2004), the user only needs to change `res_gSGCED` in lines 90–91 to `res_SGCED`. The commands in lines 103–106 and 107–110 add error bars to the x and y coordinates, respectively. The commands in lines 112–114 use the **R** internal function `cor()` to calculate the Pearson correlation coefficient between SAR and SGC D_e.

```
88 sarED <- res_SARED$sarED[index,1]
89 sarEDerr <-  res_SARED$sarED[index,2]

90 sgcED <- res_gSGCED$sgcED[index,1]
91 sgcEDerr <- res_gSGCED$sgcED[index,2]

92 min_xy <- min(sarED-sarEDerr,
93   sgcED-sgcEDerr)
94 max_xy <- max(sarED+sarEDerr,
95   sgcED+sgcEDerr)

96 plot(sarED, sgcED,
97   xlim=c(min_xy,max_xy),
98   ylim=c(min_xy,max_xy),
99   xlab="SAR De (s)",
100  ylab="SGC De (s)",
101  pch=21, bg="skyblue3",
102  col="skyblue3", cex=1.5)

103 arrows(x0=sarED-sarEDerr/2,
104   x1=sarED+sarEDerr/2,
105   y0=sgcED, y1=sgcED, code=3,
106   angle=90, length=0.05)

107 arrows(x0=sarED,
108   y0=sgcED-sgcEDerr/2,
109   x1=sarED, y1=sgcED+sgcEDerr/2, code=3,
110   angle=90, length=0.05)

111 abline(a=0, b=1, lty="dashed")

112 R2 <- round(
113   (cor(x=sarED, y=sgcED,
114   method="pearson"))^2, 3L)

115 legend("bottomright",
116   legend=c(paste("N=",
117   length(index)),
118   paste("R^2=", R2)), bty="n")
```

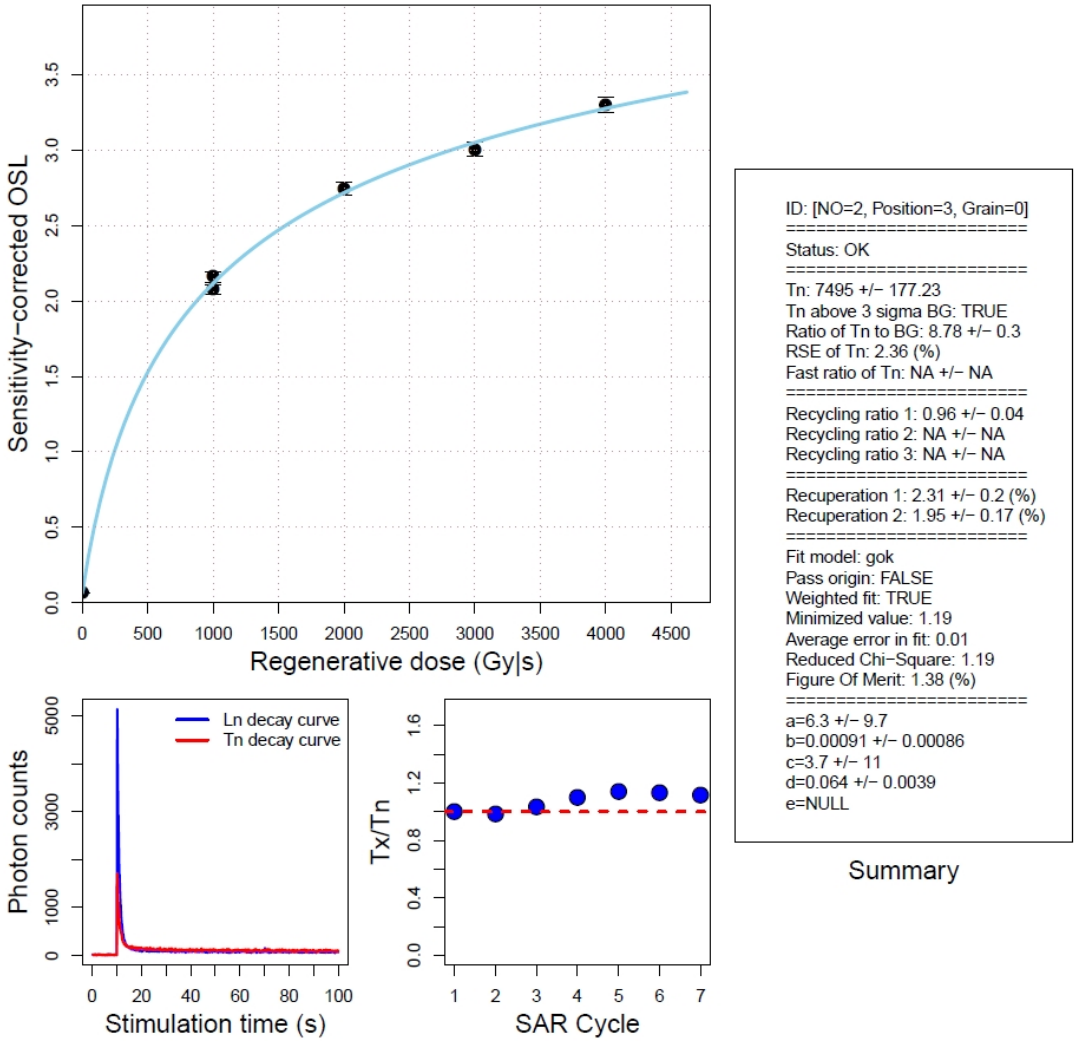

Figure 11. Results of growth curve selection produced using function `pickSARdata()` for one of the aliquots of a fluvial sample from Shanxi province in China. The upper plot shows result of growth curve fitting. The lower left plot shows the decay curves for the natural dose and its test dose. The lower right plot demonstrates the variation in the ratio of T_x to T_n for different SAR cycles. The right panel summarises the results of growth curve fitting. Note that the unit of dose is in irradiation time (second) rather than in Gy.

The commands in lines 119–127 visualize the distribution of ratios of SGC to SAR D_e using the pseudo radial plot. The standard errors of the ratios were calculated using command line 120–122. The commands in lines 123–127 use function `psRadialPlot()` from package '`numOSL`' to visualize the distribution of the ratios with a simplified (pseudo) radial plot. The central value was set equal to 1.0 (`dose=1.0`). The size of points can be modified using argument `psize`. Figure 14 shows comparisons between SAR D_e and SGC D_e calculated using two different methods.

```
119 Ratio <- sgcED/sarED

120 seRatio <- Ratio*
121   sqrt((sarEDerr/sarED)^2+
122   (sgcEDerr/sgcED)^2)

123 psRadialPlot(
124   cbind(Ratio,seRatio),
125   dose=1.0, zmin=0.7,
126   zmax=1.5, psize=1.5,
127   zlabel="Ratio of SGC to SAR De")
```

4. Discussion

A number of functions have been provided to flexibly import, select and analyse OSL data measured using a SAR procedure. The commonly used method for assessing the error estimate of the net OSL response is based on the assumption that the variance of photon counts follows a Poisson distribution (Galbraith, 2002). However, recent studies (Li, 2007; Adamiec et al., 2012) suggest that the variation in photon counts are dispersed more than would be expected from a Poisson distribution. The function `analyseBINdata()` estimates the standard error of net OSL signal using the newly derived formula outlined by Bluszcz et al. (2015) when count numbers do not follow a Poisson distribution. The function

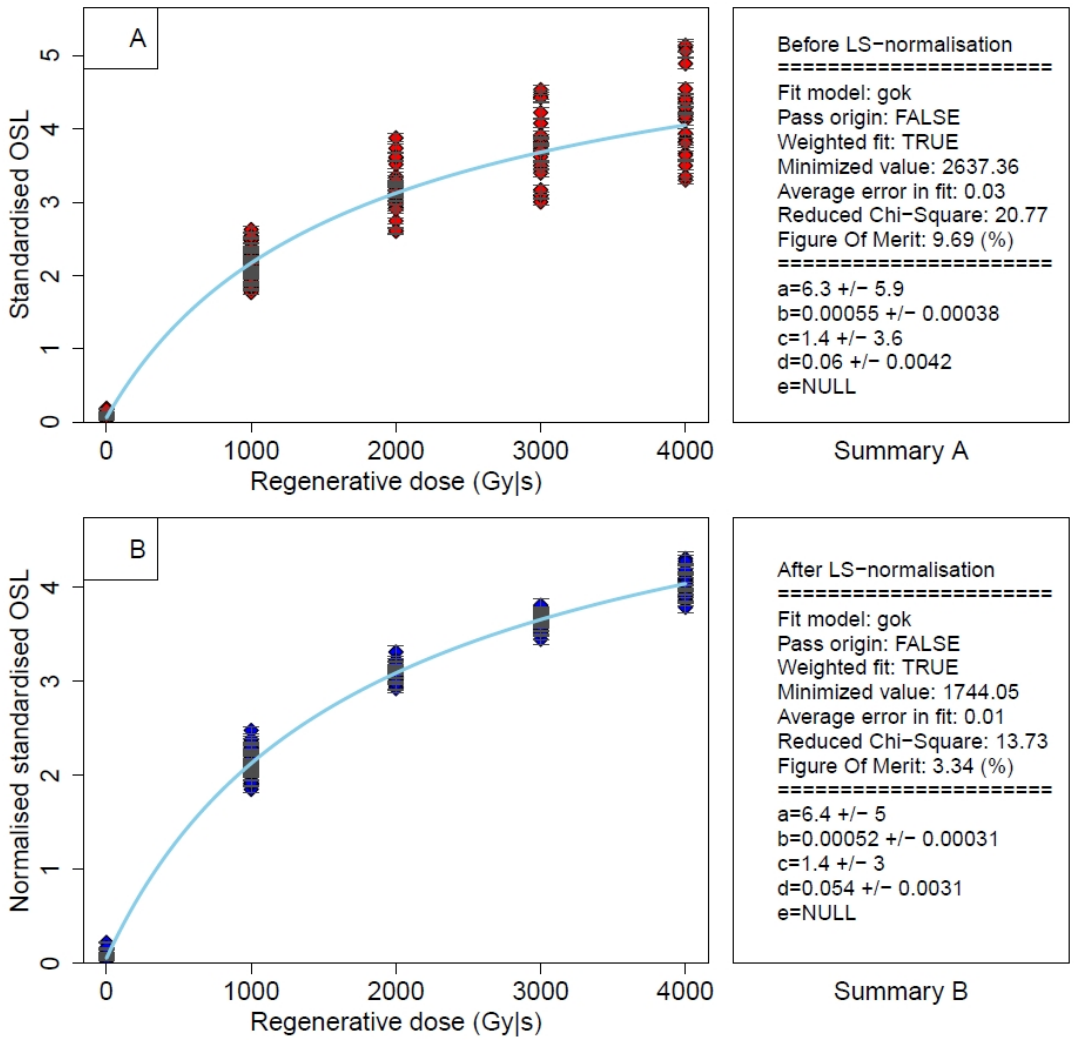

Figure 12. Results of LS-normalisation generated using function `lsNORM()`. The parameters (*a*, *b*, *c*, and *d*) shown in the right panel are obtained by fitting the data shown in the left panels using the GOK model. It should be noted that if the fitting is performed using a weighted procedure (i.e., `weight=TRUE`) then the "Minimized value" denotes the minimized chi-square value. For un-weighted fitting procedures (i.e., `weight=FALSE`), the "Minimized value" represents the minimized sum of squared residuals. The "Average error in fit" denotes the average deviation (*avgDev*) of the fitted growth curve data. Note that the unit of dose is in irradiation time (second) rather than in Gy.

was used to analyse single-grain data from sample HF11 (Li et al., 2016) and the results were compared to those analysed using *Analyst*. This comparison suggests that the sensitivity-corrected natural signal and associated standard error estimated using the two software packages are identical to each other when a Poisson distribution is assumed (Fig. 4A–B), but greater standard errors are obtained when photon counts do not follow a Poisson distribution (Fig. 4C).

Several strategies have been adopted to improve the efficiency, applicability, and practicability of the function `calSARED()` for SAR D_e analysis. Firstly, the core function has been programmed using the Fortran 90, instead of using pure **R** language, and wrapped by **R** using an interface. Compared to Fortran 90, pure **R** language has much less efficiency in the routine if a large number of SAR data sets are analysed (as shown in the worked example of Sec. 3.1). Secondly, the general applicability and robustness of the model used for growth curve fitting are critical for ensuring determination of a large number of D_e values in a batch model without the need for manual interference. Accordingly, besides the most commonly used models (i.e., the LINE, EXP, LEXP, and DEXP), the newly developed GOK model (Guralnik et al., 2015) has been included in our program. We tested the performance of this model using a large number of single-grain growth curve data from sample HF11 and other samples (data not shown here). Our results demonstrate the general applicability and robustness of the GOK model in growth curve fitting (as shown in Fig. 5). Moreover, setting argument `trial=TRUE` ensures that the growth curve will be fitted using other models if the specified model fails. This further increases the flexibility and adaptability of the function in growth curve fitting. Finally, we have integrated the commonly used rejection criteria for selecting and rejecting SAR D_e estimates into the function `calSARED()`. These cri-

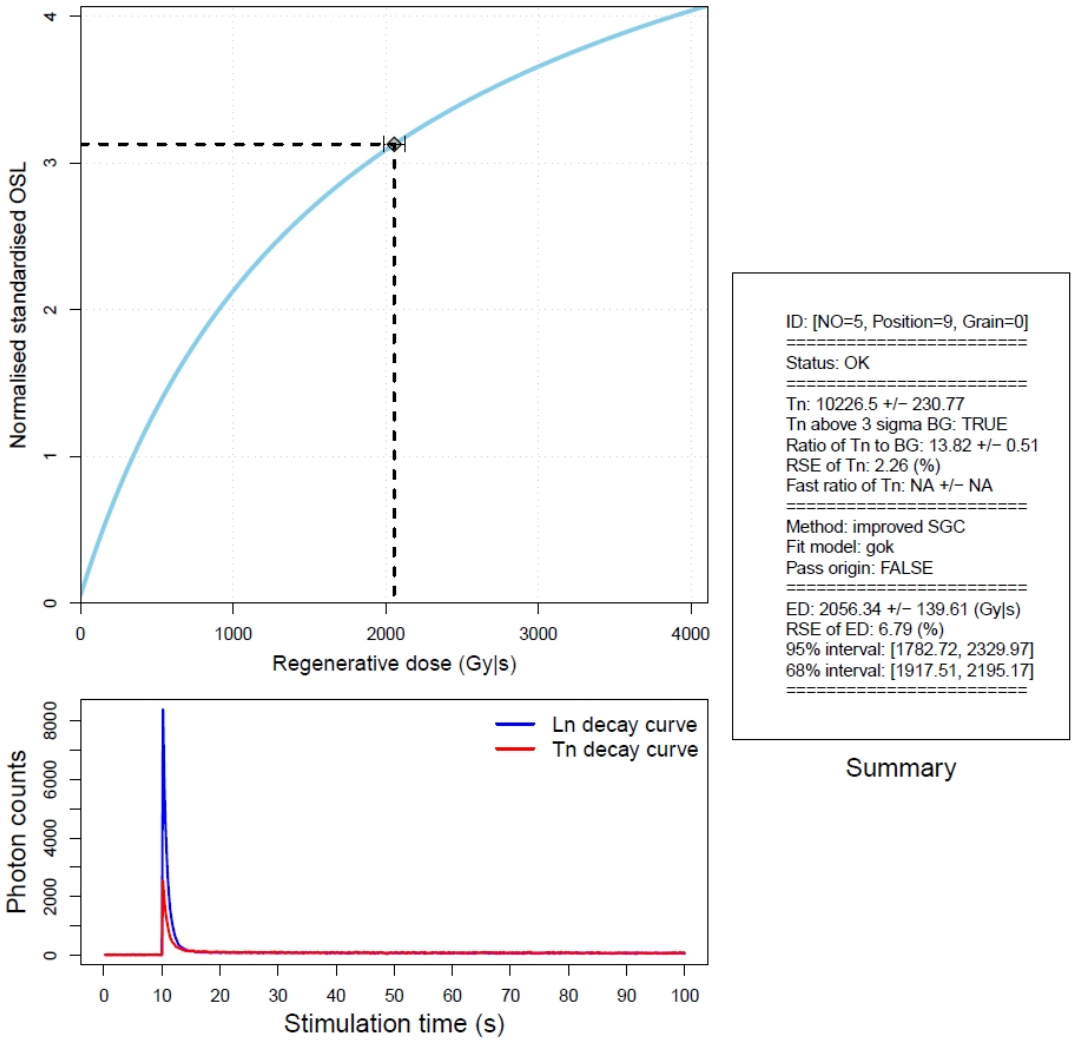

Figure 13. Results of SGC D_e calculation produced using function `calSGCED()` for one of the aliquots of a fluvial sample from Shanxi province in China. The upper plot shows result of SGC D_e calculation. The blue line denotes the SGC established using LS-normalisation. The lower plot shows the decay curves for the natural dose and its test dose. The right panel summarises the results of D_e calculation. The 68% (one sigma) and 95% (two sigma) confidence intervals of D_e were determined by normal approximation (not Monte Carlo simulation) as the simple transformation method is applied here for D_e error assessment. Note that the unit of dose is in irradiation time (second) rather than in Gy.

teria are applied in a manner that save calculation resources as much as possible. For this purpose, signal-related criteria are applied first, then the growth-curve-related criteria, and the D_e-related criteria are considered last. We compared SAR D_e and associated standard errors obtained from the function `calSARED()` with those estimated from *Analyst* (as shown in Fig. 7). The results between two software packages are indistinguishable.

Two criteria (FOM and RCS) are adopted to select reliable growth curves for SGC establishment. Generally, the FOM is useful in selecting "absolutely perfect" growth curves by ignoring their standard errors, while RCS also takes the standard errors into account. Note that the upper limits on FOM and RCS used to extract "acceptable" growth curves may be sample dependent, which needs to be further investigated and is beyond the scope of this study.

The performance of the LS-normalisation procedure implemented using the function `lsNORM()` was tested using randomly simulated growth curve data (as shown in Fig. 8). The results suggest that the LS-normalisation procedure is a generally reliable method for reducing variation in growth curves between aliquots (grains) measured from the same or different samples. However, we would like to emphasise here that the SGC method should only be applied on the basis of a careful validation, i.e., by comparing SAR and SGC D_e estimates using a large number of measured SAR data sets. It is necessary to first test whether reliable D_e estimates can be obtained using a full SAR procedure, and assess the effect and importance of each of the rejection criteria used to select SAR D_e; the latter is especially important because the SGC approach involves only the measurements of natural-dose and an additional regenerative-dose cycles, so

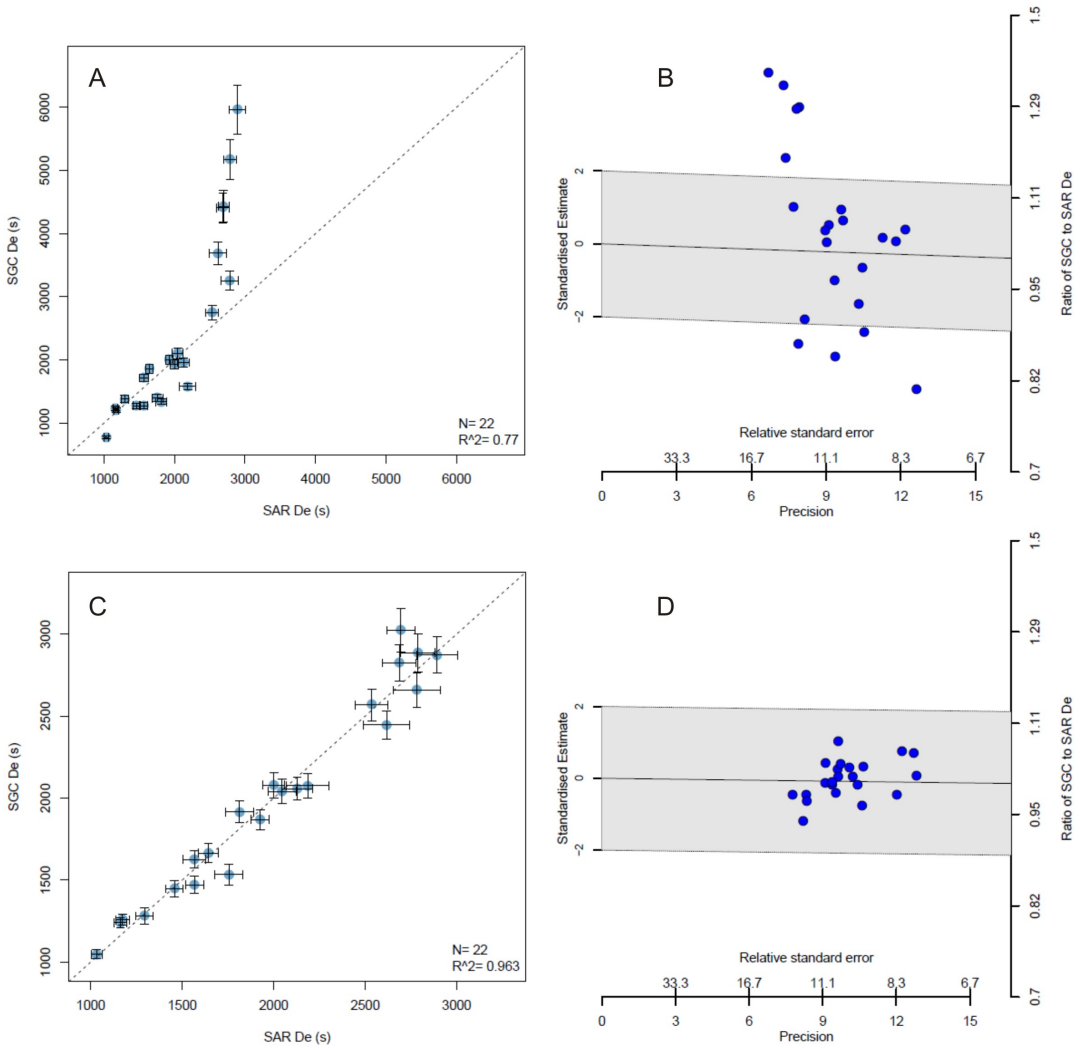

Figure 14. Comparison between SAR and SGC D_e estimates. (A) and (C) plot SAR D_e against SGC D_e determined using the methods of Roberts & Duller (2004) and Li et al. (2016), respectively. (B) and (D) show distributions of ratios of SGC D_e determined using the methods of Roberts & Duller (2004) and Li et al. (2016) to SAR D_e, respectively. The grey bands in (B) and (D) show the 2 sigma range around the central value at 1.

application of growth-curve-related rejection criteria (such as recuperation, recycling ratio, FOM, and RCS) is not possible. Consequently, the user may incorporate some poorly-behaved grains (e.g., Duller et al., 2000; Jacobs et al., 2003, 2006; Duller, 2008) into the final calculation, which may not only induce additional uncertainty in the final results but also may produce erroneous results.

Batch analysis of SAR and SGC data offers benefits for standardisation of analyses and elimination of user error, and, therefore, can substantially reduce the amount of data-handling time. At the same time, however, we would emphasis and maintain that manual data analysis also has its own advantages. We would like to suggest that one should conduct manual data analysis at least for some of their samples or some of the measured grains, particularly for understanding potentially problematic OSL behaviours, better characterisation of variable OSL properties between samples, and for identifying behavioural trends that might go unnoticed when using automated procedures. In reality, the optimum approach for SAR analysis of a large number of data sets undoubtedly lies in combining both practices together, particularly when working on previously unstudied samples: i.e., undertaking batch analysis for implementation of quality assurance criteria and for deriving accepted D_e populations, and then manually cross-checking the OSL properties of the rejected and accepted grain populations to ensure that sample-specific luminescence properties are fully understood by the user.

5. Conclusions

We present several general **R** functions to flexibly analyse SAR data and determine SAR and SGC D_e in a batch model under the framework of the '`numOSL`' package. The intended use of these functions is to enable the user to rapidly and flexibly perform D_e analysis for a large number of SAR

data sets. We have provided practical workflows, including data import (selection), signal analysis, SAR D_e determination, application of rejection criteria, growth curve selection, LS-normalisation, and SGC D_e calculation, using simple **R** code templates. We demonstrate that a combination of the small number of **R** functions can be used to perform SAR and SGC D_e analysis in a flexible and efficient manner. These functions are totally self-contained and do not depend on any external **R** packages. Users are encouraged to combine our program with other software packages (e.g., *Analyst*, **R** package `'Luminescence'`, etc.) for their specific SAR (SGC) application requirements.

Acknowledgments

Zenobia Jacobs is thanked for providing the example data from sample HF11. Valuable and constructive comments were provided by Lee Arnold. BL was supported by an Australian Research Council Future Fellowship grant (FT140100384). JP was supported by the National Natural Science Foundation of China (41701004).

References

Adamiec, G., Heer, A. J., and Bluszcz, A. *Statistics of count numbers from a photomultiplier tube and its implications for error estimation*. Radiation Measurements, 47(9): 746–751, 2012.

Armitage, S. J., Jasim, S. A., Marks, A. E., Parker, A. G., Usik, V. I., and Uerpmann, H. P. *The Southern Route "Out of Africa": Evidence for an Early Expansion of Modern Humans into Arabia*. Science, 331(6016): 453–456, 2011.

Arnold, L. J., Demuro, M., Navazo, M., Benito-Calvo, A., and Pérez-González, A. *OSL dating of the Middle Palaeolithic Hotel California site, Sierra de Atapuerca, north-central Spain*. Boreas, 42(2): 285–305, 2012.

Bailey, R. M. *Towards a general kinetic model for optically and thermally stimulated luminescence of quartz*. Radiation Measurements, 33(1): 17–45, 2001.

Balian, H. G. and Eddy, N. W. *Figure-of-merit (FOM), an improved criterion over the normalized chi-squared test for assessing goodness-of-fit of gamma-ray spectral peaks*. Nuclear Instruments and Methods, 145(2): 389–395, 1977.

Ballarini, M., Wallinga, J., Wintle, A. G., and Bos, A. J. J. *Analysis of equivalent-dose distributions for single grains of quartz from modern deposits*. Quaternary Geochronology, 2(1-4): 77–82, 2007.

Bevington, P. R. and Robinson, D. K. *Data Reduction and Error Analysis for the Physical Sciences*. McGraw-Hill Education, 2002. pp194–195.

Bluszcz, A., Adamiec, G., and Heer, A. J. *Estimation of equivalent dose and its uncertainty in the OSL SAR protocol when count numbers do not follow a Poisson distribution*. Radiation Measurements, 81: 46–54, 2015.

Bos, A. J. J., Piters, T. M., Gómez-Ros, J. M., and Delgado, A. *An Intercomparison of Glow Curve Analysis Computer Programs: II. Measured Glow Curves*. Radiation Protection Dosimetry, 51(4): 257–264, 1994.

Burbidge, C. I., Duller, G. A. T., and Roberts, H. M. *D_e determination for young samples using the standardised OSL response of coarse-grain quartz*. Radiation Measurements, 41(3): 278–288, 2006.

Douka, K., Jacobs, Z., Lane, C., Grün, R., Farr, L., Hunt, C., Inglis, R. H., Reynolds, T., Albert, P., Aubert, M., Cullen, V., Hill, E., Kinsley, L., Roberts, R. G., Tomlinson, E. L., Wulf, S., and Barker, G. *The chronostratigraphy of the Haua Fteah cave (Cyrenaica, northeast Libya)*. Journal of Human Evolution, 66: 39–63, 2014.

Duller, G. A. T. *Distinguishing quartz and feldspar in single grain luminescence measurements*. Radiation Measurements, 37(2): 161–165, 2003.

Duller, G. A. T. *Assessing the error on equivalent dose estimates derived from single aliquot regenerative dose measurements*. Ancient TL, 25(1): 15–24, 2007.

Duller, G. A. T. *Single-grain optical dating of Quaternary sediments: why aliquot size matters in luminescence dating*. Boreas, 37(4): 589–612, 2008.

Duller, G. A. T. *Improving the accuracy and precision of equivalent doses determined using the optically stimulated luminescence signal from single grains of quartz*. Radiation Measurements, 47(9): 770–777, 2012.

Duller, G. A. T. *The Analyst software package for luminescence data: overview and recent improvements* . Ancient TL, 33(1): 35–42, 2015.

Duller, G. A. T., Bøtter-Jensen, L., and Murray, A. S. *Optical dating of single sand-sized grains of quartz: sources of variability*. Radiation Measurements, 32(5-6): 453–457, 2000.

Durcan, J. A. and Duller, G. A. T. *The fast ratio: A rapid measure for testing the dominance of the fast component in the initial OSL signal from quartz*. Radiation Measurements, 46(10): 1065–1072, 2011.

Feathers, J. K. *Single-grain OSL dating of sediments from the Southern High Plains, USA*. Quaternary Science Reviews, 22(10-13): 1035–1042, 2003.

Fu, X., Li, B., and Li, S. H. *Testing a multi-step post-IR IRSL dating method using polymineral fine grains from Chinese loess*. Quaternary Geochronology, 10: 8–15, 2012.

Fu, X., Cohen, T. J., and Arnold, L. J. *Extending the record of lacustrine phases beyond the last interglacial for Lake Eyre in central Australia using luminescence dating*. Quaternary Science Reviews, 162: 88–110, 2017.

Galbraith, R. F. *Graphical Display of Estimates Having Differing Standard Errors*. Technometrics, 30(3): 271–281, 1988.

Galbraith, R. F. *A note on the variance of a background-corrected OSL count*. Ancient TL, 20(2): 49–51, 2002.

Galbraith, R. F. and Roberts, R. G. *Statistical aspects of equivalent dose and error calculation and display in OSL dating: An overview and some recommendations*. Quaternary Geochronology, 11: 1–27, 2012.

Galbraith, R. F., Roberts, R. G., Laslett, G. M., Yoshida, H., and Olley, J. M. *Optical dating of single and multiple grains of Quartz from Jinmium Rock Shelter, Northern Australia: Part I, Experimental design and statistical models*. Archaeometry, 41(2): 339–364, 1999.

Guo, Y. J., Li, B., Zhang, J. F., Yuan, B. Y., Xie, F., and Roberts, R. G. *Luminescence ages for three 'Middle Palaeolithic' sites in the Nihewan Basin, northern China, and their archaeological and palaeoenvironmental implications*. Quaternary Research, 85(3): 456–470, 2016.

Guralnik, B., Li, B., Jain, M., Chen, R., Paris, R. B., Murray, A. S., Li, S. H., Pagonis, V., Valla, P. G., and Herman, F. *Radiation-induced growth and isothermal decay of infrared-stimulated luminescence from feldspar*. Radiation Measurements, 81: 224–231, 2015.

Horowitz, Y. S. and Yossian, D. *Computerised Glow Curve Deconvolution: Application to Thermoluminescence Dosimetry*. Radiation Protection Dosimetry, 60(1): 3–111, 1995.

Hu, G., Yi, C. L., Zhang, J. F., Liu, J. H., Jiang, T., and Li, S. H. *Late Quaternary glacial advances in the eastern Qilianshan, north-eastern Tibet, as inferred from luminescence dating of fluvioglacial sediments*. Journal of Quaternary Science, 31(6): 587–597, 2016.

Jacobs, Z., Duller, G. A. T., and Wintle, A. G. *Optical dating of dune sand from Blombos Cave, South Africa: II—single grain data*. Journal of Human Evolution, 44(5): 613–625, 2003.

Jacobs, Z., Duller, G. A. T., and Wintle, A. G. *IInterpretation of single grain D_e distributions and calculation of D_e*. Radiation Measurements, 41(3): 264–277, 2006.

Jacobs, Z., Li, B., Jankowski, N., and Soressi, M. *Testing of a single grain OSL chronology across the Middle to Upper Palaeolithic transition at Les Cates (France)*. Journal of Archaeological Science, 54: 110–122, 2015.

Jacobs, Z., Li, B., Farr, L., Hill, E., Hunt, C., Jones, S., Rabett, R., Reynolds, T., Roberts, R. G., Simpson, D., and Barker, G. *The chronostratigraphy of the Haua Fteah cave (Cyrenaica, northeast Libya) - Optical dating of early human occupation during Marine Isotope Stages 4, 5 and 6*. Journal of Human Evolution, 105: 69–88, 2017.

Kreutzer, S., Schmidt, C., Fuchs, M., Dietze, M., Fischer, M., and Fuchs, M. *Introducing an R package for luminescence dating analysis* . Ancient TL, 30(1): 1–8, 2012.

Lai, Z. P. *Testing the use of an OSL standardised growth curve (SGC) for D_e determination on quartz from the Chinese Loess Plateau*. Radiation Measurements, 41(1): 9–16, 2006.

Li, B. *A note on estimating the error when subtracting background counts from weak OSL signals*. Ancient TL, 25(1): 9–14, 2007.

Li, B., Jacobs, Z., Roberts, R. G., and Li, S. H. *Extending the age limit of luminescence dating using the dose-dependent sensitivity of MET-pIRIR signals from K-feldspar*. Quaternary Geochronology, 17: 55–67, 2013.

Li, B., Roberts, R. G., Jacobs, Z., and Li, S. H. *A single-aliquot luminescence dating procedure for K-feldspar based on the dose-dependent MET-pIRIR signal sensitivity*. Quaternary Geochronology, 20: 51–64, 2014.

Li, B., Roberts, R. G., Jacobs, Z., and Li, S. H. *Potential of establishing a 'global standardised growth curve' (gSGC) for optical dating of quartz from sediments*. Quaternary Geochronology, 27: 94–104, 2015a.

Li, B., Roberts, R. G., Jacobs, Z., Li, S. H., and Guo, Y. J. *Construction of a 'global standardised growth curve' (gSGC) for infrared stimulated luminescence dating of K-feldspar*. Quaternary Geochronology, 27: 119–130, 2015b.

Li, B., Jacobs, Z., and Roberts, R. G. *Investigation of the applicability of standardised growth curves for OSL dating of quartz from Haua Fteah cave, Libya*. Quaternary Geochronology, 35: 1–15, 2016.

Long, H., Lai, Z. P., Fan, Q. S., Sun, Y. J., and Liu, X. J. *Applicability of a quartz OSL standardised growth curve for De determination up to 400Gy for lacustrine sediments from the Qaidam Basin of the Qinghai-Tibetan Plateau*. Quaternary Geochronology, 5(2-3): 212–217, 2010.

Madsen, A. T., Duller, G. A. T., Donnelly, J. P., Roberts, H. M., and Wintle, A. G. *A chronology of hurricane landfalls at Little Sippewissett Marsh, Massachusetts, USA, using optical dating*. Geomorphology, 109(1-2): 36–45, 2009.

Moré, J. J. *The Levenberg-Marquardt algorithm: Implementation and theory*. In *Numerical Analysis*, pp. 105–116. Springer, Berlin, Heidelberg, 1978.

Murray, A. S. and Olley, J. M. *Precision and Accuracy in the optically stimulated luminescence dating of sedimentary quartz: a status review*. Geochronometria, 21: 1–16, 2002.

Murray, A. S. and Wintle, A. G. *Luminescence dating of quartz using an improved single-aliquot regenerative-dose protocol*. Radiation Measurements, 32(1): 57–73, 2000.

Pagonis, V. and Kitis, G. *On the Possibility of using Commercial Software Packages for Thermoluminescence Glow Curve Deconvolution Analysis*. Radiation Protection Dosimetry, 101(1–4): 93–98, 2002.

Peng, J. and Pagonis, V. *Simulating comprehensive kinetic models for quartz luminescence using the R program KMS*. Radiation Measurements, 86: 63–70, 2016.

Peng, J., Dong, Z., Han, F. Q., Long, H., and Liu, X. J. *R package numOSL: numeric routines for optically stimulated luminescence dating*. Ancient TL, 31(2): 41–48, 2013.

Peng, J., Pagonis, V., and Li, B. *On the intrinsic accuracy and precision of the standardised growth curve (SGC) and global-SGC (gSGC) methods for equivalent dose determination: A simulation study*. Radiation Measurements, 94: 53–64, 2016.

Roberts, H. M. and Duller, G. A. T. *Standardised growth curves for optical dating of sediment using multiple-grain aliquots*. Radiation Measurements, 38(2): 241–252, 2004.

Roberts, R. G., Jacobs, Z., Li, B., Jankowski, N. R., Cunningham, A. C., and Rosenfeld, A. B. *Optical dating in archaeology: thirty years in retrospect and grand challenges for the future*. Journal of Archaeological Science, 56: 41–60, 2015.

Shen, Z. and Mauz, B. *Estimating the equivalent dose of late Pleistocene fine silt quartz from the Lower Mississippi Valley using a standardized OSL growth curve*. Radiation Measurements, 46(8): 649–654, 2011.

Stevens, T., Armitage, S. J., Lu, H., and Thomas, D. S. G. *Examining the potential of high sampling resolution OSL dating of Chinese loess*. Quaternary Geochronology, 2(1–4): 15–22, 2007.

Telfer, M. W., Bateman, M. D., Carr, A. S., and Chase, B. M. *Testing the applicability of a standardized growth curve (SGC) for quartz OSL dating: Kalahari dunes, South African coastal dunes and Florida dune cordons*. Quaternary Geochronology, 3(1–2): 137–142, 2008.

Wintle, A. G. and Murray, A. S. *A review of quartz optically stimulated luminescence characteristics and their relevance in single-aliquot regeneration dating protocols*. Radiation Measurements, 41(4): 369–391, 2006.

Xie, Y. H. *Dynamic Documents with R and knitr*. Chapman & Hall/CRC Press, 2015. pp17–18.

Yang, L. H., Lai, Z. P., Long, H., and Zhang, J. R. *Construction of a quartz OSL standardised growth curve (SGC) for aeolian samples from the Horqin dunefield in northeastern China*. Geochronometria, 38(4): 391–396, 2011.

Reviewer

Lee Arnold

Ancient TL

40 Years of Ancient TL

Steve Sutton[1], Ian Bailiff[2], Didier Miallier[3], Geoff Duller[4], Regina DeWitt[5*]

[1]Department of Geophysical Sciences and Center for Advanced Radiation Sources, University of Chicago, Building 434A, 9700 South Cass Avenue, Argonne National Laboratory, Argonne, IL 60439, USA
[2]Department of Archaeology, Durham University, South Road, Durham, DH1 3LE, United Kingdom
[3]Clermont Université, Université Blaise Pascal, CNRS/IN2P3, Laboratoire de Physique Corpusculaire, BP 10448, F-63000 Clermont-Ferrand, France
[4]Aberystwyth Luminescence Research Laboratory, Department of Geography and Earth Sciences, Aberystwyth University, Ceredigion, United Kingdom SY23 3DB
[5]Department of Physics, East Carolina University, Howell Sciences C-209, 1000 E. 5th St., Greenville, NC, 27858, USA

*Corresponding Author: dewittr@ecu.edu

Abstract

The first issue of Ancient TL was published in September 1977, 40 years ago. The journal was started by the late David Zimmerman at Washington University in Missouri (USA) as an informal newsletter for thermoluminescence practitioners. Since then editors Steve Sutton (then Washington University; editor until 1984), Ian Bailiff (Durham, UK; 1984–1994), Didier Miallier (Clermont-Ferrand, France; 1995–2004), Geoff Duller (Aberystwyth, UK; 2004–2014) and Regina DeWitt (Greenville, NC, USA; since 2015) have continued the tradition and continually modernized the journal. Despite many changes the scope of the journal has been and still is to provide the luminescence and ESR community with ideas and essential information for laboratory work and serve as an outlet for community news.

Birth of the Ancient TL Newsletter and the Washington University TL Laboratory (1977–1984)

by Steve Sutton

Ancient TL began as an informal newsletter for thermoluminescence practitioners initiated in 1977 by David Zimmerman at Washington University (WU) in St. Louis, Missouri, USA (Figure 1). In the beginning, it was hand-typed (Figure 2, left; with camera-ready contributions included), duplicated, and mailed in hand-stuffed envelopes. It contained short articles, announcements, publication lists and job openings. The mailing list contained about 30 names.

But the story began long before that. A native of Wisconsin, David attended the University of Wisconsin at Madison where he received an MS degree. David did his doctoral work at Oxford University receiving his DPhil in 1970 for his thesis entitled "The dependence of thermoluminescence on energy and type of ionizing radiation and its significance for archaeologic age determination." He met his wife Joan there who was also completing a DPhil on thermoluminescence properties. Both were working in the Research Laboratory for Archaeology and the History of Art directed by Martin Aitken.

In 1971, David and Joan moved to the Physics Department at WU and even shared an office for a time. They worked in the McDonnell Center for the Space Sciences led by Robert Walker. Prof. Walker had an interest in dating methods stemming from his groundbreaking work on fission track methods (Fleischer et al., 1975). Prof. Walker enlisted both David and Joan (and others) to develop a TL lab primarily for studying the radiation and thermal histories of lunar samples being returned by the Apollo astronauts, but also to develop an archaeological dating capability.

The TL effort was supported by NASA and NSF research grants. In 1973, the WU group received a NSF-EAR grant entitled "Study of Geological Materials by the Methods of Particle Tracks, Thermoluminescence and Rare Gases." which together with NASA support got the TL effort going. The NSF support was ongoing through the early 80s. There was also an NSF-Anthropology grant in 1979 on "TL Dating

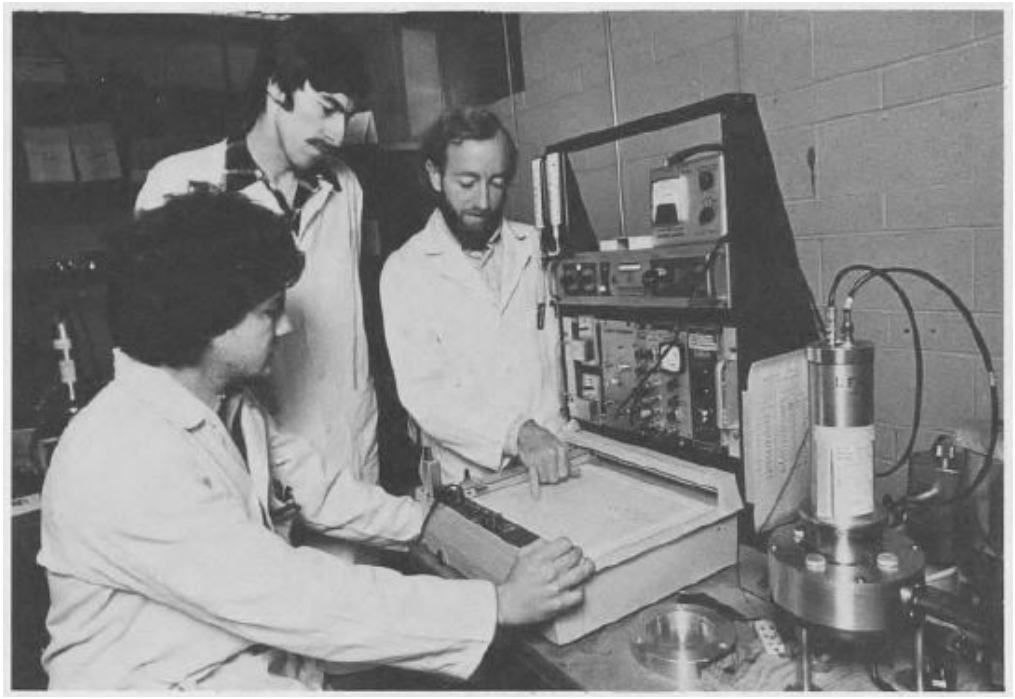

Figure 1. The late David W. Zimmerman (far right), senior research associate in physics and director of the Center for Archaeometry, studies a "glow" test for dating an ancient object with Charles Melcher (seated), a graduate student in physics, and Steve Sutton, space engineer, McDonnell Center for the Space Sciences. Reprinted from Washington University Record (Book 120, 1978)

in Archaeology" with Walker as the Principal Investigator. In the early 70s, there was a diverse array of TL projects ongoing, many related to PhD theses. The "extraterrestrial" component was measuring lunar rocks and cores (Phil Hoyt and Tony Plachy) as well as the radiation exposures of meteorites (Chuck Melcher). David was more interested in archaeological applications and was focusing on TL dating methods development with the help of Margie Yuhas and me.

Zimmerman's efforts led to the establishment in 1975 of "The Center for Archaeometry" at WU which formalized the activities related to the application of scientific methods in art and archaeology. The Center involved not only the TL dating effort but also an art conservation collaboration already in progress involving a local conservator (Phoebe Weil), and WU chemists (Peter Gaspar), anthropologists (Patty Jo Watson) and physicists (Walker) (see accompanying WU Record

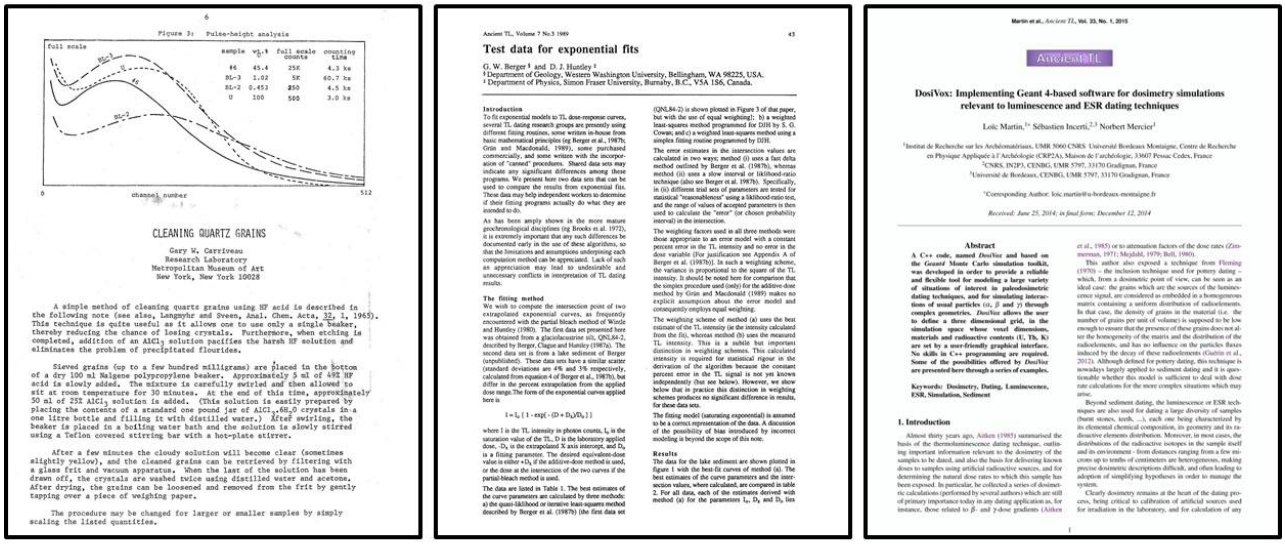

CLEANING QUARTZ GRAINS

Gary W. Carriveau
Research Laboratory
Metropolitan Museum of Art
New York, New York 10028

Test data for exponential fits

G. W. Berger † and D. J. Huntley ‡
† Department of Geology, Western Washington University, Bellingham, WA 98225, USA.
‡ Department of Physics, Simon Fraser University, Burnaby, B.C., V5A 1S6, Canada.

DosiVox: Implementing Geant 4-based software for dosimetry simulations relevant to luminescence and ESR dating techniques

Loïc Martin,[1,*] Sébastien Incerti,[2,3] Norbert Mercier[1]

Figure 2. Example pages from the very first issue from 1977 (left), Vol. 7 no. 3 from 1989 (center) and Vol. 33 no.1 from 2015 (right)

article in Supplement 1). Other members included curators of the St. Louis Art Museum just down the road (Richard Cleveland, Lee Parsons), an association that led to rewarding TL dating/authentication applications. The Ancient TL newsletter grew out of this Center.

When David died in November of 1978 (see accompanying WU Record article in Supplement 2), I continued producing the newsletter. I worked on various TL projects including dating Midwest shards for National Park Service and completed a PhD on TL of shocked rocks from Meteor Crater including dating the crater.

Ancient TL Vol. 2 no. 1 (1984) was the last issue published by WU at which point I moved on to other research and Ian Bailiff (Univ. of Durham, UK, Figure 3) took over as editor. The TL apparatus was donated to William Cassidy at the University of Pittsburgh who was leading the ANSMET project, the US Antarctic meteorite search.

The birth of Ancient TL was an exciting time at Washington University and I will always remember it fondly.

Ancient TL in Durham (1984–1994)

by Ian Bailiff

It was with some hesitation that I agreed to be persuaded by Ann Wintle to take over the production of Ancient TL from Martin Aitken who was acting as the Editorial Caretaker while a new home was found for the newsletter. At that time my laboratory was based in the attic room of the Fulling Mill on the banks of the River Wear in Durham and, although in an idyllic setting, it required a ca 50 m hike up the banks to reach my department and to access its resources. This was towards the end of an era where even the innovative development of "word processing" was something done on an electric typewriter where the typist often needed an array of "golf ball" type heads to type anything more sophisticated than an equals font. To produce the early issues, papers were re-typed, printed, cut blocks of text, insert headings with the now forgotten "Letraset", and all pasted with "artwork" (figures) onto master pages that were submitted for offset lithographic printing. Fortunately 1985 was the year a Mac landed on my desk and with the availability of Word we could set about page layout resembling the word processing packages of today (Figure 2, center), and we progressively made use of the advances provided by PCs and their word processing software. In 1989 we acted on an excellent suggestion made by Ashok Singhvi to help transform the newsletter into the format of a small journal by producing it within covers as a stapled booklet. At the outset of its move to Durham, the Editorial Board agreed to set up an open reviewing system and this provided the means to rapidly publishing material sent to the newsletter (as it was at that time). We also set up a system for publishing (thermo) luminescence dating results in the form of the Ancient TL Date List. During the decade of its production in Durham, Ancient TL was sustained by valuable contributions from members of our community as authors and reviewers, and it was intended that the publication should provide a platform for work that could be subsequently submitted to one of the major journals. As well as having the opportunity to air vexed issues such as functions fitted to dose response curves and present new ideas such as the lateral thinking of the Australian slide method, the beginnings of many aspects what we now take for granted - LED light stimulation sources for example - are also seen on the pages of Ancient TL.

Figure 3. Ian Bailiff

Ancient TL in Clermont-Ferrand (1995 - 2004)

by Didier Miallier

Ancient TL was edited by the TL group of Clermont-Ferrand in France (Laboratoire de Physique Corpusculaire, LPC, Université Blaise Pascal) between 1995 (Vol. 13 no. 1) and 2004 (Vol. 21 no. 2). Its production was held by a staff composed of Jean Faïn, Didier Miallier, Thierry Pilleyre and Serge Sanzelle. Jean Faïn (Figure 4) was responsible for finances. He very sadly left us on July 2nd 2010, and we want to take this opportunity to commemorate him. All those who met him, appreciated both his high human qualities and deep expertise in physics. We must also mention Ann Wintle who significantly helped us by compiling comprehensive bibliographic lists which were regularly published in Ancient TL.

Ancient TL at Clermont continued the preceding edition at Durham, as well in content as in presentation. We only just dared to slightly modify the colour of the title caption so as to personalize the Clermont edition. Incidentally, the first batch of printed covers ever produced appeared to have a basis weight which was too high for being correctly assembled with the inner pages, so that we had to order lighter ones. Consequently, our stock of unused wrong covers still provides us with convenient folders. We were not specialists in page layout, and therefore the presentation of the articles was

Figure 4. Jean Faïn

often the result of a plodding fight with a word-processing program that we did not completely control.

In 1995, the number of subscribers, either institutional or individual, was 47 from about 20 different countries. At the time, all correspondence took place by post, since e-mail was only at the onset of its reign, and many subscribers kindly used to stick nice stamps on the envelopes, for the pleasure of stamp collectors among our colleagues. Also, the manuscripts were recorded on diskettes, which were sent with more than a single stamp because they were heavier than a simple letter (thanks once again to the authors on behalf of stamp collectors !).

The first issue ever published in Clermont-Ferrand (1995), was introduced by a short "tribute to Ian Bailiff on his retirement as Editor", co-signed by Martin Aitken, Vagn Mejdahl and Ann Wintle, as members of the Editorial Board of Ancient TL. This tribute outlined that Ian had been Editor for a decade before passing on the torch to us, and that he had "substantially raised the publication's profile as well as its importance as a means of communication within the luminescence and ESR community". This tribute was concluded by a Welcome to the Clermont team "as worthy successors". We have been deeply touched by this mark of confidence.

To some extent, by transferring the edition of Ancient TL to Clermont Ferrand, Martin Aitken, Vagn Mejdahl and Ann Wintle also wanted to acknowledge their attachment to our region, Auvergne. Actually, the three of them had produced important scientific contributions based on cases from Auvergne. In 1973, Ann Wintle revealed, for the first time, the existence of anomalous fading with the thermoluminescence of feldpars from the volcanoes of the Chaîne des Puys, near Clermont-Ferrand. In 1979, the first successful attempt at dating ancient volcanoes by TL was done by Joan Huxtable and Martin Aitken in the surroundings of Clermont-Ferrand. Their results were published in Nature (Wintle, 1973; Huxtable et al., 1979). Also Martin came several times to Auvergne, from around 1975 onwards, for trying to elucidate the controversial archaeological settlement of Glozel, in close collaboration with Doreen Stoneham. At Glozel, they could meet Vagn Mejdhal, who involved himself very eagerly in the dating of the so-called Glozelian civilization.

Finally the last issue of Ancient TL ever published in Clermont (Vol. 21 no. 2), included a section News of the Community, saying that Martin Aitken had been appointed Doctor Honoris Causa of the University Blaise Pascal of Clermont-Ferrand. The same issue contained an obituary for Georges Valladas (1920–2004), a pioneer of TL dating, excellent scientist and a person of great human qualities. So Ancient TL tried — and still tries today — to be as well a link within the community, giving good and bad news, practical information, as a medium of diffusion of the progress in our field of interest.

We do not want to highlight any article that we are particularly happy to have published, because we were happy to publish all of them. From our own experience, any article, even seemingly of secondary importance, may be, years later, with a new look, at the origin of a new scientific adventure.

Ancient TL in Aberystwyth (2004-2014)

by Geoff Duller

Since starting as a PhD student, Ancient TL has been a valuable source of ideas and essential information for laboratory work. It was therefore with great pleasure that I accepted the role of editor, bringing the journal to Aberystwyth in 2004. Ann Wintle and Helen Roberts were also based at the Aberystwyth Luminescence Research Laboratory (Figure 5), and they provided invaluable support and advice in all aspects of the editing and production. Colleagues in Clermont-Ferrand who had previously edited the journal very kindly passed on an enormous amount of information, giving a sound footing for the first few issues to be published from Wales. The first major challenge was finding someone to print the journal, and fortunately the University printers agreed to undertake the short print runs at a very reasonable rate, enabling the cost of subscription to be kept as low as possible. Assessing the number of copies of each issue to print seemed very difficult (though in hindsight I cannot see why!), with the result that we normally had 30 to 50 copies left after dispatching the subscribed copies. These back is-

Figure 5. Geoff Duller (centre), Ann Wintle (left) and Helen Roberts (right) at the Aberystwyth Luminescence Research Laboratory 2009.

sues steadily built up, so that even to this day we have a large collection of boxes lining the upper shelves of one of the luminescence offices in Aberystwyth (if anyone is interested in having copies of any issues published from 2004 to 2014 they are welcome to have them for free by contacting me).

As an editor, I always found the variety of papers in Ancient TL stimulating. Papers about drilling systems for extracting luminescence samples from dunes (Munyikwa et al., 2011) were just as much a part of Ancient TL as those dealing with phosphorescence spectra from feldspars (Haidar & Huntley, 2007). However I found some of the most satisfying papers to handle were those dealing with aspects that underpin our science, such as the paper by Rhodes & Schwenninger (2007) putting down on record the data available for the radioactivity of the concrete blocks housed in Oxford that are used by many colleagues from around the world for calibration of their portable gamma spectrometers. Such papers are the foundation of our science, and Ancient TL plays a key role as a repository for this type of work.

In 2007 the 30th Anniversary of the journal was marked by a small editorial, but more significantly by making all the issues of Ancient TL freely available online. This involved scanning all the issues from 2003 back to 1977, and uploading PDFs of the issues published since 2004. Helena Rodnight and I shared the job of scanning these back issues. This was sometimes rapid, but the pace slowed when one came across an interesting paper that you had missed (or forgotten)! Ann Wintle had an excellent collection of hard copies of Ancient TL in her archive, though a number of key issues were missing. Fortunately Daniel Richter had copies of these missing issues, and you can still see that it is his copies of some of the earlier issues that are seen online. Making the journal freely available via the web was designed to increase accessibility and readership. In the first few years I was able to monitor the number of visits to the site and it was pleasing to see the rapid adoption of electronic access. Given the free electronic access, the number of paid subscriptions inevitably declined, such that the number of paying subscribers by the end of the time that the journal was published in Aberystwyth had declined to about 20. It was therefore no surprise when the last issue of Ancient TL published in Aberystwyth (Volume 32, Issue 2, December 2014) turned out to be the last issue to be published in hard copy, reflecting the changing nature of academic publishing.

Figure 6. Regina DeWitt

Ancient TL in Greenville, NC and future of the journal (since 2015)

by Regina DeWitt

When Geoff Duller asked if I (Figure 6) would be willing to serve as editor of Ancient TL, I was very excited. Ancient TL has published some of the most-cited manuscripts in our field (e.g. Adamiec & Aitken, 1998 with more than 600 citations) and I felt very honored to be able to continue this tradition. The first issue of Ancient TL published in Greenville, NC was Vol. 33, Issue 1, 2015. Since then Ancient TL has been available online only, free of charge. Geoff Duller thankfully passed on all his files for previous issues in a very well organized manner, which tremendously helped with setting up a new webpage. We slightly modified the layout of the front page (see cover pages in Figure 7) and adopted LaTeX for typesetting of the articles (Figure 2, right). This has significantly increased the workload of the editor, since typesetting of a manuscript in LaTeX can easily take 6–10 hours, sometimes more. Volunteer help has been invaluable in this endeavour. Despite some modernizations we aimed at remaining true to the purpose of the journal: Provide the luminescence and ESR community with ideas and essential information for laboratory work and serve as an outlet for community news.

Webpages for the journal have been located on the university servers at Aberystwyth and Greenville, respectively. As a result access is limited to the editor and space restrictions apply. To remedy these issues, we have secured a permanent domain: *ancienttl.org* We are in the process of moving the entire page to an external server that can be reached under the new address. This is a lengthy process, but once it is completed we can start to work on longtime plans. Volunteers will be able to get access to the new page to help with updating the page and establishing new online services. Future plans include: (1) get the journal indexed and included in data bases such as the Chemical Abstract Index, EBSCO, or Google Scholar; (2) add doi-numbers; (3) add online services such as a comprehensive compilation of luminescence and ESR related software packages or comparison of measurement procedures for quartz and feldspar.

At the LED 2017 in Cape Town the foundation of a trapped charge dating association has been suggested. The question arises what role Ancient TL will play in the society. Different possibilities can be envisioned. Over the last few years I have collected suggestions for improvements and fu-

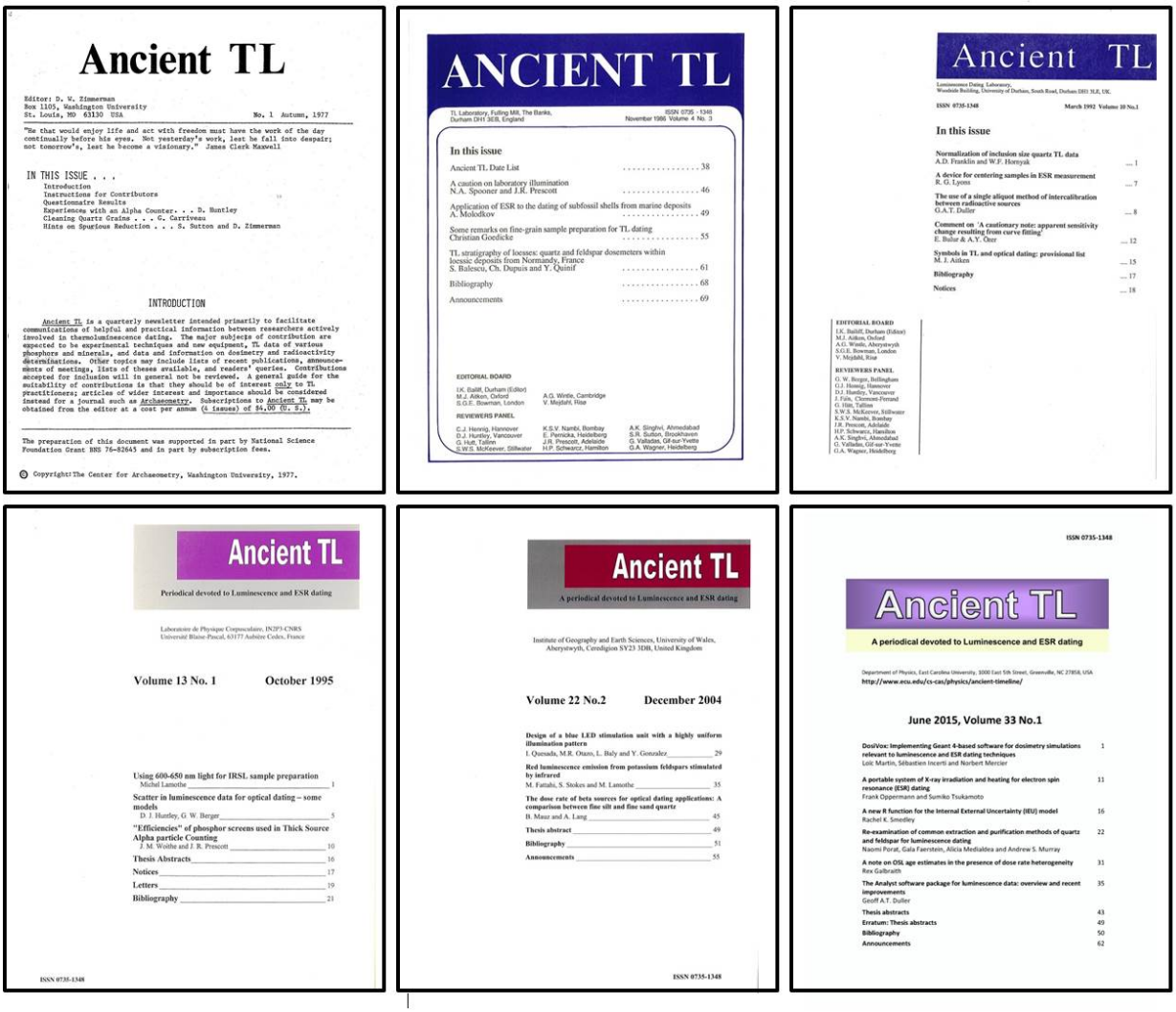

Figure 7. Evolution of the cover page of Ancient TL. From top left to bottom right: Issue 1, 1977; Vol. 4 no. 3, 1986; Vol. 10 no. 1, 1992; Vol. 13 no. 1, 1995; Vol. 22 no. 2, 2004; Vol. 33 no. 1, 2015

ture directions of the journal. Many comments concerned the fact that the journal does not have an impact factor and that the articles are not indexed by the Science Citation Index.

Thus, one route would be for Ancient TL to become an open access journal that has page charges. This could make Ancient TL financially viable and the journal could publish conference proceedings. An impact factor and indexing in the Science Citation Index would make the journal more attractive in a time, where productivity as a scientist is evaluated by number of peer reviewed articles in high-profile journals. This route would require Ancient TL being "incorporated" by some publisher, who will then take care of the actual publication process, including typesetting and webpage. It would also mean that Ancient TL could no longer perform the more diverse range of functions that it currently does (like thesis abstracts, conference announcements) and it would almost certainly lead to a drive by a publisher to reject a significant proportion of what is submitted in order to raise the impact factor.

A second route for Ancient TL is for it to become the official journal of the society, i.e. the Newsletter of the association, supported by funds from the society. Ancient TL would still perform all the functions that it currently does, and it would additionally be a forum for discussions/papers/proposals relating to Working Groups that the society may set up. This option would require more work for editor and volunteers, since no outside publisher would be involved, but all decisions about the content would be made by the editorial board. This option would not preclude the setting up of a new open access journal, or the continued use of existing journals. Over the last 40 years Ancient TL has evolved from a small newsletter to a repository for key-articles in the field of trapped charge dating. Its future role in the trapped charge dating association will have to be decided. However, Ancient TL has been and still is a journal by the community for the community. No matter in which direction the journal will head in the future, the goal should be to fulfill the needs of the community.

References

Adamiec, G. and Aitken, M. *Dose rate conversion factors: update*. Ancient TL, 16: 137–50, 1998.

Fleischer, R. L., Price, P. B., and Walker, R. M. *Nuclear Tracks in Solids: Principles and Applications*. University of California Press, 1975. 605 pages.

Haidar, S. and Huntley, D. *Phosphorescence spectra from alkali feldspars as they are cooled*. Ancient TL, 25: 49–52, 2007.

Huxtable, J., Aitken, M., and Bonhommet, N. *Thermoluminescent dating of sediment baked by lava flows of the Chaîne des Puys*. Nature, 275: 207–209, 1979.

Munyikwa, K., Telfer, M., Baker, I., and Knight, C. *Core drilling of Quaternary sediments for luminescence dating using the Dormer Drillmite^{TM}*. Ancient TL, 29: 15–23, 2011.

Rhodes, E. and Schwenninger, J.-L. *Dose rate and radioisotope concentrations in the concrete blocks at Oxford*. Ancient TL, 25: 5–8, 2007.

Washington University Record. *Washington University Record, November 30, 1978*, Book 120, 1978.

Wintle, A. *Anomalous Fading of Thermo-luminescence in Mineral Samples*. Nature, 245: 143–144, 1973.

Thesis Abstracts

Index

Weili Bi	p. 61
Michael Kenzler	p. 62
Anil Kumar	p. 62
Amit Kumar Prasad	p. 63

Weili Bi

Electron spin resonance dating of germanium center in quartz in glacial tills

December 2017

Institute of Tibetan Plateau Research, Chinese Academy of Sciences, Beijing, China

Degree: Ph.D.

Supervisors: Chaolu Yi, Haijun Yang

Electron spin resonance (ESR), provides a technique that plays an irreplaceable role in dating of quartz extracted from Quaternary deposits due to its wide dating time range. However, this technique used for dating of glacial till is limited due to lack of fundamental research in mechanisms of ESR signal depletion and test of independent dating. By using laboratory sunlight-grinding bleaching and field testing, this dissertation presents the results and conclusions of signal resetting of the germanium (Ge) center, correction of residual dose for moraine dating, and technical improvements in signal identification and measurement.

ESR dating of moraines is based on the supposition that either subglacial comminution or exposure to sunlight resets the signal. However, actual dating suggests that a signal that is initially present cannot be bleached to zero by grinding alone. We found that grinding coarse samples to fine sand reduced the signal intensity to 53-69 % of its original value. Exposure to sunlight for several days can reduce the signal intensity to 7-8 % of its original value within 1–2 mm depth of the polymineral sediment surface. However, within 5–8 mm of the sediment surface, exposure to sunlight for over one week only reduced the signal intensity to mean plateau values of 42–50 % of the initial value. The Ge signal in a modern till sample produced at 5400 m in the margin of an icecap in central Tibet is completely bleached. And the Ge signal in a modern sample in a basal moraine of a valley glacier in the Tianger Peak of the Tien Shan Mountain is partially bleached. It suggests that the level of bleaching varies spatially. Material which moraines initially deposited and which was subsequently overridden by sediments at the margins of ice caps or ice sheets may have been sufficiently exposed to sunlight to reset the clock to allow ESR dating of moraines.

The ESR signals in many sediments are not fully bleached before deposition and thus their ESR ages are overvalued. To solve this problem in fluvial and eolian sediments, residual signal intensity is reduced from the total signal intensity to correct ESR ages. However, it is not easy to determine the residual signal in glacial moraine. Here we propose that the residual dose in a modern moraine is subtracted from the total dose of a dated sample so as to correct ESR ages. The example shows that the ESR ages of tills without residual dose correction were 37.3-112.8 ka in the Tianger Peak area of the Tien Shan Mountains. After residual dose correction, the ages dropped and the corrected ESR ages are consistent with the results of 10Be surface exposure dating.

The signals in the Ge center in feldspar, mica, magnetic minerals and other heavy minerals occur in the same magnetic position as that in quartz. These signals from non-quartz minerals will interfere with the signal in quartz and therefore influence the quantification in ESR dating. Especially, feldspar has a significant impact on the signal of the Ge center in quartz due to its strong signal. In addition, the Ge signal in feldspar does not display the same decreasing trend as that in quartz when they are exposed to sunlight. The Ge signal of quartz decreases as exposure time increases. In contrast, the Ge signal of feldspar increases in the first four hours of exposure to sunlight and then decreases as the exposure time increases. After 34 to 62.5 hours of sunlight exposure, the EPR signal in feldspar reduced to 41.5-86.3 % of its original signal intensity. The procedure of heavy mineral separation and HF solution etching will greatly improve the purity of quartz.

Signal intensities in Ge and E centers in additionally irradiated samples is significantly and linearly correlated with quartz mass. Signal intensity for the Ge center is correlated with mass only if the mass is > 0.3 g for the sample without irradiation, and it is correlated with E center as the mass is reduced to < 0.45 g. The results provide a reference to general characteristics of some color centers in quartz responsive to mass increase, and also provide a solution of correction of signal intensity for the samples without sufficient mass.

We find that the smaller the microwave power, the higher the signal intensity of Ge center with the power between 0.02 to 5 mW. This abnormal phenomenon needs further study. We here suggest that small microwave power be used so as to increase ESR signal intensity to identify the weak signal in the Ge center.

Michael Kenzler

Ice-sheet dynamics and climate fluctuations during the Weichselian glaciation along the southwestern Baltic Sea coast

July 2017

Institute for Geography and Geology, University of Greifswald, Germany

Degree: Dr. rer. nat.
Supervisors: PD Dr Heiko Hüneke, Prof. Dr. Manfred Frechen

This thesis aims to develop a palaeogeographic and chronostratigraphic model of the southwestern Baltic Sea area, to improve our understanding of the depositional history of the Late Pleistocene on both a local and a transregional scale. New sedimentological, palaeontological and numerical age data are presented from three reference sites located at the coast of NE Germany. So far, the chronostratigraphic assignment of Saalian and Weichselian sediments of NE Germany has been based mainly on lithostratigraphic methods and on sparse numerical age data, resulting in a fragmentary age database. Modern sedimentological approaches, such as facies analyses, have been applied only at a few isolated profiles. Thus, a reliable reconstruction of the depositional environments and their stratigraphic positions is still missing for the study area, which makes the correlation between Pleistocene successions from NE Germany and other circum-Baltic regions problematic. To address these lithostratigraphic and geochronologic issues, three crucial profiles were re-investigated using a multiproxy approach, including sedimentological, geochronological, and palaeontological techniques. The Glowe and Kluckow sites are located on the peninsula of Jasmund (Rügen Island), whereas the Klein Klütz Höved (KKH) section is situated between Wismar and Travemünde at the coast of the Mecklenburg Bay. The age-constraining of critical horizons was conducted by luminescence dating of feldspar and quartz grain minerals. Together, these successions represent the Late Saalian to Late Weichselian period and give rise to the following picture.

The Glowe and Kluckow sections reveal that ice-free conditions dominated the study site between 47 and 42 ka. Deposition occurred in a steppe-like environment with moderate summers and cool winters. Meandering and braided river systems inhabited by various freshwater species, such as *Anodonta cygnea*, *Pisidium amnicum* and *Perca fluviatilis*, shaped the landscape. A subsequent cooling phase resulted in the establishment of a periglacial landscape and the formation of ice-wedges. This phase is shown in this thesis to be connected to the Klintholm advance documented at 34 $\pm$ 4 ka in Denmark. Furthermore, the data indicate the formation of a lacustrine basin during the transition of MIS 3 to MIS 2 under sub-arctic climate conditions. A potential link to the Kattegat ice advance (29–26 ka) will be proposed. At 23 $\pm$ 2 ka, the study area was characterised by proglacial and ice-contact lakes related to the Last Glacial Maximum ice advance of the Scandinavian Ice Sheet (SIS). This is the first documented SIS advance of Weichselian age, which reached Jasmund at 22 $\pm$ 2 ka.

The KKH sedimentary succession comprises deposits of Late Saalian to Late Weichselian age: after a period of deglaciation between ~139–134 ka (Termination II; MIS 6), which is preserved in a glaciofluvial sequence deposited in a braided river system, a lacustrine environment was established in an arctic to subarctic climate. During this time, the landscape was vegetated by typical Late Saalian flora communities. The Eemian interglacial is represented by lacustrine to brackish deposits covering the reference pollen zones 1 to 3. During this initial part of the Eemian, thermophile forest elements spread (*Quercus*, *Ulmus*), indicating a deciduous forest. The presence of brackish ostracods represents the influence of a marine transgression between 300 and 750 years after the beginning of the Eemian period. A hiatus of more than 90,000 years separates the Eemian from the overlying Late Weichselian sediments. During the Late Weichselian period, the deposition at KKH was dominated by glaciolacustrine and subglacial facies, where the first Weichselian ice advance occurred at 20 $\pm$ 2 ka.

The sedimentological and geochronological findings in this thesis provide valuable information for the reconstruction of the palaeoenvironmental history from the Late Saalian to Late Weichselian period. The Late Saalian palaeoenvironmental setting is reconstructed, including Termination II and the initial phase of the Eemian interglacial. Furthermore, the Eemian marine transgression is shown to have occurred 300 to 750 years after the beginning of this interglacial. The first proven Weichselian advance of the SIS approached NE Germany between ~23 and ~20 ka. In contrast, there is no evidence to support a pre-LGM advance of Weichselian age to the study area, as proposed by several authors, neither at Glowe and Kluckow, nor at the KKH site. Based on the presented results, and contra what was previously assumed, the MIS 3 Ristinge and Klintholm advance of the SIS, documented in Denmark, did not reach NE Germany.

A PDF of this thesis can be downloaded from: http://ub-ed.ub.uni-greifswald.de/opus/volltexte/2017/2848/pdf/diss_Kenzler_Michael.pdf

Anil Kumar

Late Quaternary landscape evolution along the Indus River: responses to climate and tectonics of Ladakh Himalaya

October 2016

Wadia Institute of Himalayan Geology, Dehradun, India

Degree: Ph.D.
Supervisor: Pradeep Srivastava

The upper Indus River flowing NW in a longitudinal valley along the SW edge of Tibet, Karakoram fault zone, Indus Tsangpo Suture Zone, Ladakh Batholith, and Zanskar ranges, represents a first order geomorphological feature

of Ladakh Himalaya. The Indus River, which arises from Mount Kailas and sinks into the Arabian Sea via the plains of Punjab (Pakistan), has a very large (1×10^6 km^2) catchment area.

Based on the longitudinal river profile and the stream length gradient index (SL index), ∼350 km stretch, the Indus River is divided into four segments. There are valley fill terraces in Segment I to III and one to two levels of strath terraces (T-2) with one cut-filled terrace (T-1) in Segment IV, which were used to calculate the aggradation and incision rates, respectively. The chronology of the channel bound and fan aggradation in Segment I to III, suggests that there are three pulses of wet phases at ∼16 ka, ∼28 ka and ∼52 ka, which facilitated fluvial aggradation. Hence aggradation was climatically controlled that occurred during the wetter phases in MIS-1 and MIS-3.

The SL index quantifies the variation in the bedrock erosion along a channel and any changes in this index indicate, (1) lithological contacts with varied erodibility, and/or (2) differential uplift along an active fault. In Segment-I, where, the Indus flows through the Indus Molasse, the SL index is low, whereas in Segment-II, between Kiari and Tirido, it attains higher values with batholith as bedrock. In the Segment-III, where channel follows the molasse-batholith contact, the SL values are again low. In Segment-IV, downstream of Spituk to Skyurbuchan, river cuts through the Indus Molasse, where the SL index increases and attains high values where the channel cutting into the Ladakh Batholith. SL index in Segment-IV exhibits an overall increasing trend. Ks for the Indus also shows a similar trend, which imply that the channel steepness is controlled by the active tectonic uplift and not by the bedrock erodibility. The chronology of the alluvial cover preserved over the strath terraces indicates incision of the order of 1.1–2.8 mm/a. The average incision rate from Nimu to Nurla is 1.8 mm/a and it increases downstream to 2.3 mm/a.

Putting together the height and chronology data of terraces helped in reconstructing the levels of paleo-riverbed profiles of Indus. The upper profile running at an average elevation of 134 ± 24 m arl has a central age of 62 ± 15 ka and an average incision rate of 2.2 ± 0.6 mm/a, whereas the lower profile at 45 ± 5 m arl has an age of 44 ± 8 ka and average erosion rate of 1.0 ± 0.2 mm/a. If we interpolate these reconstructed profiles upstream in the present river profile, then (i) the lower profile truncates upstream into the fill sequences preserved in the Segment-III (Leh valley) as both bear the same ages, (ii) the upper profile is older and the sediment of equivalent age might be present in the subsurface in Segment-III and upstream. This suggests that both lower and upper profiles are divergent downstream implying a base level fall in the downstream region.

Sand ramps of Ladakh provide composite records of wet and dry climate, e.g., the aeolian facies are represented relatively arid conditions while the fluvial facies and sedimentary hiatus (hard crust) and intra-dunal lakes facies are indicative of wetter climatic conditions. The deposition of hillslope debris also suggests the dominance of wetter conditions in the region. The OSL chronology on the studied sand ramps suggests that the ramp accumulation started prior to 44 ka and continued till ∼8 ka. The period between 25-17 ka and <12–8 ka was dominated by the aeolian activities in the Leh valley. At ∼12 ka, the formation of the intra-dunal lake and at 7 ka fluvial gullying suggest wetter climate. These subsequent dry and wet phases can be linked to variations in the ISM. The clay mineralogy from the Saboo sand ramp shows illite and chlorite throughout the profile, which supports physical weathering. Here one important inference is made that although climate fluctuated between wet and dry, a signal captured by iron mineralogy, the climatic fluctuations were limited to the threshold of alteration of clay mineralogy during the late Pleistocene in the Leh valley.

Amit Kumar Prasad

Understanding defect related luminescence processes in wide bandgap materials using low temperature multi-spectroscopic techniques

January 2017

Center for Nuclear Technologies, Technical University of Denmark, Risø Campus, Roskilde 4000

Degree: Ph.D.

Supervisors: Dr. Mayank Jain (main supervisor), Dr. Torben Lapp (co-supervisor)

Feldspar is a dominant, naturally occurring mineral that comprises about 60 % of the Earths crust. It is widely used in optically stimulated luminescence (OSL) dating of sediments to obtain chronologies of past events as old as ∼0.5 Ma, and thus, plays a crucial role in understanding Quaternary climate changes, landscape development and human evolution and dispersal. Optical properties of feldspar originate from a) a wide band gap (∼7.7 eV), b) crystal defects (impurity atoms and distortions) that create localized energy states within the bandgap, and c) conduction band and the low-mobility band tail states, which play a role in charge transport.

Despite a rapid progress in the infra-red stimulated luminescence (IRSL) dating technique using feldspar, a clear understanding of luminescence process is still lacking. A better understanding of feldspar as a physical system is expected to lead to its improved exploitation as a luminescence chronometer. My Ph.D. investigates the nature of luminescence generating defects and processes in feldspar, and tests whether the intra-defect relaxation transitions may be successfully used to improve the dating technique. It includes mapping the energy states of defects individually and characterizing their emission process, understanding the dynamics of the excited-state relaxation and tunneling, and defect interactions with the crystal lattice and the band tail states. The experiments were carried out using the Risø station for CryOgenic LUminescence Research (COLUR) and a high sensitive spectrometer attached to the Risø TL/OSL reader. The key findings of my Ph.D. research are summarize as follows:

1. I discovered the excitation-energy dependent emission (a red edge effect) in the green-orange emission in feldspar, and demonstrated that this effect arises from interaction of a deep lying defect with the band tail states. This effect can be used to measure the band-tail width through relatively simple spectroscopic (photoluminescence) measurements.

2. My studies on Fe^{3+} show that its deep red emission varies with site dependence of Fe^{3+} even within a single sample. Furthermore, it is observed that there exists an excitation-energy dependence of the main radiative transition ($^4T_1 \rightarrow {}^6A_1$) in Fe^{3+}; this is possibly related to spin-lattice interaction.

3. I explored a model analogue system for feldspar called YPO_4: Ce, Sm, in order to understand OSL produced by excited-state tunneling. For the first time, a precise mapping of the energy levels of the metastable Sm^{2+} was carried out, and the temperature-dependent relaxation lifetime of Sm^{2+} excited state was determined using the defects internal radiative-transition. It was then demonstrated that OSL decay curves resulting from optically induced, sub-conduction band electron transfer ($Sm^{2+} \rightarrow Ce^{4+}$) can be adequately described using the prevalent mathematical model of excited-state tunneling.

4. Finally, inspired by the results of YPO_4: Ce, Sm, I discovered a Stokes-shifted, infra-red photoluminescence (IRPL) signal arising from the principal trap in feldspar (excitation $\sim$ 1.4 eV (885 nm), emission: $\sim$ 1.3 eV (950 nm)). Current methods of OSL rely on transfer of electrons from the principal trap to holes located elsewhere in the lattice; this is by default a destructive readout of dosimetric information. Furthermore, OSL (or IRSL) suffer from sensitivity changes because of competition in the recombination process, leading to possible uncertainties in the dose measurement. In contrast to IRSL, the IRPL signal arises from intra-defect excitation and the subsequent radiative relaxation within the principle trap (i.e. the trap giving rise to IRSL). IRPL is a non-destructive readout technique and the lifetime of the excited state relaxation is estimated to be $\sim$40 s at 7K and $\sim$29 s at 295 K. The IRPL signal increases with dose and the preliminary dating investigations indicate that this signal contains an athermal non-fading component, likely arising from the trapped electrons that do not have a nearby hole center.

There are two important technique developments in my thesis. Firstly, based on the model of the red edge effect, a simple method is proposed for estimation of the width of the band tail states in feldspar. Secondly, it is shown that the new IRPL signal can be used for non-destructive probing of dosimetric information in the IR trap. The IRPL technique is likely to provide a) a robust understanding of the behavior of electron trapping centers in feldspar, b) a possibility of selective probe of non-fading electrons without using any thermal assistance, and c) precise measurements of luminescence from very small volumes by repeated readout. These possibilities open new windows for development of robust dating methods as well as advanced imaging techniques. I envision that the IRPL signal will significantly impact the field of optical dating.

A PDF of this thesis can be downloaded from: https://www.researchgate.net/profile/Amit_Prasad10 or http://orbit.dtu.dk

Bibliography

Compiled by Sebastien Huot

From 15th May 2017 to 1st December 2017

Various geological applications

- aeolian

Arbogast, A.F., Luehmann, M.D., William Monaghan, G., Lovis, W.A., Wang, H., 2017. Paleoenvironmental and geomorphic significance of bluff-top dunes along the Au Sable River in Northeastern Lower Michigan, USA. Geomorphology 297, 112-121, http://dx.doi.org/10.1016/j.geomorph.2017.09.017.

Guedes, C.C.F., Giannini, P.C.F., Sawakuchi, A.O., DeWitt, R., Paulino de Aguiar, V.Â., 2017. Weakening of northeast trade winds during the Heinrich stadial 1 event recorded by dune field stabilization in tropical Brazil. Quaternary Research 88, 369-381, http://dx.doi.org/10.1017/qua.2017.79.

Ho, L.-D., Lüthgens, C., Wong, Y.-C., Yen, J.-Y., Chyi, S.-J., 2017. Late Holocene cliff-top dune evolution in the Hengchun Peninsula of Taiwan: Implications for palaeoenvironmental reconstruction. Journal of Asian Earth Sciences 148, 13-30, http://dx.doi.org/10.1016/j.jseaes.2017.08.024.

Hu, G., Yu, L., Dong, Z., Lu, J., Li, J., Wang, Y., Lai, Z., 2018. Holocene aeolian activity in the Zoige Basin, northeastern Tibetan Plateau, China. Catena 160, 321-328, http://dx.doi.org/10.1016/j.catena.2017.10.005.

Huntley, D.H., Hickin, A.S., Lian, O.B., 2016. The pattern and style of deglaciation at the Late Wisconsinan Laurentide and Cordilleran ice sheet limits in northeastern British Columbia. Canadian Journal of Earth Sciences 54, 52-75, http://dx.doi.org/10.1139/cjes-2016-0066.

Long, H., Shen, J., Chen, J., Tsukamoto, S., Yang, L., Cheng, H., Frechen, M., 2017. Holocene moisture variations over the arid central Asia revealed by a comprehensive sand-dune record from the central Tian Shan, NW China. Quaternary Science Reviews 174, 13-32, http://dx.doi.org/10.1016/j.quascirev.2017.08.024.

Nartišs, M., Kalińska-Nartiša, E., 2017. An aeolian or a glaciolacustrine record? A case study from Mieļupīte, Middle Gauja Lowland, northeast Latvia. Geologos 23, 15, http://dx.doi.org/10.1515/logos-2017-0002.

Zeng, F., Liu, X., Li, X., E, C., 2017. Aquatic species dominate organic matter in Qinghai Lake during the Holocene: Evidence from eolian deposits around the lake. Journal of Earth Science 28, 484-491, http://dx.doi.org/10.1007/s12583-016-0926-x.

- alluvial fan

Mouslopoulou, V., Begg, J., Fülling, A., Moraetis, D., Partsinevelos, P., Oncken, O., 2017. Distinct phases of eustatic and tectonic forcing for late Quaternary landscape evolution in southwest Crete, Greece. Earth Surface Processes and Landforms 5, 511-527, http://dx.doi.org/10.5194/esurf-5-511-2017.

- coastal (in broad term)

Bampton, M., Kelley, A., Kelley, J., Jones, M., Bigelow, G., 2017. Little Ice Age catastrophic storms and the destruction of a Shetland Island community. Journal of Archaeological Science 87, 17-29, http://dx.doi.org/10.1016/j.jas.2017.08.003.

Brill, D., May, S.M., Shah-Hosseini, M., Rufer, D., Schmidt, C., Engel, M., 2017. Luminescence dating of cyclone-induced washover fans at Point Lefroy (NW Australia). Quaternary Geochronology 41, 134-150, http://dx.doi.org/10.1016/j.quageo.2017.03.004.

Dillenburg, S.R., Barboza, E.G., Rosa, M.L.C.C., Caron, F., Sawakuchi, A.O., 2017. The complex prograded Cassino barrier in southern Brazil: Geological and morphological evolution and records of climatic, oceanographic and sea-level changes in the last 7–6ka. Marine Geology 390, 106-119, http://dx.doi.org/10.1016/j.margeo.2017.06.007.

Massuanganhe, E.A., Berntsson, A., Risberg, J., Westerberg, L.-O., Christiansson, M., Preusser, F., Bjursäter, S., Achimo, M., 2018. Palaeogeography and dynamics of the deltaic wetland of Save River, Mozambique. Palaeogeography, Palaeoclimatology, Palaeoecology 489, 64-73, http://dx.doi.org/10.1016/j.palaeo.2017.09.021.

Nooren, K., Hoek, W.Z., Winkels, T., Huizinga, A., Van der Plicht, H., Van Dam, R.L., Van Heteren, S., Van Bergen, M.J., Prins, M.A., Reimann, T., Wallinga, J., Cohen, K.M., Minderhoud, P., Middelkoop, H., 2017. The Usumacinta–Grijalva beach-ridge plain in southern Mexico: a high-resolution archive of river discharge and precipitation. Earth Surface Processes and Landforms 5, 529-556, http://dx.doi.org/10.5194/esurf-5-529-2017.

Rémillard, A.M., St-Onge, G., Bernatchez, P., Hétu, B., Buylaert, J.-P., Murray, A.S., Lajeunesse, P., 2017. Relative sea-level changes and glacio-isostatic adjustment on the Magdalen Islands archipelago (Atlantic Canada) from MIS 5 to the late Holocene. Quaternary Science Reviews 171, 216-233, http://dx.doi.org/10.1016/j.quascirev.2017.07.015.

Simms, A.R., DeWitt, R., Zurbuchen, J., Vaughan, P., 2017. Coastal erosion and recovery from a Cascadia subduction zone earthquake and tsunami. Marine Geology 392, 30-40, http://dx.doi.org/10.1016/j.margeo.2017.08.009.

- coastal (estuary)

Rossi, V., Amorosi, A., Sarti, G., Mariotti, S., 2017. Late Quaternary multiple incised valley systems: An unusually well-preserved stratigraphic record of two interglacial valley-fill successions from the Arno Plain (northern Tuscany, Italy). Sedimentology 64, 1901-1928, http://dx.doi.org/10.1111/sed.12379.

- colluvial

Veit, H., Trauerstein, M., Preusser, F., Messmer, T., Gnägi, C., Zech, R., Wüthrich, L., 2017. Late Glacial/Early Holocene slope deposits on the Swiss Plateau: Genesis and palaeo-environment. CATENA 158, 102-112, http://dx.doi.org/10.1016/j.catena.2017.06.012.

Zhao, Q., Thomsen, K.J., Murray, A.S., Wei, M., Song, B., 2017. Single-grain quartz OSL dating of debris flow deposits from Men Tou Gou, south west Beijing, China. Quaternary Geochronology 41, 62-69, http://dx.doi.org/10.1016/j.quageo.2017.06.001.

- earthquake (and fault related)

Bergen, K.J., Shaw, J.H., Leon, L.A., Dolan, J.F., Pratt, T.L., Ponti, D.J., Morrow, E., Barrera, W., Rhodes, E.J., Murari, M.K., Owen, L.A., 2017. Accelerating slip rates on the Puente Hills blind thrust fault system beneath metropolitan Los Angeles, California, USA. Geology 45, 227-230, http://dx.doi.org/10.1130/g38520.1.

Charreau, J., Saint-Carlier, D., Dominguez, S., Lavé, J., Blard, P.-H., Avouac, J.-P., Jolivet, M., Chen, Y., Wang, S., Brown, N.D., Malatesta, L.C., Rhodes, E., 2017. Denudation outpaced by crustal thickening in the eastern Tianshan. Earth and Planetary Science Letters 479, 179-191, http://dx.doi.org/10.1016/j.epsl.2017.09.025.

Druzhinina, O., Bitinas, A., Molodkov, A., Kolesnik, T., 2017. Palaeoseismic deformations in the Eastern Baltic region (Kaliningrad District of Russia). Estonian Journal of Earth Sciences 66, 119–129, http://dx.doi.org/10.3176/earth.2017.09.

Gong, Z., Sun, J., Zhang, Z., Fu, B., Jia, Y., 2017. Optical dating of an offset river terrace sequence across the Karakax fault and its implication for the late Quaternary left-lateral slip rate. Journal of Asian Earth Sciences 147, 415-423, http://dx.doi.org/10.1016/j.jseaes.2017.07.013.

He, Z., Ma, B., Long, J., Zhang, H., Liang, K., Jiang, D., 2017. Recent ground fissures in the Hetao basin, Inner Mongolia, China. Geomorphology 295, 102-114, http://dx.doi.org/10.1016/j.geomorph.2017.07.008.

Olszak, J., 2017. Late Pleistocene dip-slip faulting along the Dunajec Fault, West Carpathians: Insights from alluvial sediments. Geomorphology 295, 749-757, http://dx.doi.org/10.1016/j.geomorph.2017.08.006.

Personius, S.F., Briggs, R.W., Maharrey, J.Z., Angster, S.J., Mahan, S.A., 2017. A paleoseismic transect across the northwestern Basin and Range Province, northwestern Nevada and northeastern California, USA. Geosphere 13, 782-810, http://dx.doi.org/10.1130/GES01380.1.

Philip, G., Suresh, N.P., Jayangondaperumal, R., 2017. Late Pleistocene-Holocene strain release by normal faulting along the Main Boundary Thrust at Logar in the northwestern Kumaon Sub Himalaya, India. Quaternary International, http://dx.doi.org/10.1016/j.quaint.2017.05.022.

Poujol, A., Ritz, J.-F., Vernant, P., Huot, S., Maate, S., Tahayt, A., 2017. Which fault destroyed Fes city (Morocco) in 1755? A new insight from the Holocene deformations observed along the southern border of Gibraltar arc. Tectonophysics 712-713, 303-311, http://dx.doi.org/10.1016/j.tecto.2017.05.036.

Rossetti, D.F., Valeriano, M.M., Gribel, R., Cohen, M.C.L., Tatumi, S.H., Yee, M., 2017. The imprint of Late Holocene tectonic reactivation on a megafan landscape in the northern Amazonian wetlands. Geomorphology 295, 406-418, http://dx.doi.org/10.1016/j.geomorph.2017.07.026.

Warrell, K.F., Cox, R.T., Hatcher Jr., R.D., Vaughn, J.D., Counts, R., 2017. Paleoseismic Evidence for Multiple Mw≥6 Earthquakes in the Eastern Tennessee Seismic Zone during the Late Quaternary. Bulletin of the Seismological Society of America 107, 1610-1624, http://dx.doi.org/10.1785/0120160161.

Weissl, M., Hintersberger, E., Lomax, J., Lüthgens, C., Decker, K., 2017. Active tectonics and geomorphology of the Gaenserndorf Terrace in the Central Vienna Basin (Austria). Quaternary International 451, 209-222, http://dx.doi.org/10.1016/j.quaint.2016.11.022.

Yang, H., Yang, X., Huang, X., Li, A., Huang, W., Zhang, L., 2018. New constraints on slip rates of the Fodongmiao-Hongyazi fault in the Northern Qilian Shan, NE Tibet, from the 10Be exposure dating of offset terraces. Journal of Asian Earth Sciences 151, 131-147, http://dx.doi.org/10.1016/j.jseaes.2017.10.034.

- fluvial

Bhattacharya, F., Shukla, A.D., Patel, R.C., Rastogi, B.K., Juyal, N., 2017. Sedimentology, geochemistry and OSL dating of the alluvial succession in the northern Gujarat alluvial plain (western India) - A record to evaluate the sensitivity of a semiarid fluvial system to the climatic and tectonic forcing since the late Marine Isotopic Stage 3. Geomorphology 297, 1-19, http://dx.doi.org/10.1016/j.geomorph.2017.08.046.

Chamberlain, E.L., Wallinga, J., Reimann, T., Goodbred Jr, S.L., Steckler, M.S., Shen, Z., Sincavage, R., 2017. Luminescence dating of delta sediments: Novel approaches explored for the Ganges-Brahmaputra-Meghna Delta. Quaternary Geochronology 41, 97-111, http://dx.doi.org/10.1016/j.quageo.2017.06.006.

Daley, J., Croke, J., Thompson, C., Cohen, T., Macklin, M., Sharma, A., 2017. Late Quaternary channel and floodplain formation in a partly confined subtropical river, eastern Australia. Journal of Quaternary Science 32, 729-743, http://dx.doi.org/10.1002/jqs.2930.

Foster, M.A., Anderson, R.S., Gray, H.J., Mahan, S.A., 2017. Dating of river terraces along Lefthand Creek, western High Plains, Colorado, reveals punctuated incision. Geomorphology 295, 176-190, http://dx.doi.org/10.1016/j.geomorph.2017.04.044.

Gliganic, L.A., Cohen, T.J., Meyer, M., Molenaar, A., 2017. Variations in luminescence properties of quartz and feldspar from modern fluvial sediments in three rivers. Quaternary Geochronology 41, 70-82, http://dx.doi.org/10.1016/j.quageo.2017.06.005.

Hughes, K., Croke, J., 2017. How did rivers in the wet tropics (NE Queensland, Australia) respond to climate changes over the past 30 000 years? Journal of Quaternary Science 32, 744-759, http://dx.doi.org/10.1002/jqs.2956.

Jia, L., Hu, D., Wu, H., Zhao, X., Chang, P., You, B., Zhang, M., Wang, C., Ye, M., Wu, Z., Liang, X., 2017. Yellow River terrace sequences of the Gonghe–Guide section in the northeastern Qinghai–Tibet: Implications for plateau uplift. Geomorphology 295, 323-336, http://dx.doi.org/10.1016/j.geomorph.2017.06.007.

Kasse, C., Van Balen, R.T., Bohncke, S.J.P., Wallinga, J., Vreugdenhil, M., 2017. Climate and base-level controlled fluvial system change and incision during the last glacial–interglacial transition, Roer river, the Netherlands – western Germany. Netherlands Journal of Geosciences 96, 71-92, http://dx.doi.org/10.1017/njg.2016.50.

Kothyari, G.C., Shukla, A.D., Juyal, N., 2017. Reconstruction of Late Quaternary climate and seismicity using fluvial landforms in Pindar River valley, Central Himalaya, Uttarakhand, India. Quaternary International 443, Part B, 248-264, http://dx.doi.org/10.1016/j.quaint.2016.06.001.

Kumar, A., Srivastava, P., 2017. The role of climate and tectonics in aggradation and incision of the Indus River in the Ladakh Himalaya during the late Quaternary. Quaternary Research 87, 363-385, http://dx.doi.org/10.1017/qua.2017.19.

Kumar, A., Srivastava, P., Meena, N.K., 2017. Late Pleistocene aeolian activity in the cold desert of Ladakh: A record from sand ramps. Quaternary International 443, 13-28, http://dx.doi.org/10.1016/j.quaint.2016.04.006.

Machado, M.J., Medialdea, A., Calle, M., Rico, M.T., Sánchez-Moya, Y., Sopeña, A., Benito, G., 2017. Historical palaeohydrology and landscape resilience of a Mediterranean rambla (Castellón, NE Spain): Floods and people. Quaternary Science Reviews 171, 182-198, http://dx.doi.org/10.1016/j.quascirev.2017.07.014.

Ngangom, M., Bhandari, S., Thakkar, M.G., Shukla, A.D., Juyal, N., 2017. Mid-Holocene extreme hydrological events in the eastern Great Rann of Kachchh, western India. Quaternary International 443, Part B, 188-199, http://dx.doi.org/10.1016/j.quaint.2016.10.017.

Olszak, J., 2017. Climatically controlled terrace staircases in uplifting mountainous areas. Global and Planetary Change 156, 13-23, http://dx.doi.org/10.1016/j.gloplacha.2017.07.013.

Resmi, M.R., Achyuthan, H., Jaiswal, M.K., 2017. Middle to late Holocene paleochannels and migration of the Palar River, Tamil Nadu: Implications of neotectonic activity. Quaternary International 443, 211-222, http://dx.doi.org/10.1016/j.quaint.2016.05.002.

Rosenwinkel, S., Landgraf, A., Schwanghart, W., Volkmer, F., Dzhumabaeva, A., Merchel, S., Rugel, G., Preusser, F., Korup, O., 2017. Late Pleistocene outburst floods from Issyk Kul, Kyrgyzstan? Earth Surface Processes and Landforms 42, 1535-1548, http://dx.doi.org/10.1002/esp.4109.

Salcher, B.C., Frank-Fellner, C., Lomax, J., Preusser, F., Ottner, F., Scholger, R., Wagreich, M., 2017. Middle to Late Pleistocene multi-proxy record of environmental response to climate change from the Vienna Basin, Central Europe (Austria). Quaternary Science Reviews 173, 193-210, http://dx.doi.org/10.1016/j.quascirev.2017.08.014.

Sant'Anna, L.G., Soares, E.A.d.A., Riccomini, C., Tatumi, S.H., Yee, M., 2017. Age of depositional and weathering events in Central Amazonia. Quaternary Science Reviews 170, 82-97, http://dx.doi.org/10.1016/j.quascirev.2017.06.015.

Singh, A.K., Pattanaik, J.K., Gagan, Jaiswal, M.K., 2017. Late Quaternary evolution of Tista River terraces in Darjeeling-Sikkim-Tibet wedge: Implications to climate and tectonics. Quaternary International 443, 132-142, http://dx.doi.org/10.1016/j.quaint.2016.10.004.

Thokchom, S., Bhattacharya, F., Durga Prasad, A., Dogra, N.N., Rastogi, B.K., 2017. Paleoenvironmental implications and drainage adjustment in the middle reaches of the Sabarmati river, Gujarat: Implications towards hydrological variability. Quaternary International 454, 1-14, http://dx.doi.org/10.1016/j.quaint.2017.07.026.

Thomas, D.S.G., Durcan, J.A., Dansie, A., Wiggs, G.F.S., 2017. Holocene fluvial valley fill sources of atmospheric mineral dust in the Skeleton Coast, Namibia. Earth Surface Processes and Landforms 42, 1884-1894, http://dx.doi.org/10.1002/esp.4151.

Wang, Z., Meyer, M.C., Gliganic, L.A., Hoffmann, D.L., May, J.-H., 2017. Timing of fluvial terrace formation and concomitant travertine deposition in the upper Sutlej River (Tirthapuri, southwestern Tibet) and paleoclimatic implications. Quaternary Science Reviews 169, 357-377, http://dx.doi.org/10.1016/j.quascirev.2017.06.009.

Zhao, X., Wang, J., Wei, M., Lai, Z., Fan, M., Zhao, J., Pan, B., Zhao, Y., Li, X., Zhao, Q., 2017. Optically stimulated luminescence dating of Holocene palaeoflood deposits in the middle reach of the Yongding River, China. Quaternary International 453, 37-47, http://dx.doi.org/10.1016/j.quaint.2017.02.013.

- glacial and periglacial

Ashastina, K., Schirrmeister, L., Fuchs, M., Kienast, F., 2017. Palaeoclimate characteristics in interior Siberia of MIS 6–2: first insights from the Batagay permafrost mega-thaw slump in the Yana Highlands. Climate of the Past 13, 795-818, http://dx.doi.org/10.5194/cp-13-795-2017.

Hooke, R.L., Hanson, P.R., 2017. Late- and Post-glacial history of the East Branch of the Penobscot River, Maine, USA. Atlantic Geology 53, 285-300, http://dx.doi.org/10.4138/atlgeol.2017.012.

Hu, G., Yi, C., Zhang, J., Dong, G., Liu, J., Xu, X., Jiang, T., 2017. Extensive glacial advances during the Last Glacial Maximum near the eastern Himalayan syntaxis. Quaternary International 443, 1-12, http://dx.doi.org/10.1016/j.quaint.2016.08.005.

Huntley, D.H., Hickin, A.S., Lian, O.B., 2016. The pattern and style of deglaciation at the Late Wisconsinan Laurentide and Cordilleran ice sheet limits in northeastern British Columbia. Canadian Journal of Earth Sciences 54, 52-75, http://dx.doi.org/10.1139/cjes-2016-0066.

Opel, T., Wetterich, S., Meyer, H., Dereviagin, A.Y., Fuchs, M.C., Schirrmeister, L., 2017. Ground-ice stable isotopes and cryostratigraphy reflect late Quaternary palaeoclimate in the Northeast Siberian Arctic (Oyogos Yar coast, Dmitry Laptev Strait). Climate of the Past 13, 587-611, http://dx.doi.org/10.5194/cp-13-587-2017.

Smedley, R.K., Chiverrell, R.C., Ballantyne, C.K., Burke, M.J., Clark, C.D., Duller, G.A.T., Fabel, D., McCarroll, D., Scourse, J.D., Small, D., Thomas, G.S.P., 2017. Internal dynamics condition centennial-scale oscillations in marine-based ice-stream retreat. Geology 45, 787-790, http://dx.doi.org/10.1130/G38991.1.

Yang, J., Chen, Y., Xu, X., Cui, Z., Xiong, H., 2017. Quaternary glacial history of the Kanas Valley, Chinese Altai, NW China, constrained by electron spin resonance and optically stimulated luminescence datings. Journal of Asian Earth Sciences 147, 164-177, http://dx.doi.org/10.1016/j.jseaes.2017.07.011.

- lacustrine

Ashley, G.M., Ndiema, E.K., Spencer, J.Q.G., Harris, J.W.K., Kiura, P.W., Dibble, L., Du, A., Lordan, P.T., 2017. Paleoenvironmental Reconstruction of Dongodien, Lake Turkana, Kenya and OSL Dating of Site Occupation During Late Holocene Climate Change. African Archaeological Review 34, 345-362, http://dx.doi.org/10.1007/s10437-017-9260-4.

Fan, Y., Wang, Y., Mou, X., Zhao, H., Zhang, F., Zhang, F., Liu, W., Hui, Z., Huang, X., Ma, J., 2017. Environmental status of the Jilantai Basin, North China, on the northwestern margin of the modern Asian summer monsoon domain during Marine Isotope Stage 3. Journal of Asian Earth Sciences 147, 178-192, http://dx.doi.org/10.1016/j.jseaes.2017.07.012.

Meyer-Jacob, C., Bindler, R., Bigler, C., Leng, M.J., Lowick, S.E., Vogel, H., 2017. Regional Holocene climate and landscape changes recorded in the large subarctic lake Torneträsk, N Fennoscandia. Palaeogeography, Palaeoclimatology, Palaeoecology 487, 1-14, http://dx.doi.org/10.1016/j.palaeo.2017.08.001.

Mischke, S., Lai, Z., Aichner, B., Heinecke, L., Mahmoudov, Z., Kuessner, M., Herzschuh, U., 2017. Radiocarbon and optically stimulated luminescence dating of sediments from Lake Karakul, Tajikistan. Quaternary Geochronology 41, 51-61, http://dx.doi.org/10.1016/j.quageo.2017.05.008.

Shi, X., Kirby, E., Furlong, K.P., Meng, K., Robinson, R., Lu, H., Wang, E., 2017. Rapid and punctuated Late Holocene recession of Siling Co, central Tibet. Quaternary Science Reviews 172, 15-31, http://dx.doi.org/10.1016/j.quascirev.2017.07.017.

Tibby, J., Barr, C., Marshall, J.C., McGregor, G.B., Moss, P.T., Arnold, L.J., Page, T.J., Questiaux, D., Olley, J., Kemp, J., Spooner, N., Petherick, L., Penny, D., Mooney, S., Moss, E., 2017. Persistence of wetlands on North Stradbroke Island (south-east Queensland, Australia) during the last glacial cycle: implications for Quaternary science and biogeography. Journal of Quaternary Science 32, 770-781, http://dx.doi.org/10.1002/jqs.2981.

- loess

Fitzsimmons, K.E., 2017. Reconstructing palaeoenvironments on desert margins: New perspectives from Eurasian loess and Australian dry lake shorelines. Quaternary Science Reviews 171, 1-19, http://dx.doi.org/10.1016/j.quascirev.2017.05.018.

Guérin, G., Antoine, P., Schmidt, E., Goval, E., Hérisson, D., Jamet, G., Reyss, J.-L., Shao, Q., Philippe, A., Vibet, M.-A., Bahain, J.-J., 2017. Chronology of the Upper Pleistocene loess sequence of Havrincourt (France) and associated Palaeolithic occupations: A Bayesian approach from pedostratigraphy, OSL, radiocarbon, TL and ESR/U-series data. Quaternary Geochronology 42, 15-30, http://dx.doi.org/10.1016/j.quageo.2017.07.001.

Hošek, J., Lisá, L., Hambach, U., Petr, L., Vejrostová, L., Bajer, A., Grygar, T.M., Moska, P., Gottvald, Z., Horsák, M., 2017. Middle Pleniglacial pedogenesis on the northwestern edge of the Carpathian basin: A multidisciplinary investigation of the Bíňa pedo-sedimentary section, SW Slovakia. Palaeogeography, Palaeoclimatology, Palaeoecology 487, 321-339, http://dx.doi.org/10.1016/j.palaeo.2017.09.017.

Ito, K., Tamura, T., Kudo, T., Tsukamoto, S., 2017. Optically stimulated luminescence dating of Late Pleistocene tephric loess intercalated with Towada tephra layers in northeastern Japan. Quaternary International 456, 154-162, http://dx.doi.org/10.1016/j.quaint.2017.06.070.

Klinge, M., Lehmkuhl, F., Schulte, P., Hülle, D., Nottebaum, V., 2017. Implications of (reworked) aeolian sediments and paleosols for Holocene environmental change in Western Mongolia. Geomorphology 292, 59-71, http://dx.doi.org/10.1016/j.geomorph.2017.04.027.

Tian, S., Sun, J., Gong, Z., 2017. Loess deposits in Beijing and their paleoclimatic implications during the last interglacial-glacial cycle. Quaternary Science Reviews 177, 78-87, http://dx.doi.org/10.1016/j.quascirev.2017.10.023.

Yang, H., Yang, X., Huang, X., Li, A., Huang, W., Zhang, L., 2018. New constraints on slip rates of the Fodongmiao-Hongyazi fault in the Northern Qilian Shan, NE Tibet, from the 10Be exposure dating of offset terraces. Journal of Asian Earth Sciences 151, 131-147, http://dx.doi.org/10.1016/j.jseaes.2017.10.034.

- meteorites

Bossin, L., Kazakis, N.A., Kitis, G., Tsirliganis, N.C., 2017. Thermoluminescence characteristics of a chondrite (Holbrook) and an aubrite achondrite (Norton County) meteorites. Applied Radiation and Isotopes 127, 26-34, http://dx.doi.org/10.1016/j.apradiso.2017.05.002.

- soil

Reimann, T., Román-Sánchez, A., Vanwalleghem, T., Wallinga, J., 2017. Getting a grip on soil reworking – Single-grain feldspar luminescence as a novel tool to quantify soil reworking rates. Quaternary Geochronology 42, 1-14, http://dx.doi.org/10.1016/j.quageo.2017.07.002.

- tephra

Sun, C., Liu, J., You, H., Nemeth, K., 2017. Tephrostratigraphy of Changbaishan volcano, northeast China, since the mid-Holocene. Quaternary Science Reviews 177, 104-119, http://dx.doi.org/10.1016/j.quascirev.2017.10.021.

- thermochronology

Brown, N.D., Rhodes, E.J., Harrison, T.M., 2017. Using thermoluminescence signals from feldspars for low-temperature thermochronology. Quaternary Geochronology 42, 31-41, http://dx.doi.org/10.1016/j.quageo.2017.07.006.

- volcanic

Schmidt, C., Schaarschmidt, M., Kolb, T., Büchel, G., Richter, D., Zöller, L., 2017. Luminescence dating of Late Pleistocene eruptions in the Eifel Volcanic Field, Germany. Journal of Quaternary Science 32, 628-638, http://dx.doi.org/10.1002/jqs.2961.

Schmidt, C., Tchouankoue, J.P., Nkouamen Nemzoue, P.N., Ayaba, F., Nformidah-Ndah, S.S., Nformi Chifu, E., 2017. New thermoluminescence age estimates for the Nyos maar eruption (Cameroon Volcanic Line). PLOS ONE 12, e0178545, http://dx.doi.org/10.1371/journal.pone.0178545.

Archaeology applications

Athanassas, C.D., García Sanjuán, L., Stamoulis, K., Lineros Romero, R., Carinou, E., Anglada Curado, R., 2017. Optically stimulated luminescence (OSL) dating of an enigmatic, megalithic-like, subterranean structure in Carmona (Seville, Spain). Journal of Archaeological Science: Reports 16, 240-247, http://dx.doi.org/10.1016/j.jasrep.2017.10.012.

Bampton, M., Kelley, A., Kelley, J., Jones, M., Bigelow, G., 2017. Little Ice Age catastrophic storms and the destruction of a Shetland Island community. Journal of Archaeological Science 87, 17-29, http://dx.doi.org/10.1016/j.jas.2017.08.003.

Been, E., Hovers, E., Ekshtain, R., Malinski-Buller, A., Agha, N., Barash, A., Mayer, D.E.B.-Y., Benazzi, S., Hublin, J.-J., Levin, L., Greenbaum, N., Mitki, N., Oxilia, G., Porat, N., Roskin, J., Soudack, M., Yeshurun, R., Shahack-Gross, R., Nir, N., Stahlschmidt, M.C., Rak, Y., Barzilai, O., 2017. The first Neanderthal remains from an open-air Middle Palaeolithic site in the Levant. Scientific Reports 7, 2958, http://dx.doi.org/10.1038/s41598-017-03025-z.

Benvenuti, M., Bahain, J.-J., Capalbo, C., Capretti, C., Ciani, F., D'Amico, C., Esu, D., Giachi, G., Giuliani, C., Gliozzi, E., Lazzeri, S., Macchioni, N., Lippi, M.M., Masini, F., Mazza, P.P.A., Pallecchi, P., Revedin, A., Savorelli, A., Spadi, M., Sozzi, L., Vietti, A., Voltaggio, M., Aranguren, B., 2017. Paleoenvironmental context of the early Neanderthals of Poggetti Vecchi for the late middle Pleistocene of Central Italy. Quaternary Research 88, 327-344, http://dx.doi.org/10.1017/qua.2017.51.

Blackwell, B.A.B., Skinner, A.R., Smith, J.R., Hill, C.L., Churcher, C.S., Kieniewicz, J.M., Adelsberger, K.A., Blickstein, J.I.B., Florentin, J.A., Deely, A.E., Spillar, K.V., 2017. ESR analyses for herbivore teeth and molluscs from Kharga, Dakhleh, and Bir Tarfawi Oases: Constraining water availability and hominin paleolithic activity in the Western Desert, Egypt. Journal of African Earth Sciences 136, 216-238, http://dx.doi.org/10.1016/j.jafrearsci.2017.07.007.

Clarkson, C., Jacobs, Z., Marwick, B., Fullagar, R., Wallis, L., Smith, M., Roberts, R.G., Hayes, E., Lowe, K., Carah, X., Florin, S.A., McNeil, J., Cox, D., Arnold, L.J., Hua, Q., Huntley, J., Brand, H.E.A., Manne, T., Fairbairn, A., Shulmeister, J., Lyle, L., Salinas, M., Page, M., Connell, K., Park, G., Norman, K., Murphy, T., Pardoe, C., 2017. Human occupation of northern Australia by 65,000 years ago. Nature 547, 306-310, http://dx.doi.org/10.1038/nature22968.

Cook, R.A., Sakai, S., Genheimer, R.A., 2017. Evaluating the utility of archaeological index fossils: Optically-stimulated luminescence dating of Fort Ancient Pottery at the Hahn Site. Journal of Archaeological Science: Reports 15, 132-137, http://dx.doi.org/10.1016/j.jasrep.2017.06.026.

Daura, J., Sanz, M., Allué, E., Vaquero, M., López-García, J.M., Sánchez-Marco, A., Domènech, R., Martinell, J., Carrión, J.S., Ortiz, J.E., Torres, T., Arnold, L.J., Benson, A., Hoffmann, D.L., Skinner, A.R., Julià, R., 2017. Palaeoenvironments of the last Neanderthals in SW Europe (MIS 3): Cova del Coll Verdaguer (Barcelona, NE of Iberian Peninsula). Quaternary Science Reviews 177, 34-56, http://dx.doi.org/10.1016/j.quascirev.2017.10.005.

Fitzsimmons, K.E., Iovita, R., Sprafke, T., Glantz, M., Talamo, S., Horton, K., Beeton, T., Alipova, S., Bekseitov, G., Ospanov, Y., Deom, J.-M., Sala, R., Taimagambetov, Z., 2017. A chronological framework connecting the early Upper Palaeolithic across the Central Asian piedmont. Journal of Human Evolution 113, 107-126, http://dx.doi.org/10.1016/j.jhevol.2017.07.006.

Frouin, M., Lahaye, C., Valladas, H., Higham, T., Debénath, A., Delagnes, A., Mercier, N., 2017. Dating the Middle Paleolithic deposits of La Quina Amont (Charente, France) using luminescence methods. Journal of Human Evolution 109, 30-45, http://dx.doi.org/10.1016/j.jhevol.2017.05.002.

Guérin, G., Antoine, P., Schmidt, E., Goval, E., Hérisson, D., Jamet, G., Reyss, J.-L., Shao, Q., Philippe, A., Vibet, M.-A., Bahain, J.-J., 2017. Chronology of the Upper Pleistocene loess sequence of Havrincourt (France) and associated Palaeolithic occupations: A Bayesian approach from pedostratigraphy, OSL,

radiocarbon, TL and ESR/U-series data. Quaternary Geochronology 42, 15-30, http://dx.doi.org/10.1016/j.quageo.2017.07.001.

Ideker, C.J., Finley, J.B., Rittenour, T.M., Nelson, M.S., 2017. Single-grain optically stimulated luminescence dating of quartz temper from prehistoric Intermountain Ware ceramics, northwestern Wyoming, USA. Quaternary Geochronology 42, 42-55, http://dx.doi.org/10.1016/j.quageo.2017.07.004.

Jin, J., Li, Z., Huang, Y., Jiang, F., Fan, X., Ling, Z., Cheng, Y., Xu, X., 2017. Chronology of a late Neolithic Age site near the southern coastal region of Fujian, China. The Holocene 27, 1265-1272, http://dx.doi.org/10.1177/0959683616687383.

Obreht, I., Hambach, U., Veres, D., Zeeden, C., Bösken, J., Stevens, T., Marković, S.B., Klasen, N., Brill, D., Burow, C., Lehmkuhl, F., 2017. Shift of large-scale atmospheric systems over Europe during late MIS 3 and implications for Modern Human dispersal. Scientific Reports 7, 5848, http://dx.doi.org/10.1038/s41598-017-06285-x.

Paz, Y., Ackermann, O., Avni, Y., Ben-Hur, M., Birkenfeld, M., Langgut, D., Mizrahi, A.-S., Weiss, E., Porat, N., 2017. An early bronze age fertilized agricultural plot discovered near Tel Yarmouth, Ramat Bet Shemesh, Israel. Journal of Archaeological Science: Reports 15, 226-234, http://dx.doi.org/10.1016/j.jasrep.2017.08.001.

Pereira, A., Nomade, S., Falguères, C., Bahain, J.-J., Tombret, O., Garcia, T., Voinchet, P., Bulgarelli, G.-M., Anzidei, A.-P., 2017. 40Ar/39Ar and ESR/U-series data for the La Polledrara di Cecanibbio archaeological site (Lazio, Italy). Journal of Archaeological Science: Reports 15, 20-29, http://dx.doi.org/10.1016/j.jasrep.2017.05.025.

Richard, M., Moreno, D., Bahain, J.J., Duval, M., Falguères, C., 2017. Electron spin resonance dating of fossil teeth : some basic guidelines to ensure optimal sampling conditions. Quaternaire 28, 155-159, http://dx.doi.org/10.4000/quaternaire.8003.

Richter, D., McPherron, S.P., Dibble, H., Goldberg, P., Sandgathe, D.S., 2017. Additional chronometric data for the small flake assemblages ('Asinipodian') from Pech de l'Azé IV (France) and a comparison with similar assemblages at the nearby site of Roc de Marsal, in: Wojtczak, D., Al Najiar, M., Jagher, R., Elsuede, H., Wegmüller, F., Otte, M. (Eds.), Vocation préhistoire. Hommage à Jean-Marie Le Tensorer. Études et Récherches archéologiques de l'Université de Liège 148, Liège, pp. 323-335.

Sánchez-Pardo, J.C., Blanco-Rotea, R., Sanjurjo-Sánchez, J., 2017. The church of Santa Comba de Bande and early medieval Iberian architecture: new chronological results. Antiquity 91, 1011-1026, http://dx.doi.org/10.15184/aqy.2017.83.

Sharma, S., Singh, P., 2017. Luminescence dating of Neolithic pottery in North East India. Current Science 113, http://dx.doi.org/10.18520/cs/v113/i03/492-496.

Westaway, K.E., Louys, J., Awe, R.D., Morwood, M.J., Price, G.J., Zhao, J.x., Aubert, M., Joannes-Boyau, R., Smith, T.M., Skinner, M.M., Compton, T., Bailey, R.M., van den Bergh, G.D., de Vos, J., Pike, A.W.G., Stringer, C., Saptomo, E.W., Rizal, Y., Zaim, J., Santoso, W.D., Trihascaryo, A., Kinsley, L., Sulistyanto, B., 2017. An early modern human presence in Sumatra 73,000–63,000 years ago. Nature 548, 322-325, http://dx.doi.org/10.1038/nature23452.

Zilhão, J., Anesin, D., Aubry, T., Badal, E., Cabanes, D., Kehl, M., Klasen, N., Lucena, A., Martín-Lerma, I., Martínez, S., Matias, H., Susini, D., Steier, P., Wild, E.M., Angelucci, D.E., Villaverde, V., Zapata, J., 2017. Precise dating of the Middle-to-Upper Paleolithic transition in Murcia (Spain) supports late Neandertal persistence in Iberia. Heliyon 3, e00435, http://dx.doi.org/10.1016/j.heliyon.2017.e00435.

Various ESR applications

Blackwell, B.A.B., Skinner, A.R., Smith, J.R., Hill, C.L., Churcher, C.S., Kieniewicz, J.M., Adelsberger, K.A., Blickstein, J.I.B., Florentin, J.A., Deely, A.E., Spillar, K.V., 2017. ESR analyses for herbivore teeth and molluscs from Kharga, Dakhleh, and Bir Tarfawi Oases: Constraining water availability and hominin paleolithic activity in the Western Desert, Egypt. Journal of African Earth Sciences 136, 216-238, http://dx.doi.org/10.1016/j.jafrearsci.2017.07.007.

Daura, J., Sanz, M., Allué, E., Vaquero, M., López-García, J.M., Sánchez-Marco, A., Domènech, R., Martinell, J., Carrión, J.S., Ortiz, J.E., Torres, T., Arnold, L.J., Benson, A., Hoffmann, D.L., Skinner, A.R., Julià, R., 2017. Palaeoenvironments of the last Neanderthals in SW Europe (MIS 3): Cova del Coll Verdaguer (Barcelona, NE of Iberian Peninsula). Quaternary Science Reviews 177, 34-56, http://dx.doi.org/10.1016/j.quascirev.2017.10.005.

Guérin, G., Antoine, P., Schmidt, E., Goval, E., Hérisson, D., Jamet, G., Reyss, J.-L., Shao, Q., Philippe, A., Vibet, M.-A., Bahain, J.-J., 2017. Chronology of the Upper Pleistocene loess sequence of Havrincourt (France) and associated Palaeolithic occupations: A Bayesian approach from pedostratigraphy, OSL, radiocarbon, TL and ESR/U-series data. Quaternary Geochronology 42, 15-30, http://dx.doi.org/10.1016/j.quageo.2017.07.001.

Jia, L., Hu, D., Wu, H., Zhao, X., Chang, P., You, B., Zhang, M., Wang, C., Ye, M., Wu, Z., Liang, X., 2017. Yellow River terrace sequences of the Gonghe–Guide section in the northeastern Qinghai–Tibet: Implications for plateau uplift. Geomorphology 295, 323-336, http://dx.doi.org/10.1016/j.geomorph.2017.06.007.

Murahashi, M., Toyoda, S., Hoshi, M., Ohtaki, M., Endo, S., Tanaka, K., Yamada, Y., 2017. The sensitivity variation of the radiation induced signal in deciduous teeth to be used in ESR tooth enamel dosimetry. Radiation Measurements 106, 450-454, http://dx.doi.org/10.1016/j.radmeas.2017.06.001.

Pereira, A., Nomade, S., Falguères, C., Bahain, J.-J., Tombret, O., Garcia, T., Voinchet, P., Bulgarelli, G.-M., Anzidei, A.-P., 2017. 40Ar/39Ar and ESR/U-series data for the La Polledrara di Cecanibbio archaeological site (Lazio, Italy). Journal of Archaeological Science: Reports 15, 20-29, http://dx.doi.org/10.1016/j.jasrep.2017.05.025.

Richard, M., Moreno, D., Bahain, J.J., Duval, M., Falguères, C., 2017. Electron spin resonance dating of fossil teeth : some basic guidelines to ensure optimal sampling conditions. Quaternaire 28, 155-159, http://dx.doi.org/10.4000/quaternaire.8003.

Rossi, V., Amorosi, A., Sarti, G., Mariotti, S., 2017. Late Quaternary multiple incised valley systems: An unusually well-preserved stratigraphic record of two interglacial valley-fill successions from the Arno Plain (northern Tuscany, Italy). Sedimentology 64, 1901-1928, http://dx.doi.org/10.1111/sed.12379.

Tsukamoto, S., Porat, N., Ankjærgaard, C., 2017. Dose recovery and residual dose of quartz ESR signals using modern sediments: Implications for single aliquot ESR dating. Radiation Measurements 106, 472-476, http://dx.doi.org/10.1016/j.radmeas.2017.02.010.

Westaway, K.E., Louys, J., Awe, R.D., Morwood, M.J., Price, G.J., Zhao, J.x., Aubert, M., Joannes-Boyau, R., Smith, T.M., Skinner, M.M., Compton, T., Bailey, R.M., van den Bergh, G.D., de Vos, J., Pike, A.W.G., Stringer, C., Saptomo, E.W., Rizal, Y., Zaim, J., Santoso, W.D., Trihascaryo, A., Kinsley, L., Sulistyanto, B., 2017. An early modern human presence in Sumatra 73,000–63,000 years ago. Nature 548, 322-325, http://dx.doi.org/10.1038/nature23452.

Yang, J., Chen, Y., Xu, X., Cui, Z., Xiong, H., 2017. Quaternary glacial history of the Kanas Valley, Chinese Altai, NW China, constrained by electron spin resonance and optically stimulated luminescence datings. Journal of Asian Earth Sciences 147, 164-177, http://dx.doi.org/10.1016/j.jseaes.2017.07.011.

Basic research

Autzen, M., Guérin, G., Murray, A.S., Thomsen, K.J., Buylaert, J.P., Jain, M., 2017. The effect of backscattering on the beta dose absorbed by individual quartz grains. Radiation Measurements 106, 491-497, http://dx.doi.org/10.1016/j.radmeas.2017.05.004.

Bossin, L., Kazakis, N.A., Kitis, G., Tsirliganis, N.C., 2017. Thermoluminescence characteristics of a chondrite (Holbrook) and an aubrite achondrite (Norton County) meteorites. Applied Radiation and Isotopes 127, 26-34, http://dx.doi.org/10.1016/j.apradiso.2017.05.002.

Chen, R., Pagonis, V., 2017. A model explaining the anomalous heating-rate effect in thermoluminescence as an inverse thermal quenching based on simultaneous thermal release of electrons and holes. Radiation Measurements 106, 20-25, http://dx.doi.org/10.1016/j.radmeas.2016.11.004.

Chithambo, M.L., Niyonzima, P., 2017. Radioluminescence of annealed synthetic quartz. Radiation Measurements 106, 35-39, http://dx.doi.org/10.1016/j.radmeas.2017.02.005.

Chruścińska, A., Kijek, N., Topolewski, S., 2017. Recent development in the optical stimulation of luminescence. Radiation Measurements 106, 13-19, http://dx.doi.org/10.1016/j.radmeas.2017.01.013.

Cunningham, A.C., Clark-Balzan, L., 2017. Overcoming crosstalk in luminescence images of mineral grains. Radiation Measurements 106, 498-505, http://dx.doi.org/10.1016/j.radmeas.2017.06.004.

Druzhyna, S., Datz, H., Oster, L., Lerch, M., Rosenfeld, A., Cullen, A., Orion, I., Horowitz, Y.S., 2017. Thermoluminescence dose response of photon irradiated NaCl: Unified interaction model analysis of the dependence of the supralinearity on photon energy. Radiation Measurements 106, 455-458, http://dx.doi.org/10.1016/j.radmeas.2017.02.004.

Friedrich, J., Fasoli, M., Kreutzer, S., Schmidt, C., 2017. The basic principles of quartz radiofluorescence dynamics in the UV – analytical, numerical and experimental results. Journal of Luminescence 192, 940-948, http://dx.doi.org/10.1016/j.jlumin.2017.08.012.

Galli, A., Artesani, A., Martini, M., Sibilia, E., Panzeri, L., Maspero, F., 2017. An empirical model of the sunlight bleaching efficiency of brick surfaces. Radiation Measurements 107, 67-72, http://dx.doi.org/10.1016/j.radmeas.2017.10.004.

Guérin, G., Christophe, C., Philippe, A., Murray, A.S., Thomsen, K.J., Tribolo, C., Urbanova, P., Jain, M., Guibert, P., Mercier, N., Kreutzer, S., Lahaye, C., 2017. Absorbed dose, equivalent dose, measured dose rates, and implications for OSL age estimates: Introducing the Average Dose Model. Quaternary Geochronology 41, 163-173, http://dx.doi.org/10.1016/j.quageo.2017.04.002.

Guibert, P., Christophe, C., Urbanová, P., Guérin, G., Blain, S., 2017. Modeling incomplete and heterogeneous bleaching of mobile grains partially exposed to the light: Towards a new tool for single grain OSL dating of poorly bleached mortars. Radiation Measurements 107, 48-57, http://dx.doi.org/10.1016/j.radmeas.2017.10.003.

Guzzo, P.L., Ferreira de Souza, L.B., Barros, V.S.M., Khoury, H.J., 2017. Spectroscopic account of the point defects related to the sensitization of TL peaks beyond 220°C in natural quartz. Journal of Luminescence 188, 118-128, http://dx.doi.org/10.1016/j.jlumin.2017.04.009.

Kalita, J.M., Chithambo, M.L., 2017. Features of an annealing-induced thermoluminescence peak in α-Al2O3:C,Mg. Optical Materials 70, 158-164, http://dx.doi.org/10.1016/j.optmat.2017.05.034.

Karmakar, M., Bhattacharyya, S., Sarkar, A., Mazumdar, P.S., Singh, S.D., 2017. Analysis of Thermoluminescence Glow Curves using Derivatives of different Orders. Radiation Protection Dosimetry 175, 493-502, http://dx.doi.org/10.1093/rpd/ncw378.

Kijek, N., Chruścińska, A., 2017. On the equivalence of natural and laboratory growth curves in luminescence dating - The effect of deep traps and luminescence centres. Radiation Measurements 106, 477-482, http://dx.doi.org/10.1016/j.radmeas.2017.05.014.

Li, B., Jacobs, Z., Roberts, R.G., Galbraith, R., Peng, J., 2017. Variability in quartz OSL signals caused by measurement uncertainties: Problems and solutions. Quaternary Geochronology 41, 11-25, http://dx.doi.org/10.1016/j.quageo.2017.05.006.

Lowick, S.E., Valla, P.G., 2018. Characterising the luminescence behaviour of 'infinitely old' quartz samples from Switzerland. Quaternary Geochronology 43, 1-11, http://dx.doi.org/10.1016/j.quageo.2017.09.004.

Nikiforov, S.V., Pagonis, V., Merezhnikov, A.S., 2017. Sublinear dose dependence of thermoluminescence as a result of competition between electron and hole trapping centers. Radiation Measurements 105, 54-61, http://dx.doi.org/10.1016/j.radmeas.2017.08.003.

Nyirenda, A.N., Chithambo, M.L., 2017. Factors influencing the shape of CW-OSL signal obtained by stimulation of very deep traps in carbon-doped aluminium oxide: An experimental study. Journal of Luminescence 192, 436-442, http://dx.doi.org/10.1016/j.jlumin.2017.07.016.

Pagonis, V., Chen, R., Kulp, C., Kitis, G., 2017. An overview of recent developments in luminescence models with a focus on localized transitions. Radiation Measurements 106, 3-12, http://dx.doi.org/10.1016/j.radmeas.2017.01.001.

Pagonis, V., Kulp, C., Chaney, C.-G., Tachiya, M., 2017. Quantum tunneling recombination in a system of randomly distributed trapped electrons and positive ions. Journal of Physics: Condensed Matter 29, 365701, http://dx.doi.org/10.1088/1361-648X/aa7db5.

Rengers, F.K., Pagonis, V., Mahan, S.A., 2017. Can thermoluminescence be used to determine soil heating from a wildfire? Radiation Measurements 107, 119-127, http://dx.doi.org/10.1016/j.radmeas.2017.09.002.

Sadek, A.M., Kitis, G., 2017. A critical look at the kinetic parameter values used in simulating the thermoluminescence glow-curve. Journal of Luminescence 183, 533-541, http://dx.doi.org/10.1016/j.jlumin.2016.12.002.

Şahiner, E., Kitis, G., Pagonis, V., Meriç, N., Polymeris, G.S., 2017. Tunnelling recombination in conventional, post-infrared and post-infrared multi-elevated temperature IRSL signals in microcline K-feldspar. Journal of Luminescence 188, 514-523, http://dx.doi.org/10.1016/j.jlumin.2017.05.010.

Sánchez-Muñoz, L., García-Guinea, J., Townsend, P.D., Juwono, T., Cremades, A., 2016. Gaussian thermoluminescence in long-range disordered K-feldspar. American Mineralogist 101, 2118-2122, http://dx.doi.org/10.2138/am-2016-5697.

Sharma, S.K., Chawla, S., Sastry, M.D., Gaonkar, M., Mane, S., Balaram, V., Singhvi, A.K., 2017. Understanding the reasons for variations in luminescence sensitivity of natural quartz using spectroscopic and chemical studies. Proceedings of the Indian National Science Academy 83, 645-653, http://dx.doi.org/10.16943/ptinsa/2017/49024.

Timar-Gabor, A., Buylaert, J.P., Guralnik, B., Trandafir-Antohi, O., Constantin, D., Anechitei-Deacu, V., Jain, M., Murray, A.S., Porat, N., Hao, Q., Wintle, A.G., 2017. On the importance of grain size in luminescence dating using quartz. Radiation Measurements 106, 464-471, http://dx.doi.org/10.1016/j.radmeas.2017.01.009.

Townsend, P.D., Finch, A.A., Maghrabi, M., Ramachandran, V., Vázquez, G.V., Wang, Y., White, D.R., 2017. Spectral changes and wavelength dependent thermoluminescence of rare earth ions after X-ray irradiation. Journal of Luminescence 192, 574-581, http://dx.doi.org/10.1016/j.jlumin.2017.07.041.

Trukhin, A.N., 2017. Luminescence of α-quartz crystal and silica glass under excitation of excimer lasers ArF (193nm), KrF (248nm). Journal of Luminescence 188, 524-528, http://dx.doi.org/10.1016/j.jlumin.2017.05.018.

Tsukamoto, S., Kondo, R., Lauer, T., Jain, M., 2017. Pulsed IRSL: A stable and fast bleaching luminescence signal from feldspar for dating Quaternary sediments. Quaternary Geochronology 41, 26-36, http://dx.doi.org/10.1016/j.quageo.2017.05.004.

Tsukamoto, S., Porat, N., Ankjærgaard, C., 2017. Dose recovery and residual dose of quartz ESR signals using modern sediments: Implications for single aliquot ESR dating. Radiation Measurements 106, 472-476, http://dx.doi.org/10.1016/j.radmeas.2017.02.010.

Dose rate issues

Brill, D., May, S.M., Shah-Hosseini, M., Rufer, D., Schmidt, C., Engel, M., 2017. Luminescence dating of cyclone-induced washover fans at Point Lefroy (NW Australia). Quaternary Geochronology 41, 134-150, http://dx.doi.org/10.1016/j.quageo.2017.03.004.

Romanyukha, A.A., Cunningham, A.C., George, S.P., Guatelli, S., Petasecca, M., Rosenfeld, A.B., Roberts, R.G., 2017. Deriving spatially resolved beta dose rates in sediment using the Timepix pixelated detector. Radiation Measurements 106, 483-490, http://dx.doi.org/10.1016/j.radmeas.2017.04.007.

Instruments

Maraba, D., Bulur, E., 2017. Design and construction of an automated OSL reader with open source software and hardware. Radiation Measurements 106, 632-637, http://dx.doi.org/10.1016/j.radmeas.2017.04.011.

computer coding

Gieszczyk, W., Bilski, P., 2017. A simplified numerical approach to non-radiation induced high-temperature signals in thermoluminescence. GlowVIEW – a useful tool for a multiple glow-curve analysis. Radiation Measurements 107, 102-110, http://dx.doi.org/10.1016/j.radmeas.2017.09.005.

Sature, K.R., Patil, B.J., Dahiwale, S.S., Bhoraskar, V.N., Dhole, S.D., 2017. Development of computer code for deconvolution of thermoluminescence glow curve and DFT simulation. Journal of Luminescence 192, 486-495, http://dx.doi.org/10.1016/j.jlumin.2017.06.016.

Zeeden, C., Dietze, M., Kreutzer, S., 2018. Discriminating luminescence age uncertainty composition for a robust Bayesian modelling. Quaternary Geochronology 43, 30-39, http://dx.doi.org/10.1016/j.quageo.2017.10.001.

Review

Fitzsimmons, K.E., 2017. Reconstructing palaeoenvironments on desert margins: New perspectives from Eurasian loess and Australian dry lake shorelines. Quaternary Science Reviews 171, 1-19, http://dx.doi.org/10.1016/j.quascirev.2017.05.018.

Liritzis, I., Panou, E., Exarhos, M., 2017. Novel approaches in surface luminescence dating of rock art: A brief review. Mediterranean Archaeology and Archaeometry 17, 89-102, http://dx.doi.org/10.5281/zenodo.893194.

Richard, M., Moreno, D., Bahain, J.J., Duval, M., Falguères, C., 2017. Electron spin resonance dating of fossil teeth : some basic guidelines to ensure optimal sampling conditions. Quaternaire 28, 155-159, http://dx.doi.org/10.4000/quaternaire.8003.

Conference Announcements: 12th NWLDW

12th New World Luminescence Dating Workshop June 27-30, Greenville NC

The 12th New World Luminescence Dating Workshop (NWLDW) will be held in Greenville, North Carolina, June 27-June 30. Both poster and oral presentations are planned for Thursday June 28 and Friday June 29.

In the afternoon of Wednesday June 27 we will discuss the foundation of a Trapped Charge Dating Association which was suggested at the Luminescence and Electron Spin Resonance Dating conference (LED 2017) held in Cape Town. We also suggest electing regional representatives for the working group during that time.

We will be offering an optional field trip to the North Carolina coast on Saturday, June 30. Details will follow later.

For questions contact **Regina DeWitt (dewittr@ecu.edu)**
We look forward to seeing you in June!

Regina DeWitt and Shannon Mahan

Conference Announcements: LumiDoz-11

The 11th International Conference on Luminescence and ESR Dosimetry

September 5 to 7, 2018 at the University of Gaziantep, Turkey

On behalf of the organizing committee, we are pleased to announce that the 11th International Conference on Luminescence and ESR Dosimetry (LumiDoz-11) will be held from September 05 to 07, 2018 at University of Gaziantep, Turkey.

The conference will cover topics such as radiation, dosimetry, luminescence materials, archaeological and geological dating, food irradiation, ESR and other related issues. LumiDoz-11 provides an ideal academic platform for researchers to present the latest research findings. The Organizing Committee also encourages companies and institutions to showcase their modern products and equipment in the conference area.

For more detailed information, please kindly visit the conference official website:

http://lumidoz11.gantep.edu.tr/index.php

We are looking forward to meeting you at LumiDoz-11

With our best regards,
LumiDoz-11 Organizing Committee

Conference Announcements: UKLUM2018

UK Luminescence and ESR Meeting 2018
University of Sheffield

11th-12th September, 2018

This is the first announcement for the 2018 UK luminescence and ESR dating (UKLUM2018). This is to be hosted by the Sheffield Luminescence Laboratory at the University of Sheffield, UK. It will be held in Sheffield from 11th-12th September, 2018.

The meeting seeks to provide an informal forum for discussion of luminescence and electron spin resonance research, with an emphasis on recent development, ongoing work and student projects. Both oral and poster presentations are encouraged so that we have a full, interesting and varied programme. To register an interest or request further details please contact Mark Bateman (m.d.bateman@Sheffield.ac.uk).

We look forward to welcoming you to Sheffield.

Mark Bateman and Edward Rhodes

Conference Announcements: APLED-5

Fifth Asia-Pacific Conference on Luminescence and Electron Spin Resonance Dating

Peking University in Beijing, China on 15–17 October 2018

Dear Colleagues,

With the attached First Circular APLED-5, we send you further information about the Fifth Asia-Pacific Conference on Luminescence and Electron Spin Resonance Dating (APLED2018) which will be held at Peking University in Beijing, China on 15–17 October 2018, and hosted by the Luminescence Dating Laboratory in the Key Laboratory for Earth Surface Processes at Peking University.

The conference contact email is: apled2018@urban.pku.edu.cn. Please send all your requests and suggestions to this address. The website of the conference is
http://webues.pku.edu.cn/apled2018/index.html
where you can find details about registration, abstract submission, accommodation and proceedings. The online registration will be open on 1st June 2018.

Please feel free to pass this announcement around to interested colleagues.

We look forward to welcoming you in Beijing!

Conference Announcements: LAIS 2019

Luminescence in Archaeology International Symposium

Institute of Earth and Environmental Sciences
University of Freiburg, Germany
April 3rd to 6th, 2019

The 4th Luminescence in Archaeology International Symposium will be hosted by the Sedimentary Geology and Quaternary Research Group at the University of Freiburg (Germany). LAIS 2018 continues the series of symposia initiated in Delphi 2009, Lisbon 2012 and Paris 2015. It is an international initiative focussing on the use of luminescence for the dating and analysis of materials in archaeological and geoarchaeological context. In addition, it supports archaeological and archaeometrical communities to further develop and expose luminescence methodology.

Topics

- Advances in luminescence methodology
- Dose rate determination
- Innovative materials
- Application in all fields of archaeological sciences
- (Geo-)Archaeological case studies

Local organiser: F. Preusser
International standing committee: I. Liritzis (Chairman, Rhodes, Greece), N. Zacharias, (Kalamata, Greece), A. Zink (Paris, France), Ana Luisa Rodrigues (Lisbon, Portugal).

Deadlines and costs
Registration: November 1st to December 31st 2018
Late registration: January 1st, 2019 to March 31st 2019
Abstract submission: until December 1st 2018
Abstract confirmation: December 15th 2018
Conference fee: EUR 240,-
Student fee: EUR 160,-
Accompanying persons: EUR 100,-

Conference email: LAIS2019@geologie.uni-freiburg.de
Web page: www.sedimentologie.uni-freiburg.de/lais2019

Obituary: Dr. K. S. V. Nambi (1938 – 2017)

Dr. K. S. V. Nambi
1938 – 2017
Former Head, Environmental Assessment Division
Bhabha Atomic Research Centre, Mumbai, India

Dr. K. S. V. Nambi (Kalakad Sankarnarayan Vadivaligia Nambi) was born on July 10, 1938 at Palayamkottai in Tamilnadu, India. As a student, Dr. Nambi had a brilliant career and he received Gold Medals for excellent performance at B.Sc. and M.Sc. (Physics) degree examinations of the University of Madras. Through a difficult national competition, Dr. Nambi was selected by the Atomic Energy Establishment of India to work at the Bhabha Atomic Research Centre (BARC). He worked at BARC till his superannuation in 1998 as the Head, Environmental Assessment Division. His Ph.D. Degree was based on a thesis on Thermoluminescence of Rare- earth Doped Calcium Sulphate Phosphors under Prof. A. K. Ganguly from the Gujarat University, Ahmedabad, India in 1974.

In the seventies, Drs. A. K. Ganguly, C. M. Sunta and K. S. V Nambi and their illustrious colleagues like, S. P. Kathuria, V. K. Jain, V. N. Bapat, B. D. Bhasin, A. Sunderarajan, M. David, R. Sashidharan, A. S. Pradhan, B.C. Bhatt, A. R. Lakshmanan and many others became a formidable dosimetry group that earned international acclaim through, its work on Ca-based and other phosphors and for its contribution to the overall development of thermoluminescence dosimetry and the physics behind it. This group also developed instrumentation for TL dosimetry (TLD readers, low temperature systems, exo-electron systems and many others) and developed new ideas on understanding the luminescence processes in materials. This group carried out large scale radiation survey using TLDs. Nambi's Redox Model has been widely used to understand luminescence process in various rare earth doped phosphors. To an extent, during the seventies, the TLD group at BARC became important movers and shakers of the TL dosimetry field and was highly productive in terms of their publications. Dr. Nambi organized the first Indian conference on Thermoluminescence and its Applications in 1990. This meeting provided the seeds for the initiation of the Luminescence Society of India (LSI) that is now providing a vibrant platform for all luminescence workers to meet annually. He served as the first President of the LSI and laid out good practices for its functioning.

Though not its direct mandate, this group also took upon a pilot study on the dating of archeological pottery and established the protocols. Later on, jointly with Martin Aitken, Dr. Nambi provided the conversion values for the computation of annual radiation dose from elemental concentration of radio-elements. The dating community used these factors for close to two decades. Drs. Nambi and Sunta were regular

features at the Luminescence and Electron Spin Resonance dating meetings organized by Martin Aitken - simply as Martin always felt the need for basic physics inputs to understand luminescence processes in minerals. He once mentioned to one of us, as to how much he respected the work by the Indian groups led by Sunta and Nambi and that he immensely applauded their 'established reputation'. Dr. Nambi served on the Editorial Board for Ancient TL and also contributed widely to ESR dating and more importantly on TL-ESR correlation. Even to-date, this is an area that needs further impetus, if TL/OSL has to really go beyond their present status.

In the area of environmental radiation dosimetry, based on their work on the coastal regions of Kerala, India, Nambi and Soman suggested a negative correlation between cancer incidences rates with gamma radiation levels measured using TLD's. This was in consonance with the concept of radiation hormesis. Though this work was criticized on some grounds, it none-the-less led to the establishment of two major programs in India. One was the establishment of cancer registry for cancer epidemiology in the high background areas of Kerala and the other one was on the occurrences of cancer mortality among workers in the Atomic Energy establishments. These programs have gone a long way in providing the scientific basis for understanding the effects of minimally low, but constant radiation exposure to humans.

Nambi was an enabler and always welcomed colleagues to join the team TLD and contribute to it. He led by example. He contributed through monographs. Notable was was his monongraph titled *Progress of Thermoluminescence Research on Geological Materials* with Dr. A.V. Sankaran and C. M. Sunta in Proceedings of the Indian National Science Academy. This close to 100 page monograph is a magnum opus on the TL properties of natural minerals. His lecture notes on *Thermoluminescence: its understanding and applications*, published in Brazil by Instituto de Energia Atomica, Cidade Uniersitaria has been landmark contributions and is a must read for all workers in TL. A report titled *U, Th and K distributions inferred from regional geology and the terrestrial radiation profiles in India*, based on field deployment and analysis of about 5000 TLD monitors across India demonstrates the breadth of work he covered. Many of us still advise new students in luminescence applications to read these articles as the basic introduction for understanding luminescence as a physical process and its applications.

In 1991, Nambi was given the responsibility to Head the Environmental Assessment Division at BARC. This was a responsibility that he led with rare aplomb by establishing environmental monitoring program around nuclear facilities in India using natural CaF_2 based environmental dosimeters. He also took up the Nuclear Aerosol Project to assess effects after nuclear accidents. He developed a nuclear aerosol test facility; initiated measurement of indoor radon; developed atmospheric gamma ray radiation program with solar powered systems; initiated measurement of heavy metals in herbal medicines and their impact on human health; developed protocols to measure aluminum build up during dialysis and for accentuated selenium level during treatment of depression. These activities were noteworthy and once again depicted the range of themes he covered. Dr. Nambi was an avid reader and this habit sculpted his vision and helped him understand quickly, the nitty-gritty of new areas that he initiated. Some of these studies compelled removal of lead from Indian gasoline as anti knocking agent. His group also developed rugged continuous air particulate and gas monitoring system to measure a range of parameters from Solar radiation flux to Chemical and Industrial pollutants. He buttressed these with modeling and computational efforts.

It was not known to many that post superannuation, Dr. Nambi devoted his time in the study of ancient Tamil literature and that he wrote several books on Thirukural. Thirukural is a classic Tamil text consisting of 1330 couplets or kurals, dealing with the everyday virtues of an individual and is considered as one of the magnum opus of written work on ethics, morality and secular ethics. This activity resonated with the persona that Dr. Nambi was. As a scientist, Dr. Nambi impacted the Indian Environmental Assessment and monitoring studies in a big way. He built instrumentations where none existed, applied and explored new avenues and always buttressed experimental observations with models. And, as a person, Dr. Nambi touched many a lives with his ever affable and pleasant nature, and through his ever willingness to help a scientific cause. These were his landmark traits. Nambi was a friend in the truest sense of word and never hesitated giving his frank views and advice.

In his demise, the community lost a brilliant and a fearless individual, a close and a well meaning friend and a mentor to many. Analogous to the geological parlance, he was an extreme event in Indian environmental sciences that modulated and sculpted the landscape of radiation environmental sciences in India. Dr. Nambi breathed his last on April 29, 2017 and is survived by his wife (Sundari), daughter (Vijaya), son (Shankar), daughter-in-law (Kaushi) and five grand children (Preethi, Vikram, Adithi, Adarsh and Sarika). We will remember him and miss him, for his camaraderie, his benevolent friendship sans boundaries and the wholesome manner he touched our lives and scientific careers. We pray for Peace to him and for Strength to his family.

A. K. Singhvi, Y. S. Mayya, and B. C. Bhatt

Obituary: Professor Martin Aitken (1922 – 2017)

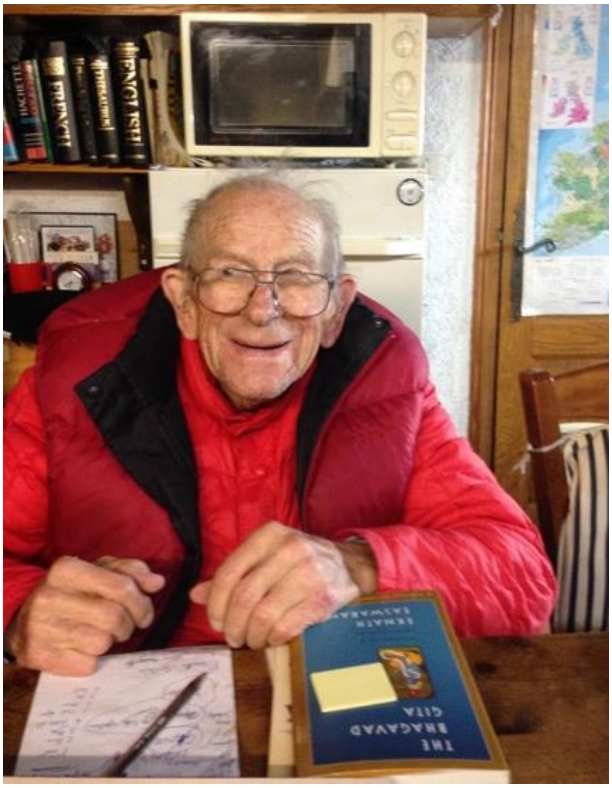

Martin Aitken
11 March 1922 – 15 June 2017

Remembering Martin Aitken

Several obituaries have been written for Martin Aitken, but here we focus on his key contributions to the field of luminescence, his influence on the community and the 'Aitkenesque' quirks which all who worked with him will remember well.

Martin inherited a very practical disposition, born into a line of fen farmers with his father and elder brother taking up careers in engineering. At school he thrived in the Boy Scouts and became a Home Guard in the early days of the war. He won a bursary to the University of Oxford to study physics-with-radio but before completion became a ground Radar Officer in the RAFVR, serving in Ceylon, India and Burma. Anyone who visited the Research Laboratory for Archaeology and the History of Art (RLAHA), 6 Keble Road, will remember the incessant morse-code buzzing: each lab member had their own personalised buzz-code and so could be called to the phone wherever they were in the rabbit-warren of a building. This was one of Martin's very practical implementations.

After the war Martin moved back to Oxford to complete his studies and in 1947 married Joan, who he had met at one of the radar stations. He went on to complete a DPhil. based on the development of a 120-MeV electron synchrotron in the Clarendon Laboratory. However, in 1957 he joined the newly-formed RLAHA - Martin's desire to work in an area where 'individual effort could still be effective' will resonate with many in the luminescence community.

When Martin first joined the RLAHA the areas of research were limited to radiocarbon dating and resistivity surveying. By the time he retired in 1989 the Laboratory was the recognised world-centre for 'archaeometry', embracing many branches of science. Martin, together with the Laboratory's first Director, the late Teddy Hall, supplied the key

impetus for this success. Martin could be a hard task master, and many of his 11 MSc. and 12 DPhil. students will attest to the expectation that their dissertations would stand up to the highest level of scientific scrutiny. The depth of knowledge he expected from his students was evidenced by his comment that "PhD students are no use until after three years".

Martin's first projects involved successful use of a proton magnetometer, pulsed induction detector and fluxgate gradiometer for archaeological magnetic prospection. After a few years he moved on to laboratory archaeomagnetic measurements of field direction, and later field intensity. Martin worked on the development of the first cryogenic SQUID magnetometer in Britain, and his interest in this field continued until his retirement.

In the early 1960's a member of the Laboratory's governing committee returned from a visit to California where at UCLA he had been greatly enthused by the use of TL for ceramic authentication. TL was chosen as thesis topics for two students (Mike Tite and Jeanette Waine) and an abstract submitted for a conference in Rome. It was somewhat embarrassing when Martin heard shortly afterwards that TL authenticity testing had been abandoned at UCLA due to frequent false positives from unidentified causes! However, Martin and his team persisted, implementing a suggestion from a visiting geologist to suppress the non-radiation-induced TL by use of an inert atmosphere and 'the rest is history'.

Martin and his growing team of researchers then designed and constructed the first practical TL glow oven (the "Alldred set"), subsequently commercialised as the well-known "Littlemore TL glow oven", and used these advances to pioneer TL dating techniques for burnt flint, calcite and windblown sediment. This enabled the dates to reach back beyond the range of radiocarbon to the lower palaeolithic period, greatly raising the profile of TL dating. The range of datable materials was extended to volcanic products and Martin's interest in magnetic reversals and the Laschamp Geomagnetic Event led him to the Chane des Puys in the Auvergne region of central France. This was also the region of the infamous Glozel archaeological site which initially gave TL a bad rap, but was later resolved as a complicated mix of Gallo-Roman, medieval and modern-era objects. It was here that Martin and Joan fell in love with the countryside (and wine!), subsequently settling in a small hamlet in the Monts de Forez in retirement.

Martin and Joan lived for forty years in the picturesque White Cottage in Islip, just north of Oxford. Staff and students will remember many excellent lunches there on the banks of the River Cherwell, and the obligatory visit to see the pet goat. They may also remember the tour conveniently ending at the cloak closet where coats had been left on arrival!

In 1985 Martin began his last major research thrust. Enthused by the landmark optical dating paper by Huntley et al. in Nature, Martin immediately set up a team to investigate and apply the new technique. For the four years until his retirement the RLAHA led the development of the technique, investigating applications to feldspar and zircon, and developing the core quartz dating protocols which remain until this day. The optical dating research was centred in the "Laser Hut" out in the car park at the back of the RLAHA. The Laser Hut was heavily used during that period, starting with a recurring 7:00 am booking by Martin during which he would eat a garlic sandwich for breakfast. Martin's car was to be avoided in France as he had the penchant to stop and buy fresh garlic from local farmers. Martin had a pretty good appreciation of food and always tried to plan or attend fieldwork which was within convenient lunchtime travel distance of a good restaurant, particularly when in France.

Martin was always very open and generous towards other researchers and genuinely desired to propagate his research around the world. For example, he had a standing purchase arrangement with EMI for about 20 years to ensure that RLAHA got any 9635Q PMT produced which was "A" standard with very low background counts. Whilst most of these were used within his lab, over time many were donated to other laboratories. The 'Aitken academic tree' has been published elsewhere and shows just some of the links to current luminescence research across the world.

China held a warm place in Martin's heart. He had received an invitation out of the blue through the Royal Society and visited only a few years after the downfall of the Gang of Four. Yielding to marital pressure, Martin requested that Joan accompany him and the request was granted on condition that she gave a course of lectures on the use of English. He recounted that she was in the room next to him and he was repeatedly distracted by the bursts of laugher from next door. Martin and Joan visited China several times over the years, and Martin's favourite outfit was a Chinese suit. He wore it once when visiting his first Chinese student in Oxford (Li Sheng Hua). He was greeted by 'Ah, very fashionable' and his face lit up until after a pause Sheng Hua added '30 years ago'.

Martin published over 150 papers, but is best known for his textbooks. *Physics and Archaeology* (1961, second edition 1974) was followed by the TL dating 'bible', *Thermoluminescence Dating*, in 1985. His book on *Science-Based Dating in Archaeology* (1990) immediately became a standard undergraduate text, and he followed up with *Introduction to Optical Dating* in 1998. Martin was quietly proud of his books, in particular that *Physics and Archaeology* had given him access to the inner circles of the Chinese elite. He was due to visit China again at the time of release of his seminal TL dating book in 1985 and he badgered the publishers to courier an advance copy to him so he could take it on his travels. On its arrival he was so keen to read it that it accompanied him even to the loo, but unfortunately the book slid from under his arm and the lab staff spent the rest of the day drying it out. In subsequent years students visited that same loo to ceremoniously christen theses immediately before their viva.

Martin also instigated two enduring conferences. He preferred the term 'symposia' as this implied an opportunity for informal discussion over refreshments. The first of these

evolved into the International Symposium on Archaeometry and the second was the Specialist Seminars on TL at Oxford which morphed into the current International Conference on Luminescence and ESR Dating. He also started the journal Archaeometry which began as a cyclostyle duplicated Laboratory Bulletin in 1958, and remained editor for many years.

In 1983 Martin was elected a Fellow of the Royal Society, and in 1985 made the ad hominem Chair of Archaeometry at Oxford. He won the Gemant Award from the American Institute of Physics and the Pomerance Award of the Archaeological Institute of America for scientific contributions to archaeology. These accolades attest to the breadth of his research endeavour and his success in applying hard science to often complex problems. He sometimes called himself 'the 10% man', emphasising the need to forget about the majority of the complications and to concentrate on the priorities. This meant that he could take an analytical approach to find solutions which worked even when he didn't fully understand the physical processes, and so move forward while leaving later researchers to tease out the detail. Many of us who follow his footsteps in luminescence research will appreciate his vision, achievements and impact on our lives.

Barnaby Smith, Nigel Spooner and Danielle Questiaux

Martin Aitken's contributions to Ancient TL

Several obituaries for Martin Aitken list his complete bibliography. Here I want to focus on his contributions to Ancient TL. Martin Aitken briefly served as the Editorial Caretaker after Steve Sutton moved on to other research. Martin Aitken and Ian Bailiff worked together on Volume 2, Issue 2 (September 1984), before Ian Bailiff took over production. He reviewed numerous manuscripts and authored or co-authored 13 articles. Many of these articles were landmark papers for luminescence dating and were later integrated in his books. The most notable among them is his work with G. Adamiec on dose rate conversion factors, which has been cited more than 600 times since its publication.

Regina DeWitt

Bibliography

A.K. Singhvi and M.J. Aitken. *Americium - 241 for Alpha Irradiations*; Ancient TL, 1978, No.3.

M.J. Aitken. *The alpha particle response of fluorite*; Ancient TL, 1979, No.9.

M.J. Aitken, G.D. Bussell and H.S.T. Driver. *Zero-glow Monitoring (ZGM)*; Ancient TL. 1979, No.9.

M.J. Aitken. *TL dating in China*; Ancient TL, 1980, No.13.

M.J. Aitken. *Non-linear growth: allowance for alpha particle contribution*; Ancient TL, 1984, Vol. 2, No.1.

M.J. Aitken. *Alpha particle effectiveness: numerical relationship between systems*; Ancient TL, 1985, Vol. 3, No.3.

M.J. Aitken. *Alpha dose to a thin layer*; Ancient TL, 1987, Vol. 5, No.3.

M.J. Aitken. *Pairs precision required in alpha counting*; Ancient TL, 1990, Vol. 8, No.2.

M.J. Aitken and J. Xie. *Moisture correction for annual gamma dose*; Ancient TL, 1990, Vol. 8, No.2.

J. Xie and M.J. Aitken. *The hypothesis of mid-term fading and its trial on Chinese loess*; Ancient TL, 1991, Vol. 9, No.2.

M.J. Aitken. *Symbols in TL and optical dating: provisional list*; Ancient TL, 1992, Vol. 10, No.1.

G. Adamiec and M. Aitken. *Dose rate conversion factors: update*; Ancient TL, 1998, Vol. 16, No.2.

N.A. Spooner, D.G. Questiaux, and M.J. Aitken. *The use of sodium lamps for low-intensity laboratory safelighting for optical dating*; Ancient TL, 2000, Vol. 18, No.2.

Ancient TL

ISSN 0735-1348

Aims and Scope

Ancient TL is a journal devoted to Luminescence dating, Electron Spin Resonance (ESR) dating, and related techniques. It aims to publish papers dealing with experimental and theoretical results in this field, with a minimum of delay between submission and publication. Ancient TL also publishes a current bibliography, thesis abstracts, letters, and miscellaneous information, e.g., announcements for meetings.

Frequency

Two issues per annum in June and December

Submission of articles to Ancient TL

Ancient TL has a reviewing system in which direct dialogue is encouraged between reviewers and authors. For instructions to authors and information on how to submit to Ancient TL, please visit the website at:
http://www.ecu.edu/cs-cas/physics/ancient-timeline/ancient-tl1.cfm

Journal Enquiries

For enquiries please contact the editor:
Regina DeWitt, Department of Physics, East Carolina University, Howell Science Complex, 1000 E. 5th Street, Greenville, NC 27858, USA; Tel: +252-328-4980; Fax: +252-328-0753 (dewittr@ecu.edu)

Subscriptions to Ancient TL

Ancient TL Vol. 32 No.2 December 2014 was the last issue to be published in print. Past and current issues are available for download free of charge from the Ancient TL website:
http://www.ecu.edu/cs-cas/physics/ancient-timeline/ancient-tl5.cfm